Supplementary Figure 1

Supplementary Figure 1. Venn diagram per entity, describing the data types available for each of the 35 patients in our cohort.

Supplementary Figure 2

a

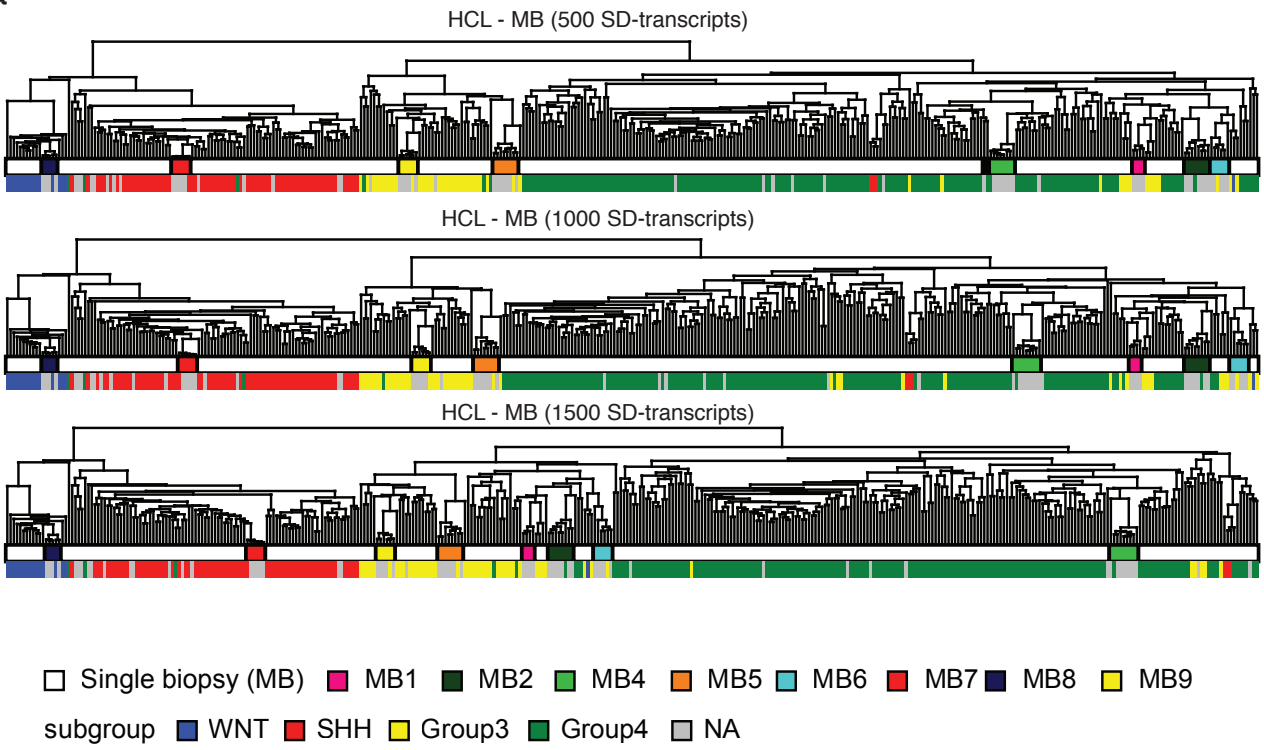

b

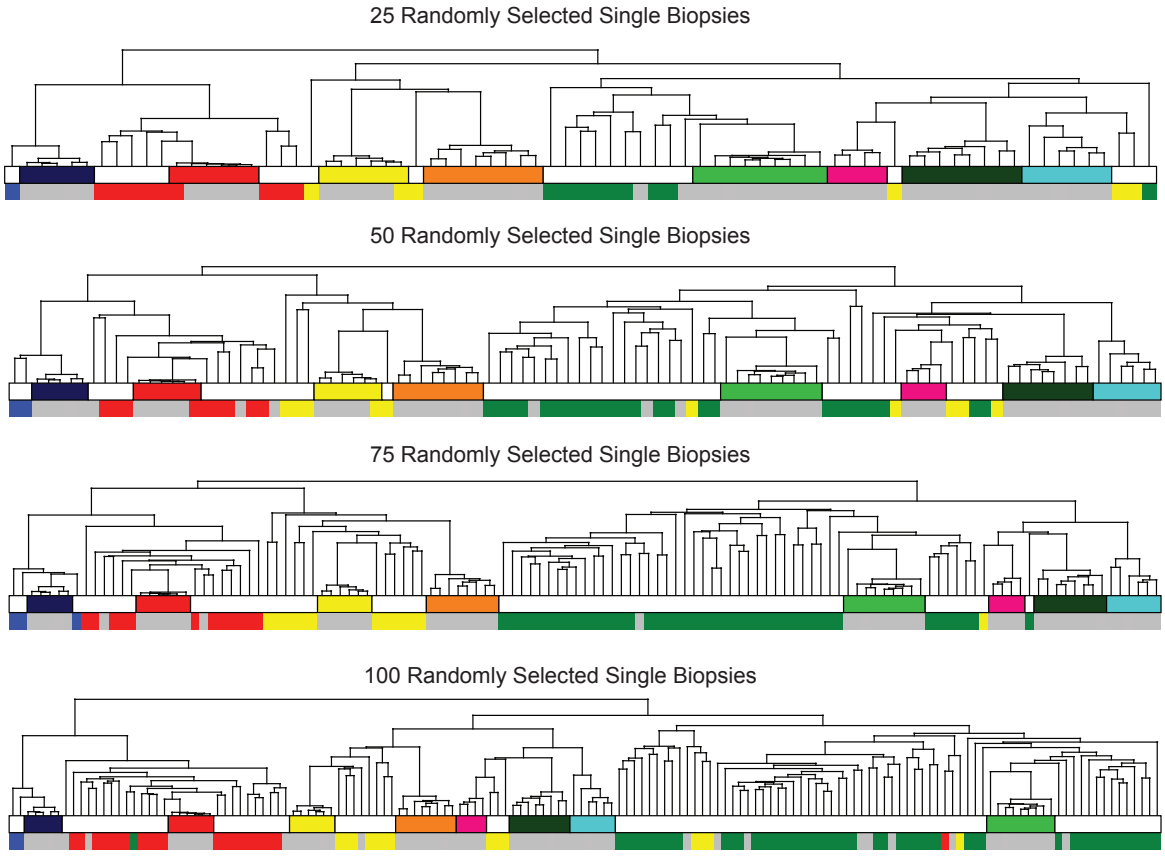

(cont..)

Supplementary Figure 2

b (cont)

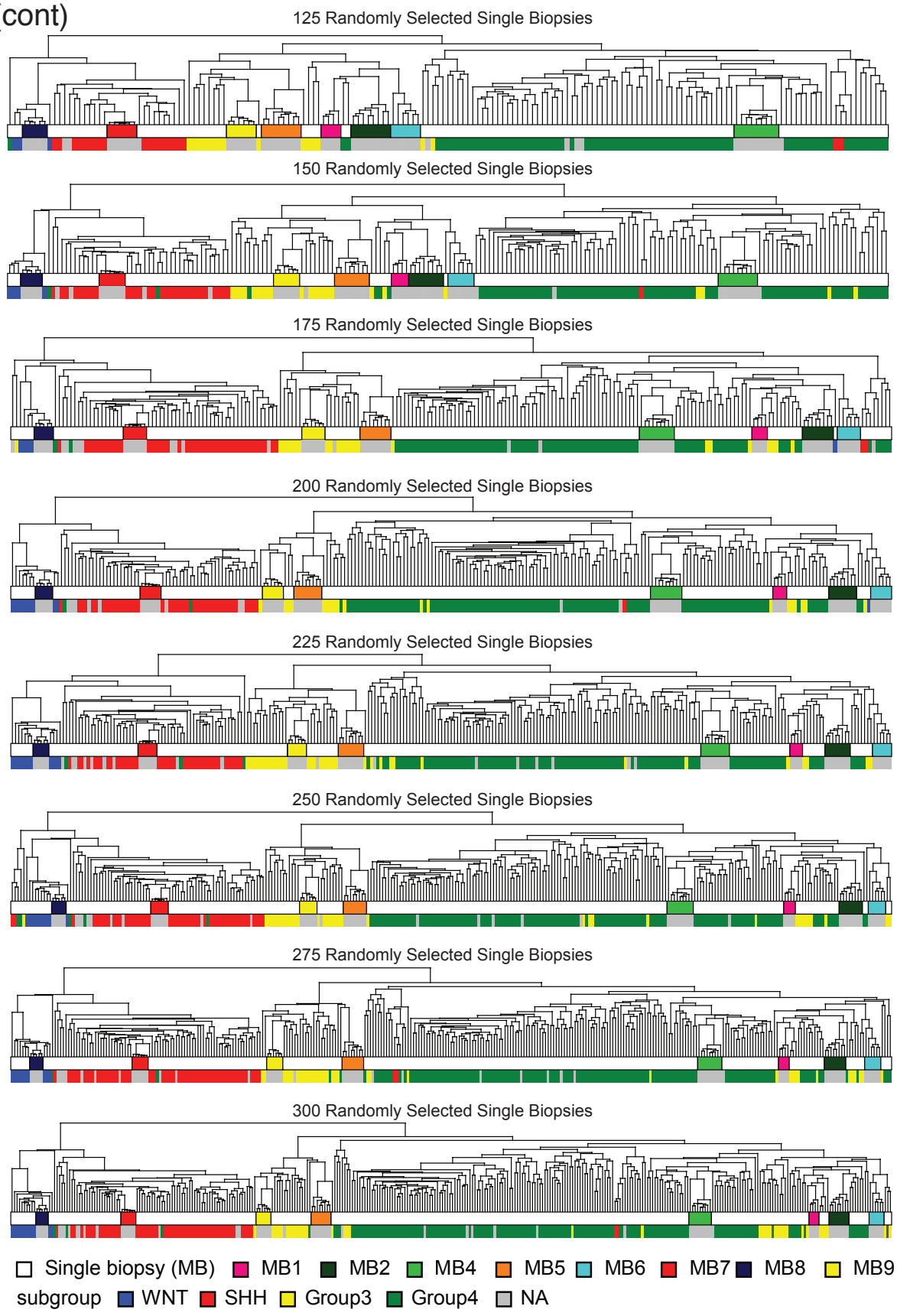

Supplementary Figure 2

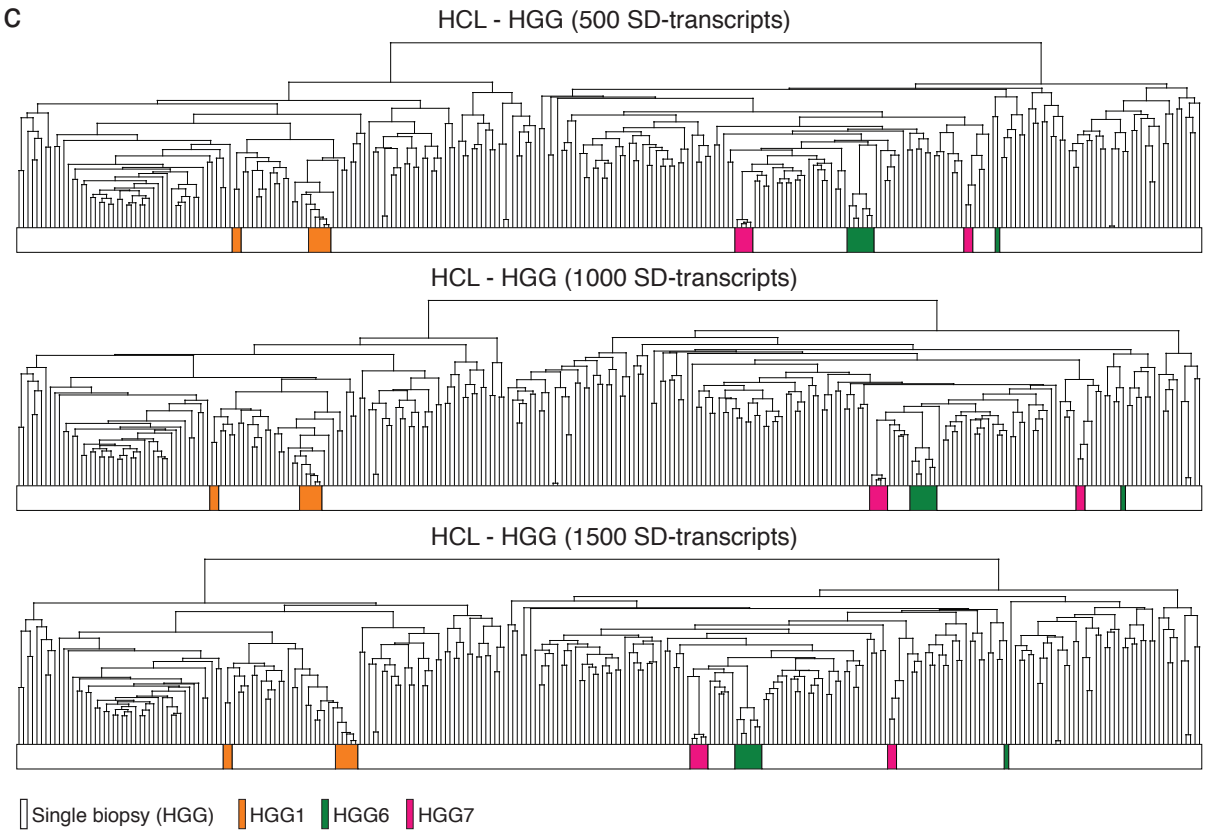

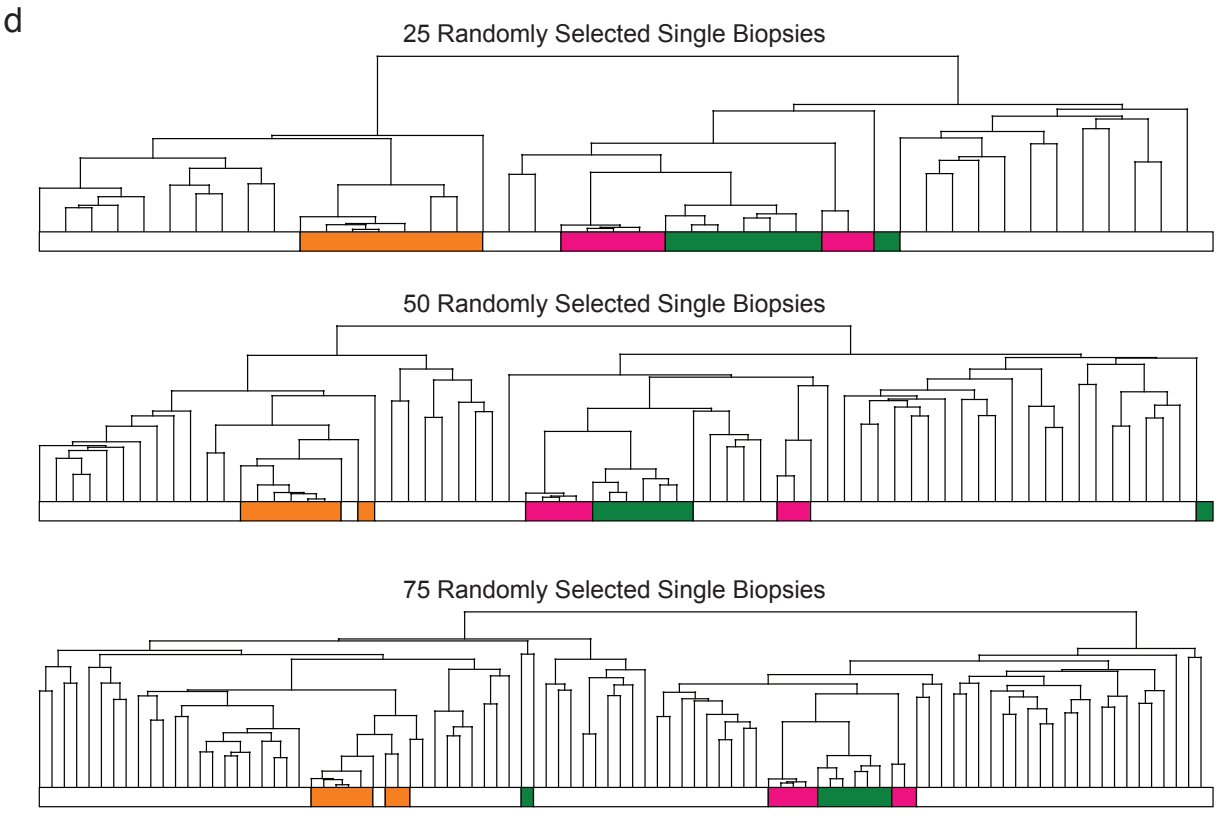

(cont...)

Supplementary Figure 2

d (cont)

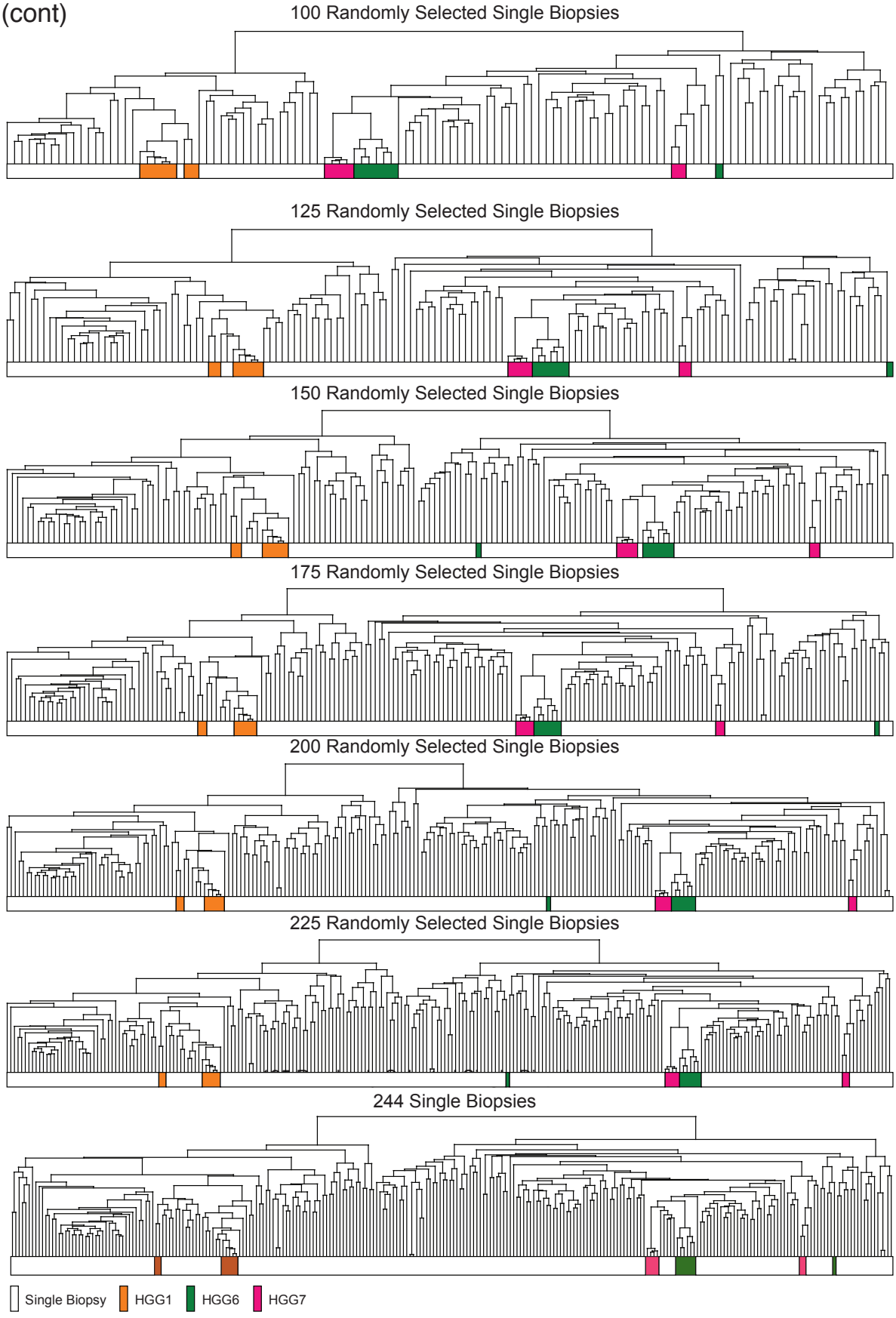

Supplementary Figure 2

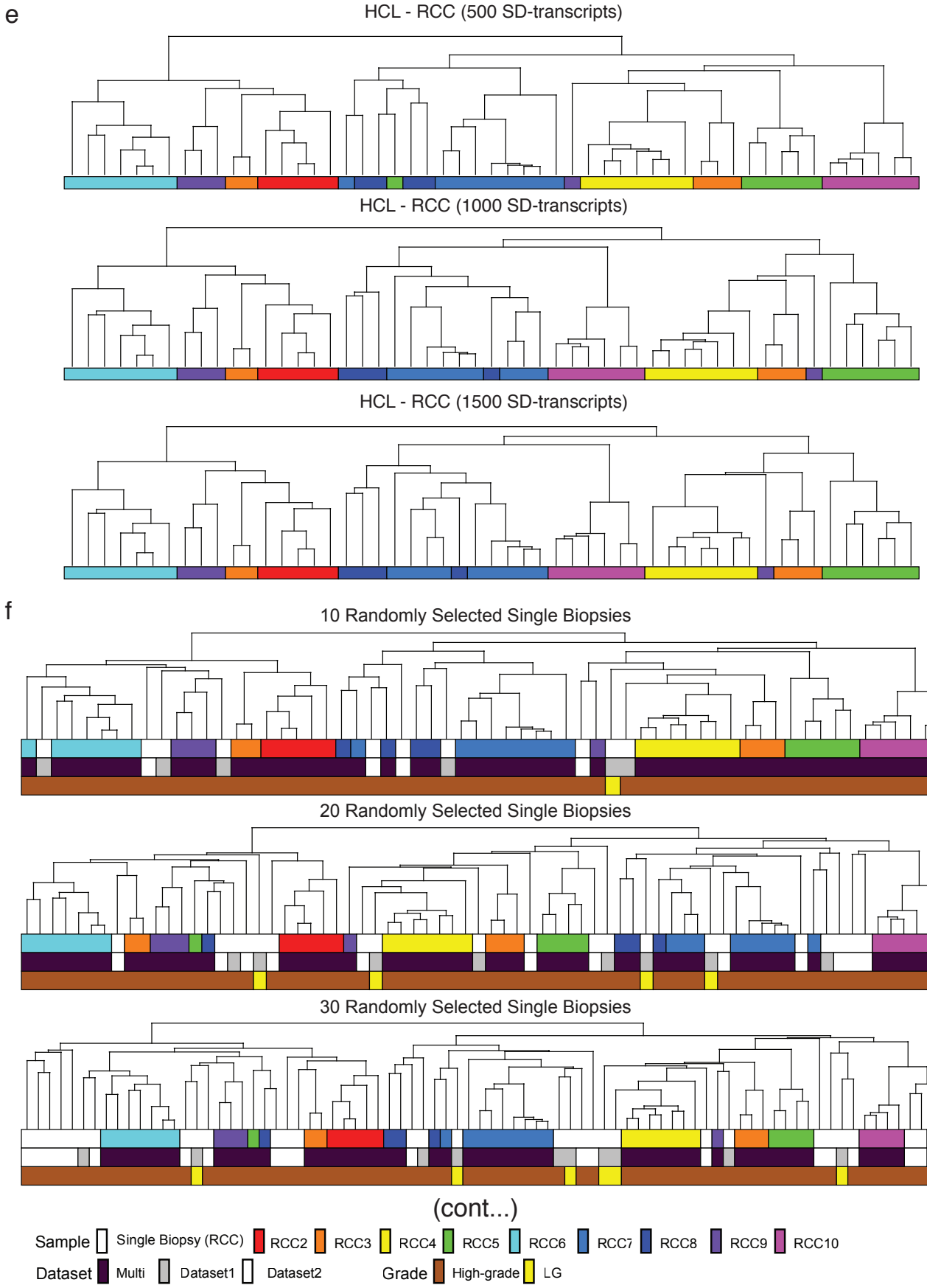

Supplementary Figure 2

f (cont)

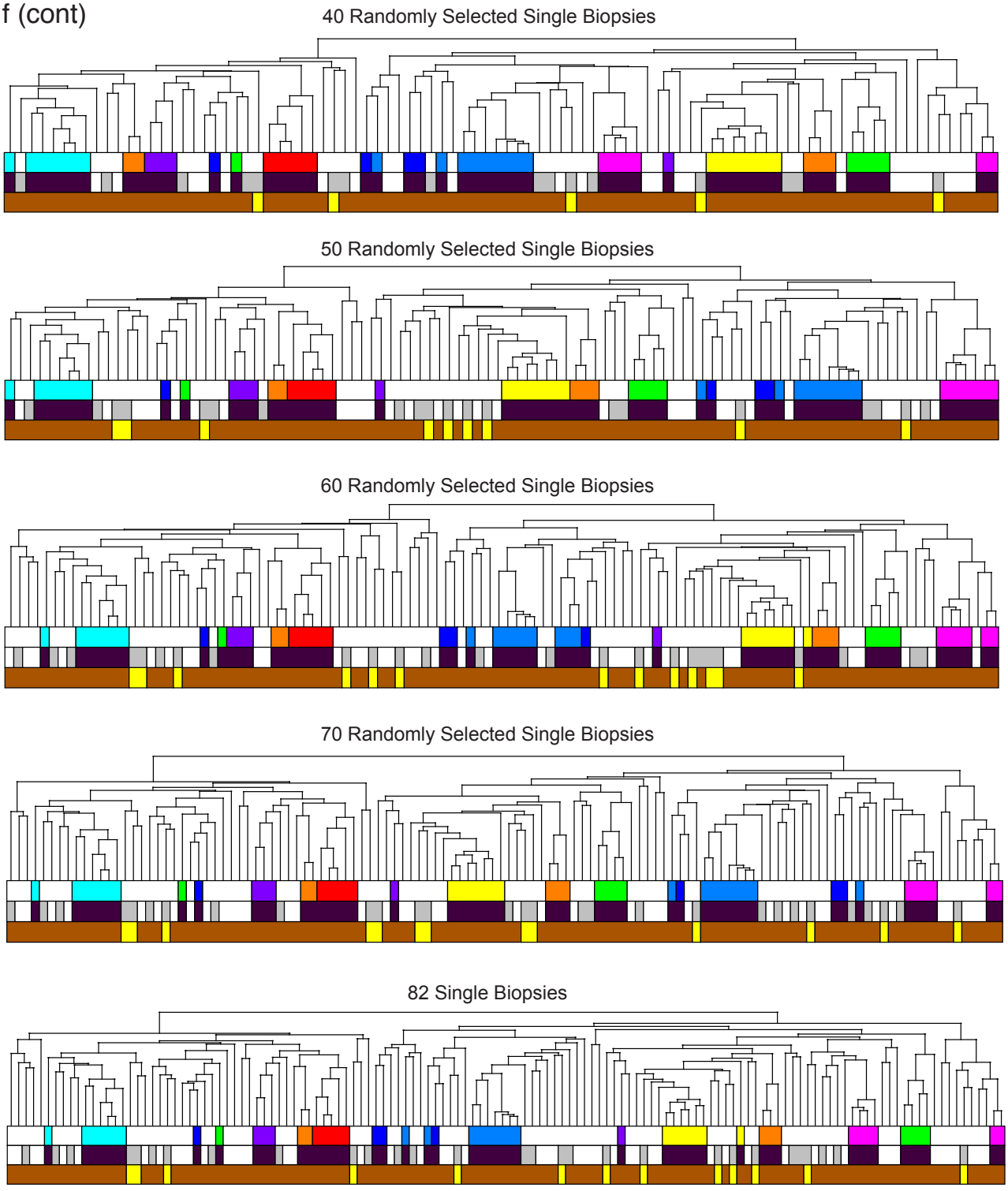

Supplementary Figure 2. Gene expression clustering of MB, HGG and RCC samples. (**a**) Unsupervised hierarchical clustering (HCL) of multi-region medulloblastoma (MB) samples combined with single biopsies (n=334) using the 500, 1,000, and 1,500 highest-SD transcripts. (**b**) Unsupervised HCL of multi-region medulloblastoma (MB) samples combined with increasing number of randomly picked single biopsies (from 10 to 300 in increments of 25; 1,000 highest-SD transcripts). Medullobastoma subgroups are indicated on the 2nd color bar. (**c**) Unsupervised HCL of multi-region high-grade glioma (HGG) samples combined with single biopsies (n=244) using the 500, 1,000, and 1,500 highest–standard deviation (SD) transcripts. (**d**) Unsupervised HCL of multi-region high-grade glioma combined with increasing number of randomly picked single biopsies (from 25 to 244 in increments of 25; 1,000 highest-SD transcripts). (**e**) Unsupervised HCL of multi-region RCC biopsies using the 500, 1,000, and 1,500 highest–standard deviation (SD) transcripts. (**f**) Unsupervised HCL of multi-region RCC samples combined with increasing number of randomly picked single biopsies (from 10 to 82 in increments of 10; 1,000 highest-SD transcripts). The single biopsies come from 2 different datasets (dataset1[19], dataset2[18]) as indicated on the 2nd color bar. Dataset1 has some low-grade RCC samples indicated in yellow on the 3rd color bar.

Supplementary Figure 3

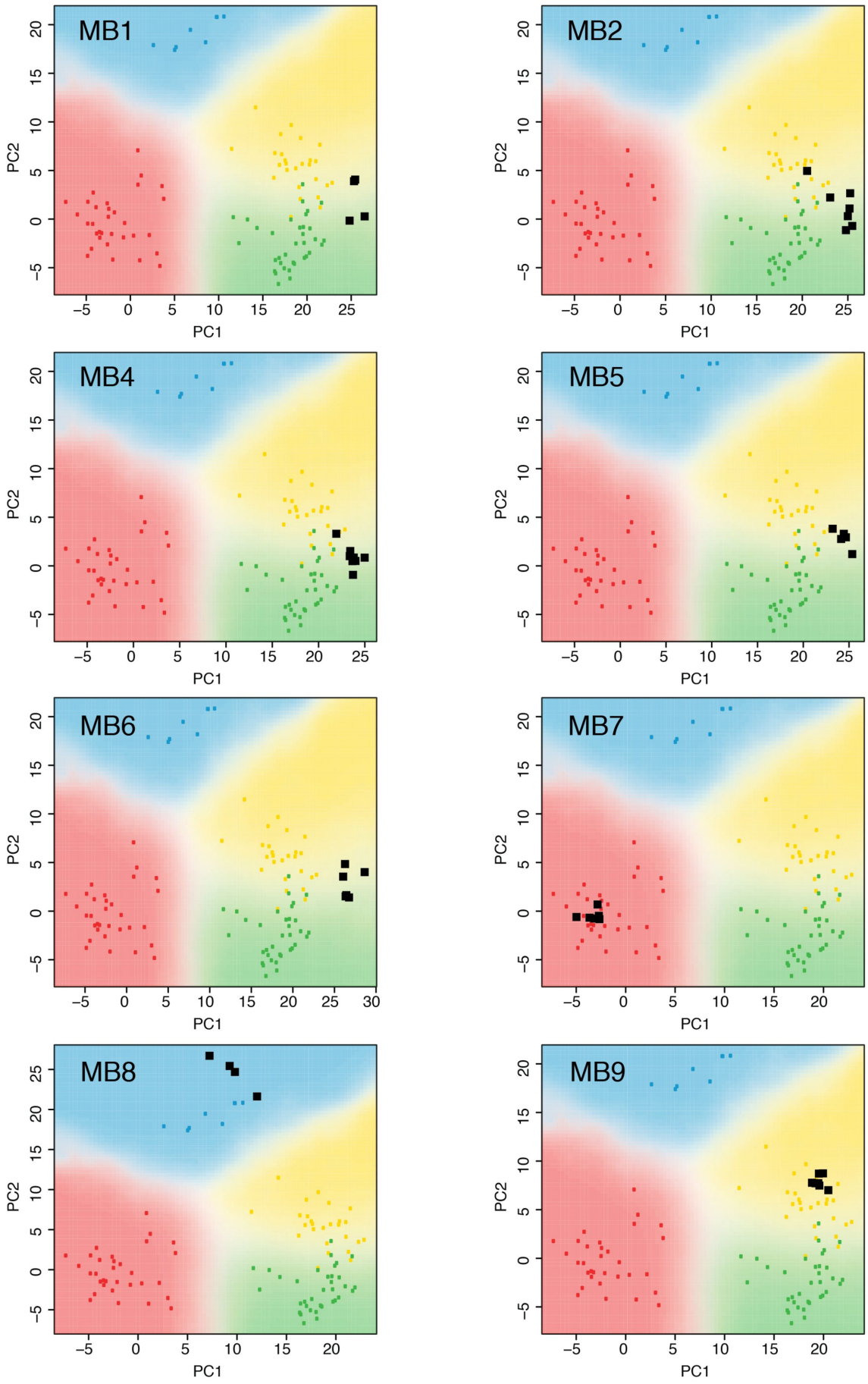

Supplementary Figure 3. Principal component analysis (PCA) confirms a low degree of spatial heterogeneity using expression of 22 MB subgroup marker genes. Multi-region biopsies are indicated by black squares, and illustrated along with 103 single-biopsy MB samples (small squares colored according to predicted subgroup).

Supplementary Figure 4

a

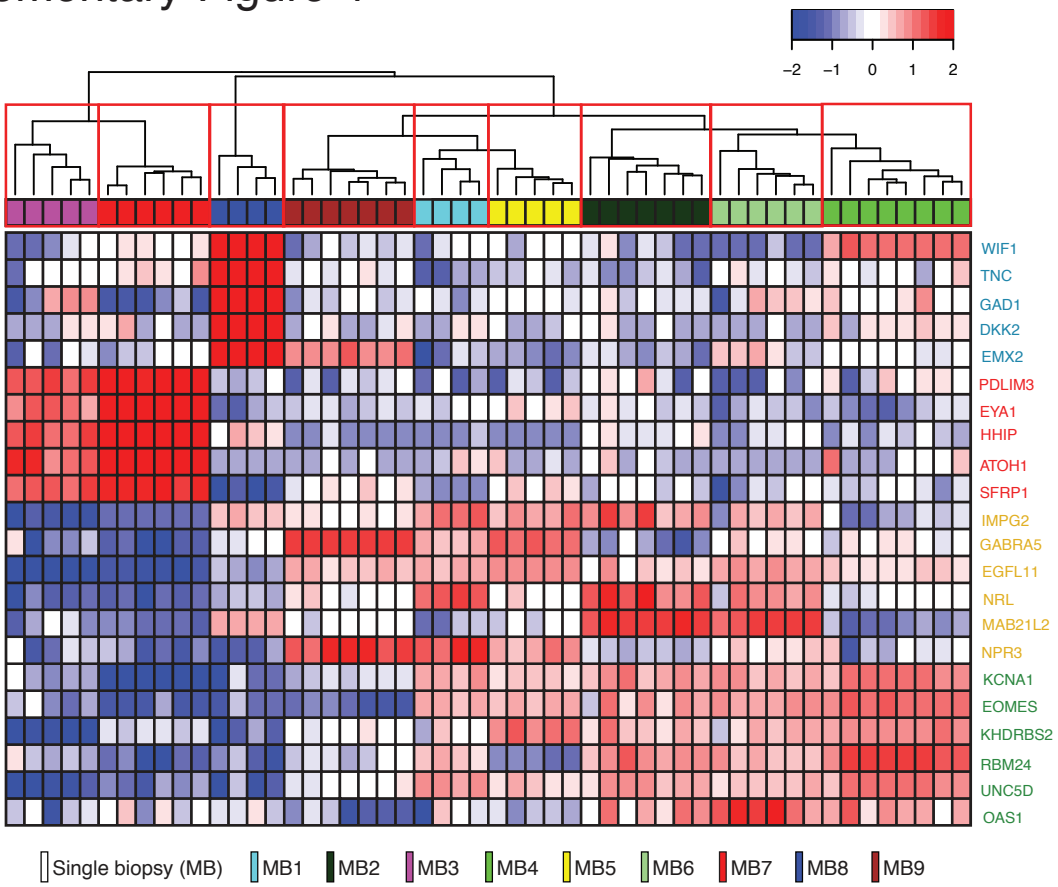

b

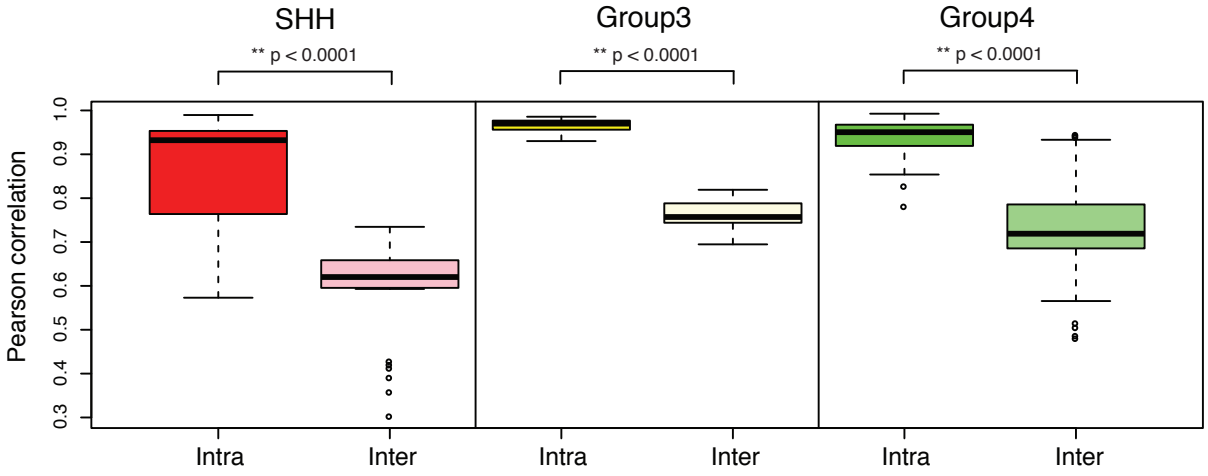

Supplementary Figure 4. Low degree of subgroup marker expression differences in MB multi-region samples. (**a**) Unsupervised hierarchical clustering (HCL) results from NanoString gene expression profiling reveal reproducible MB subgroup marker expression across MB tumors. Gene label colors denote subgroup: blue (WNT), red (SHH), dark yellow (Group3), green (Group4). (**b**) Pearson correlation was used to compare the similarity of marker gene expression between multi-region biopsies of each patient (intra) versus the similarity of expression between different patient samples (inter), stratified by subgroup. Marker gene expression was significantly more similar between biopsies of the same patient (intra) compared to biopsies from different patients from the same subgroup (inter), and this pattern remained consistent across subgroups (Wilcoxon rank sum test).

Supplementary Figure 5

MB1

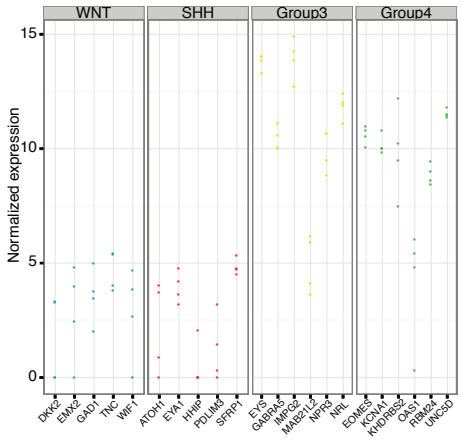

MB2

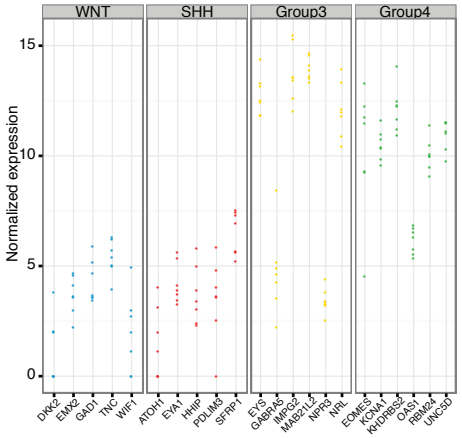

MB4

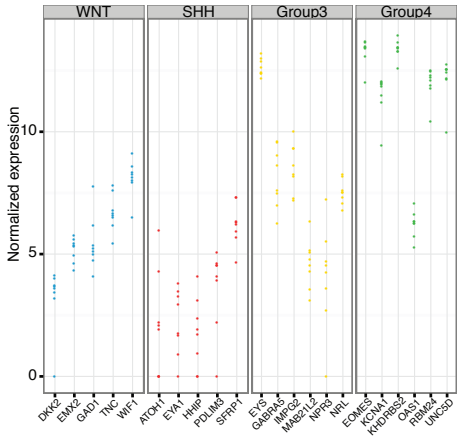

MB5

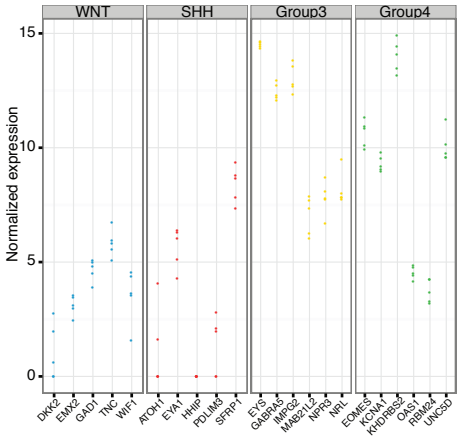

MB6

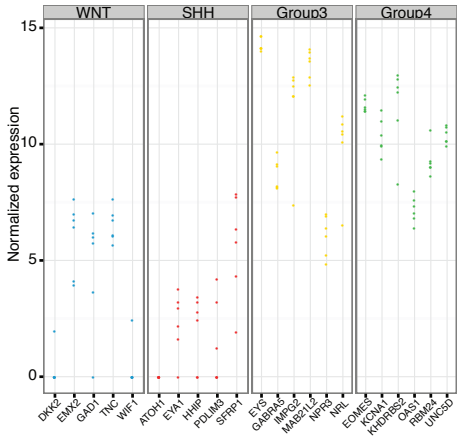

MB7

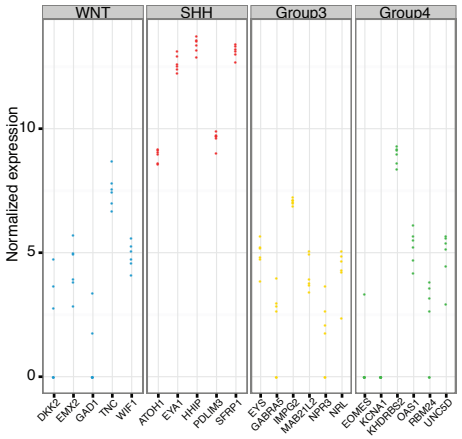

MB8

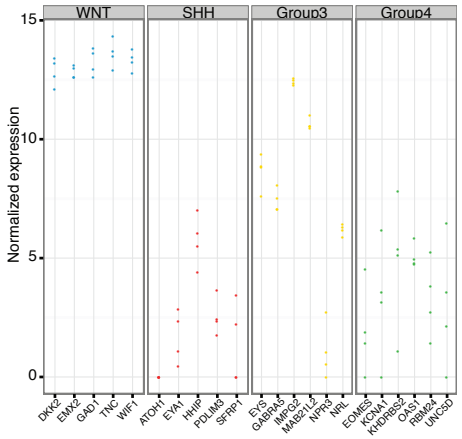

MB9

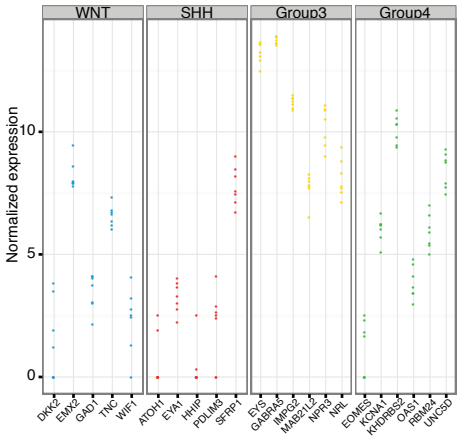

Supplementary Figure 5. Highly comparable marker gene expression is evident in all multi-region biopsies from individual MB patients. For each marker gene, the corresponding expression in each biopsy is indicated by a dot. Colors correspond to the subgroup with which the respective gene expression is affiliated: blue (WNT), red (SHH), yellow (Group3), green (Group4).

Supplementary Figure 6

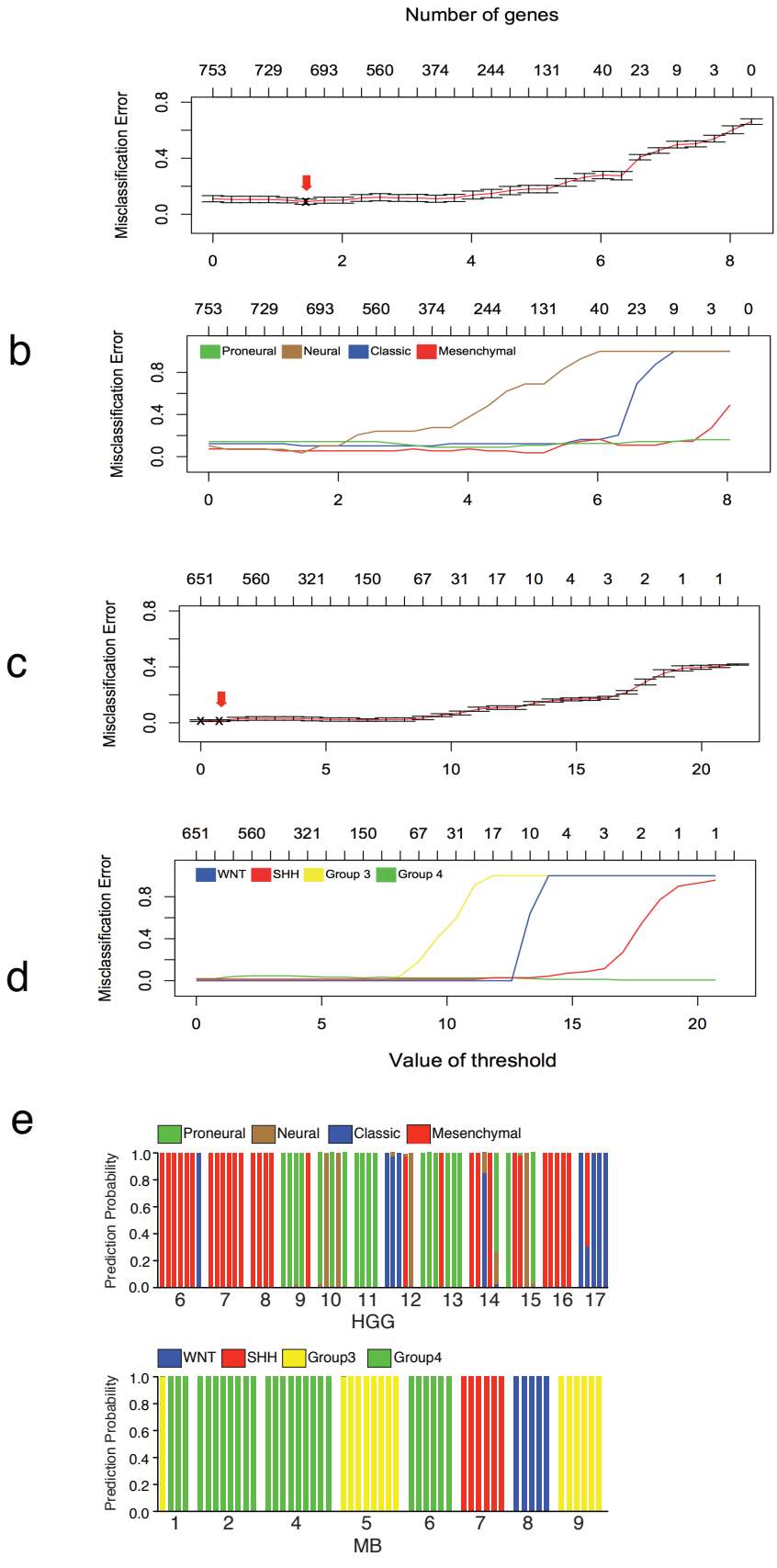

Supplementary Figure 6. Feature selection for predictive analysis of microarrays (PAM) in glioblastoma (HGG) and medulloblastoma (MB) training sets. Threshold selection for the optimal number of marker genes (**a**) based on the misclassification error (**b**) in the GBM training set. Threshold selection for the optimal number of marker genes (**c**) based on the misclassification error (**d**) in the MB training set. Optimal threshold is indicated by **x** and a red arrow. (**e**) Predictive analysis of microarrays (PAM) highlights discordant subtyping in glioblastomas (HGG; upper panel) and highly concordant subgrouping in MB (lower panel).

Supplementary Figure 7

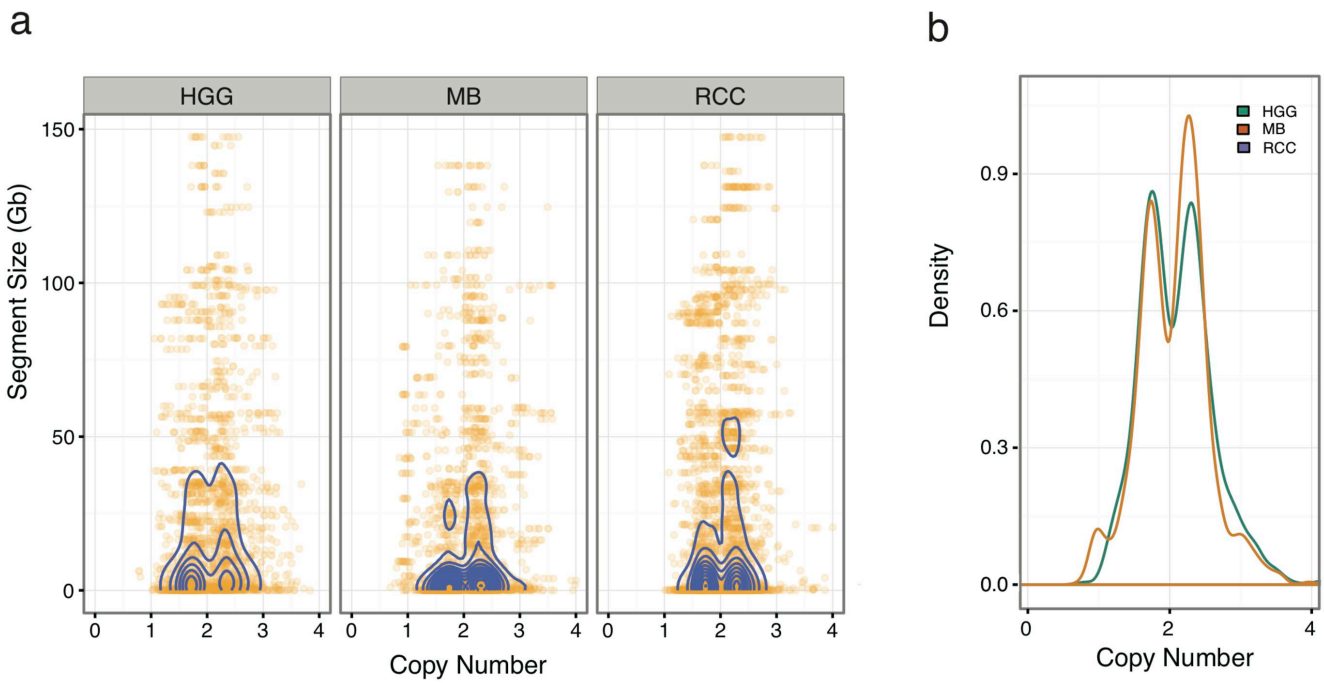

Supplementary Figure 7. Density plots of gain and loss segment sizes (Gb) show a similar distribution across entities, with the majority of events having a size under 50Gb, and approximately equal numbers of gains and losses, with MBs having slightly more gains (blue lines: density contour; orange: data points). **(b)** Gain and loss density profiles in HGGs, MBs, and RCCs show that despite the greater of normal contamination in RCCs vs HGGs and MBs, the TITAN algorithm performs equally well at identifying copy number events, without underestimating the copy number of events in RCCs (i.e. all curves overlap).

Supplementary Figure 8

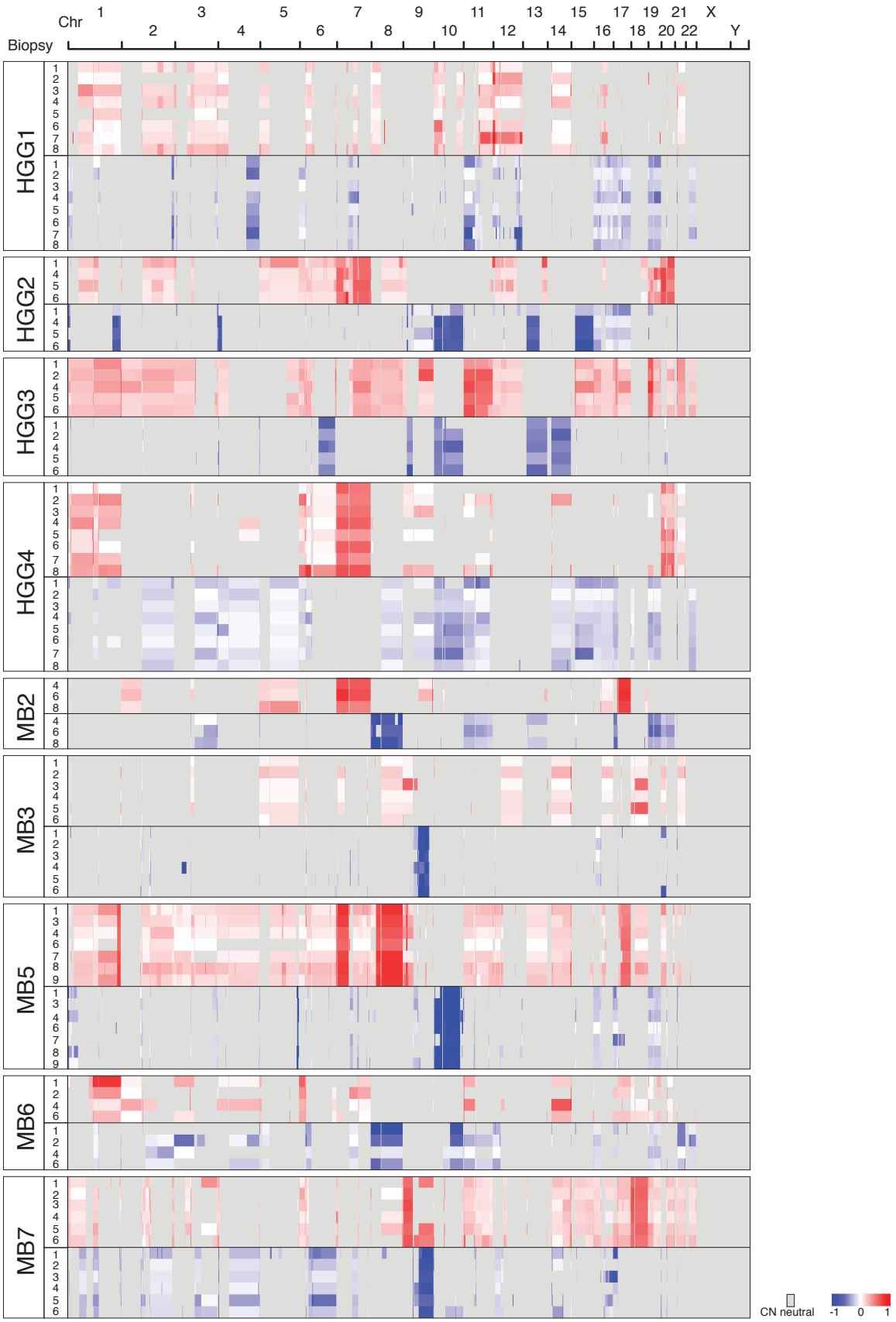

Supplementary Figure 8

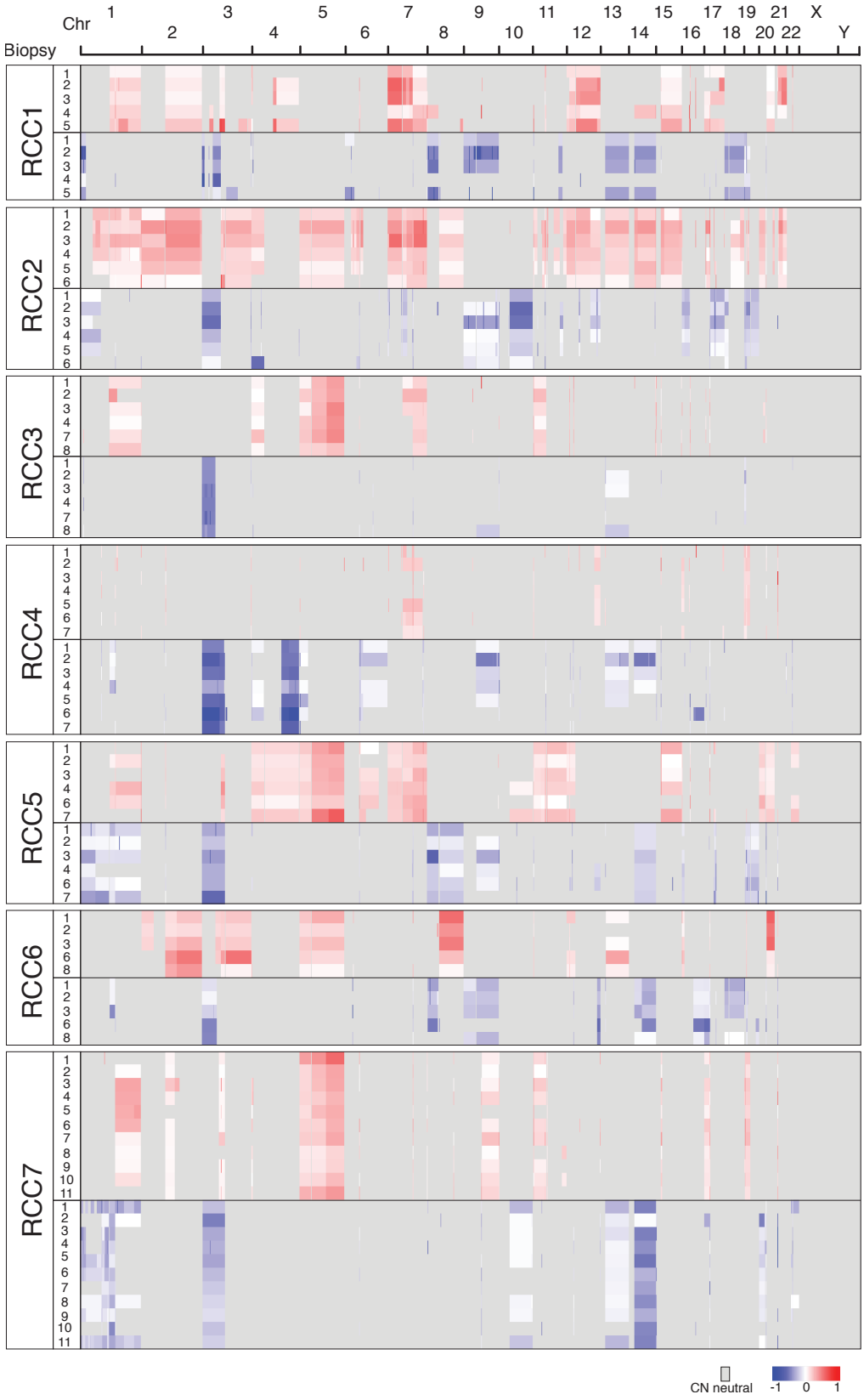

Supplementary Figure 8

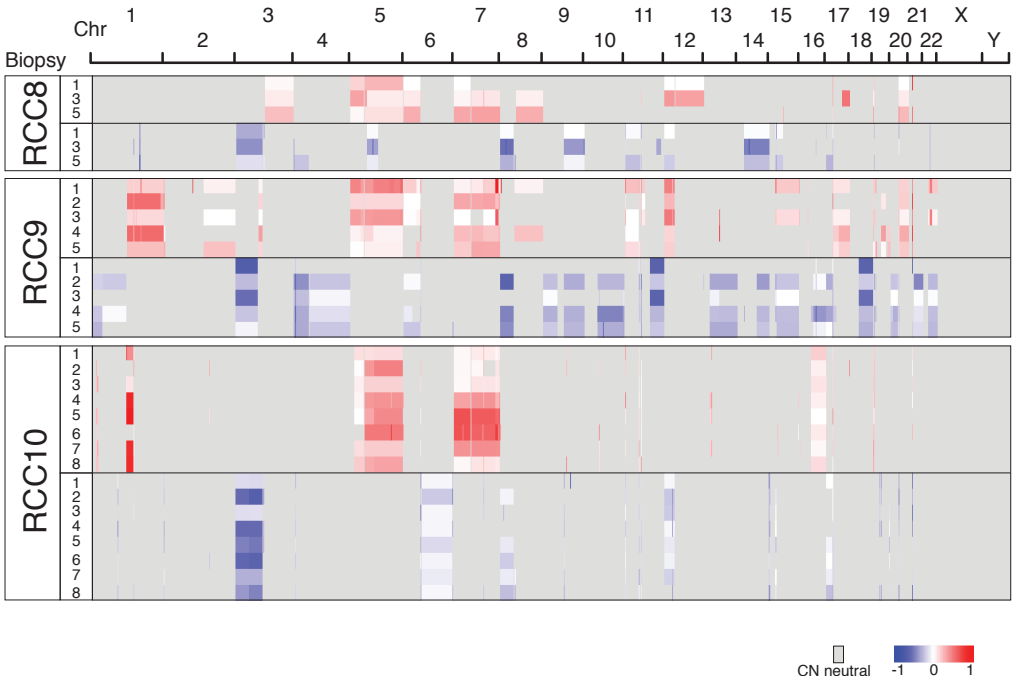

Supplementary Figure 8. Copy number segments of gain (red) or loss (blue) are shown across the genome of individual patients for each biopsy.

Supplementary Figure 9

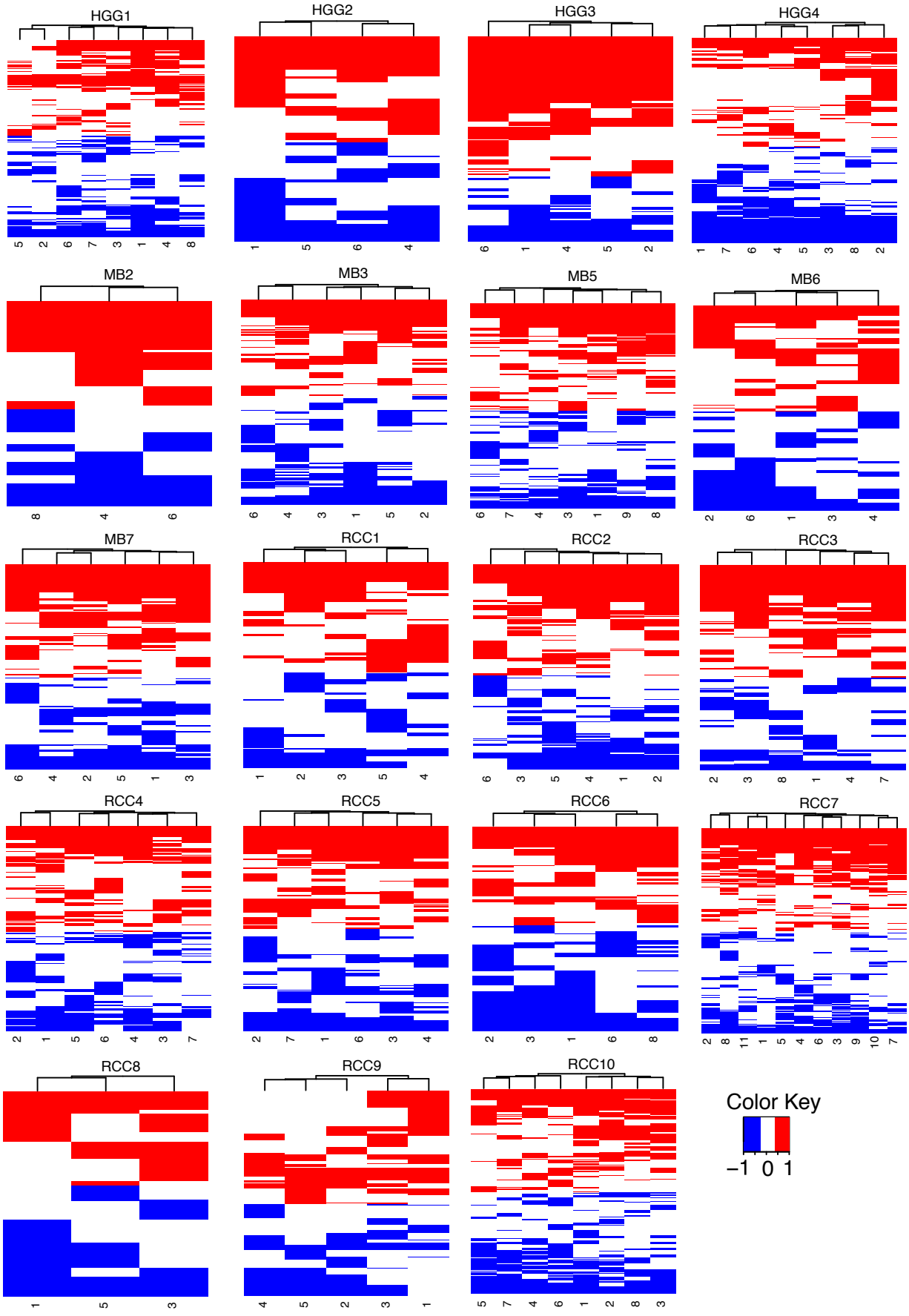

Supplementary Figure 9. CNA-based clustering per patient shows the similarity between biopsies. Unsupervised hierarchical clustering of copy number segments from individual biopsies per patient across all tumors in the cohort with copy number data in at least 3 biopsies. Gains: red; Losses: blue

Supplementary Figure 10

a

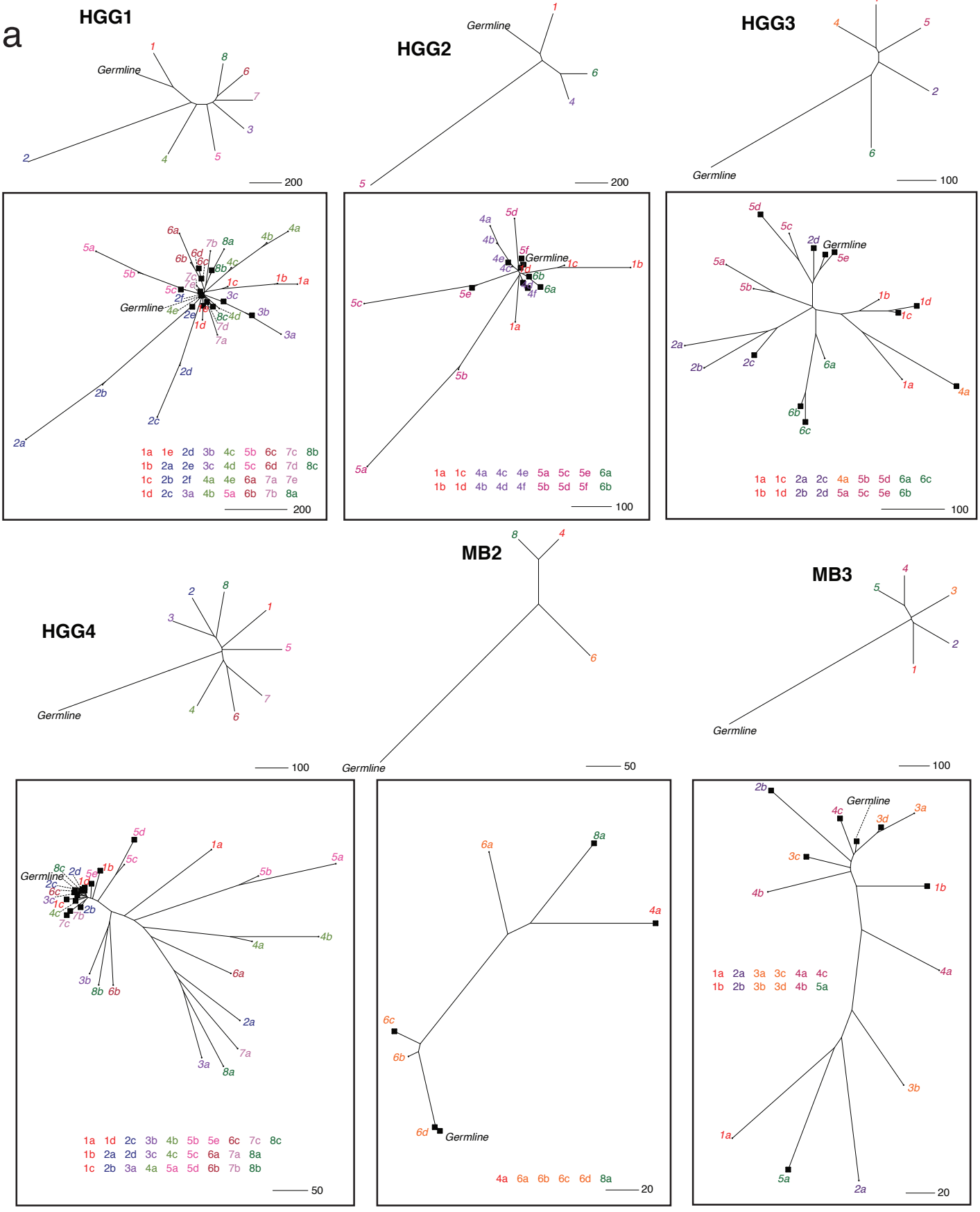

Supplementary Figure 10

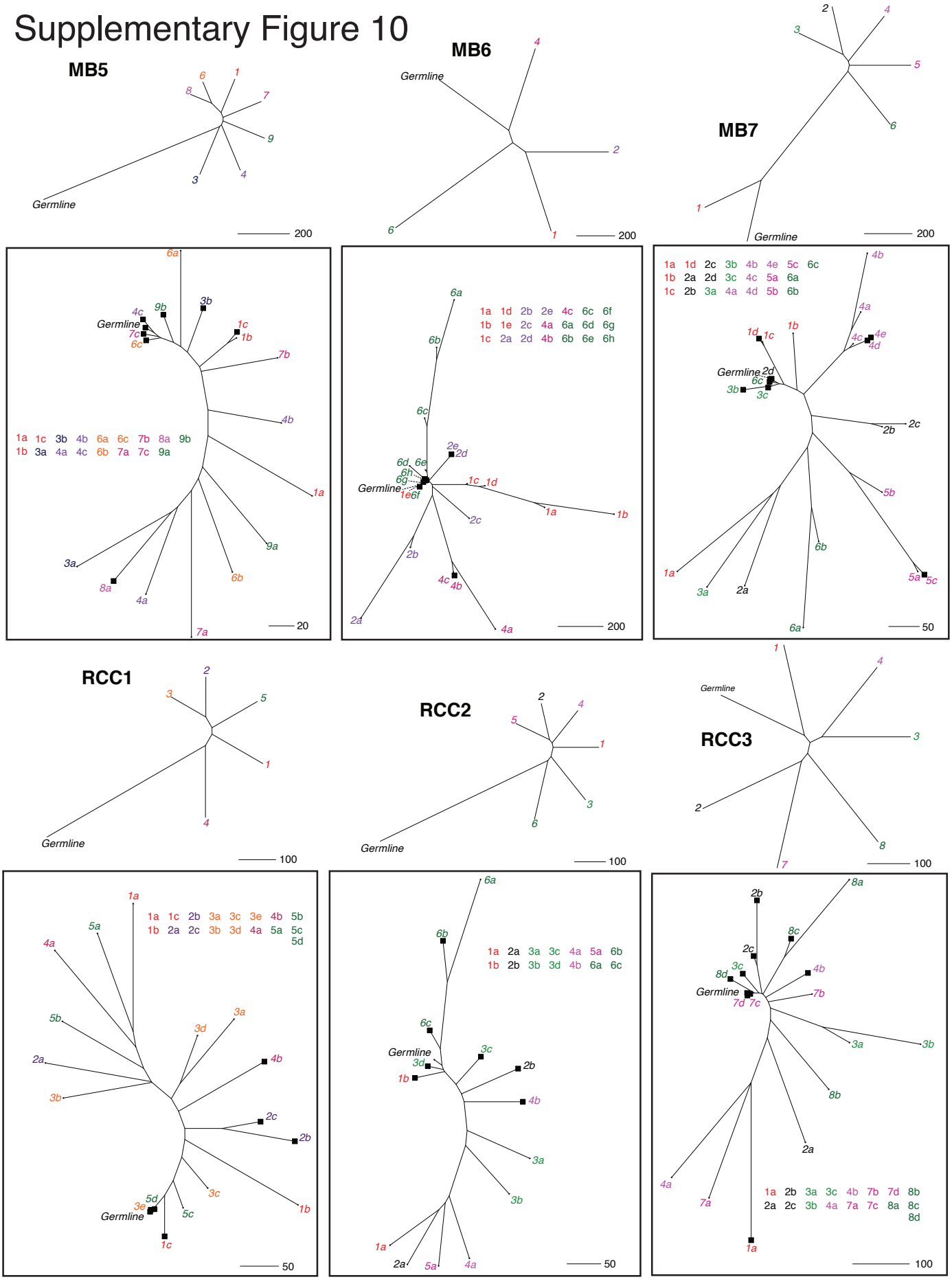

Supplementary Figure 10

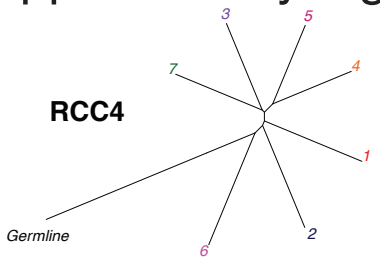

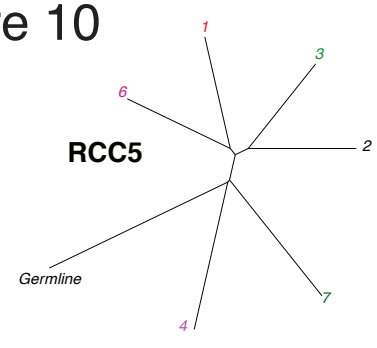

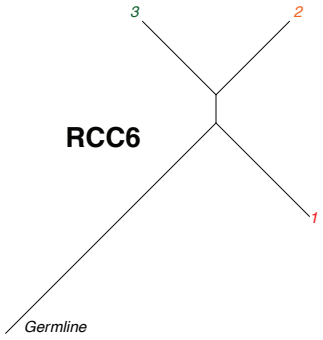

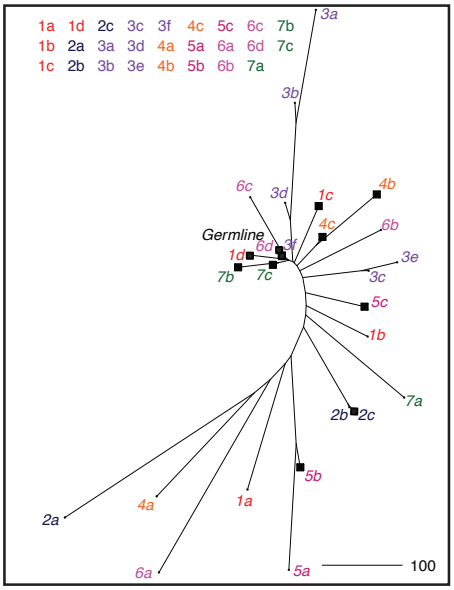

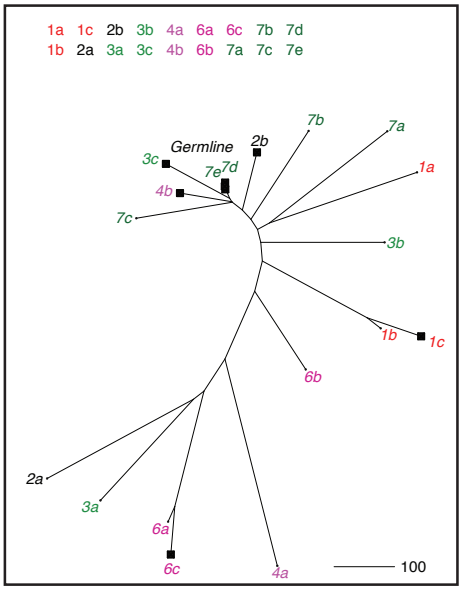

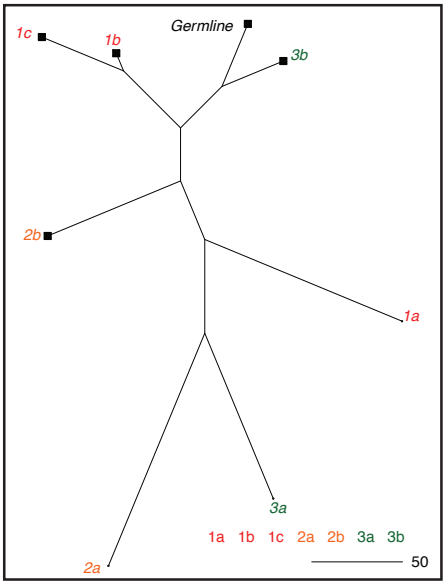

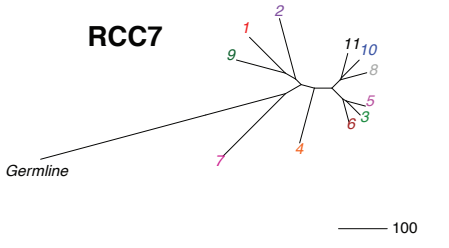

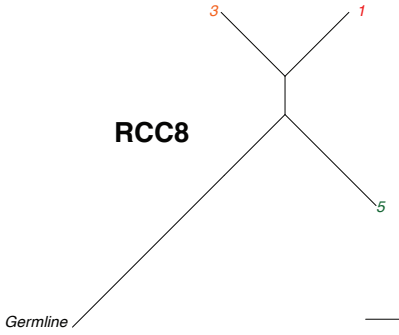

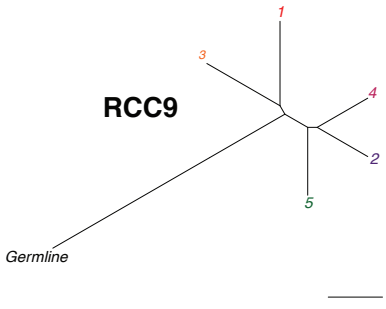

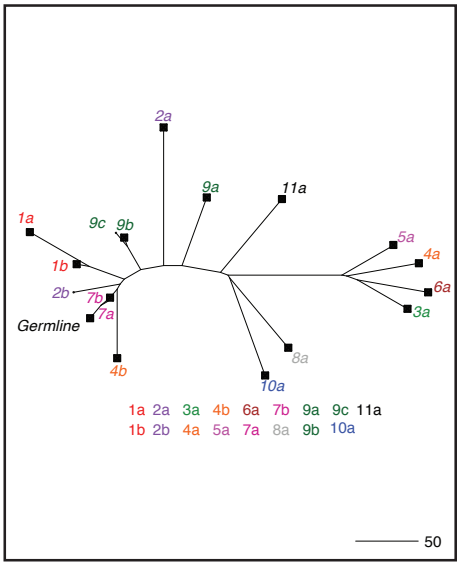

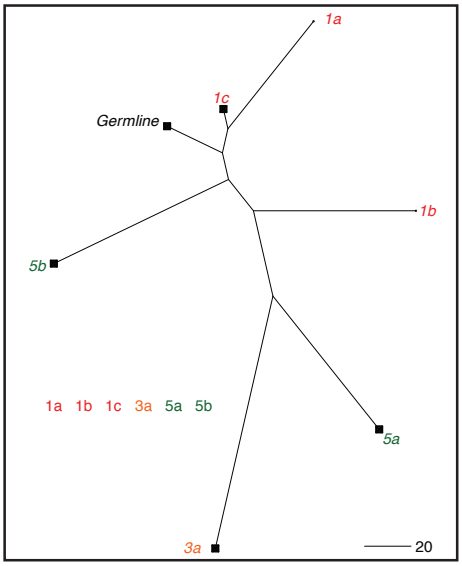

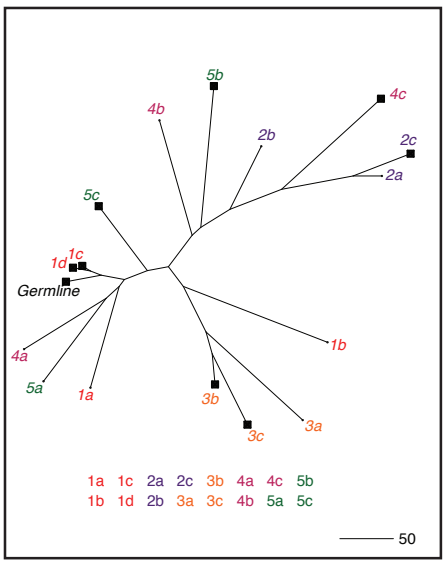

Supplementary Figure 10

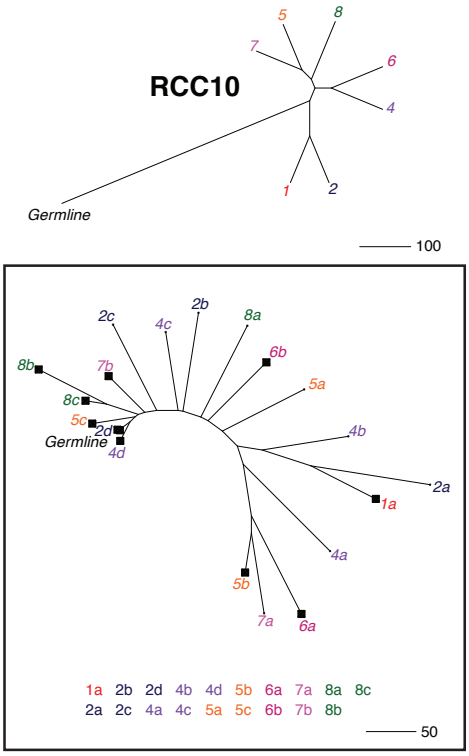

b

HGG2 (CCF)

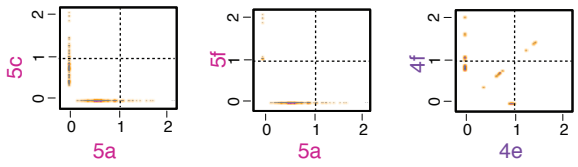

MB7 (CCF)

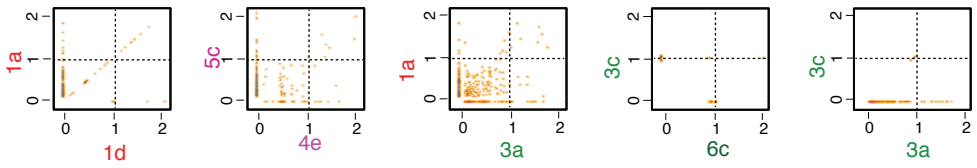

RCC7 (CCF)

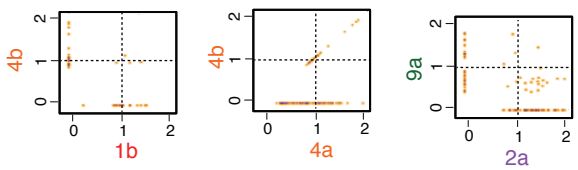

Supplementary Figure 10. (a) Phylogenetic relationships between biopsies. Phylogenetic trees based on SNV and CNA events of each biopsy in MB, HGG, and RCC tumors indicate the degree of genetic divergence from germline. A classic biopsy-level phylogenetic tree is presented for each case, as well as a subpopulation-level phylogeny (boxed). Branch tips are colored according to biopsy number, and labeled according to biopsy number (1,2,3…) and clonal lineage (a,b,c…). Black squares indicate major cellular lineages (>70% of tumor cells in the biopsy; adjusted frequency). All genetically-distinct lineages identified in each tumor are listed next to the corresponding subpopulation-level phylogeny. Those main branches corresponding to a major cellular lineage, and which in addition have a high similarity to minor lineages in other biopsies, cluster together, suggesting a high degree of genetic-lineage intermixing. Some branches (e.g. bottom left in MB6) do not correspond to a majority of cells in any biopsy, potentially indicating the existence of a genetically distinct clone that only has a few cells in a subset of the currently-profiled biopsies. Branch lengths are proportional to the number of SNVs and CNAs (scale at the bottom right of each tree). (b) Cancer cell fraction (CCF) values of mutations are shown for pairs of biopsies or subpopulations, as in main Figure 3d. CCF scatter plots have a smoothed color density; black dots represent individual mutations.

Supplementary Figure 11

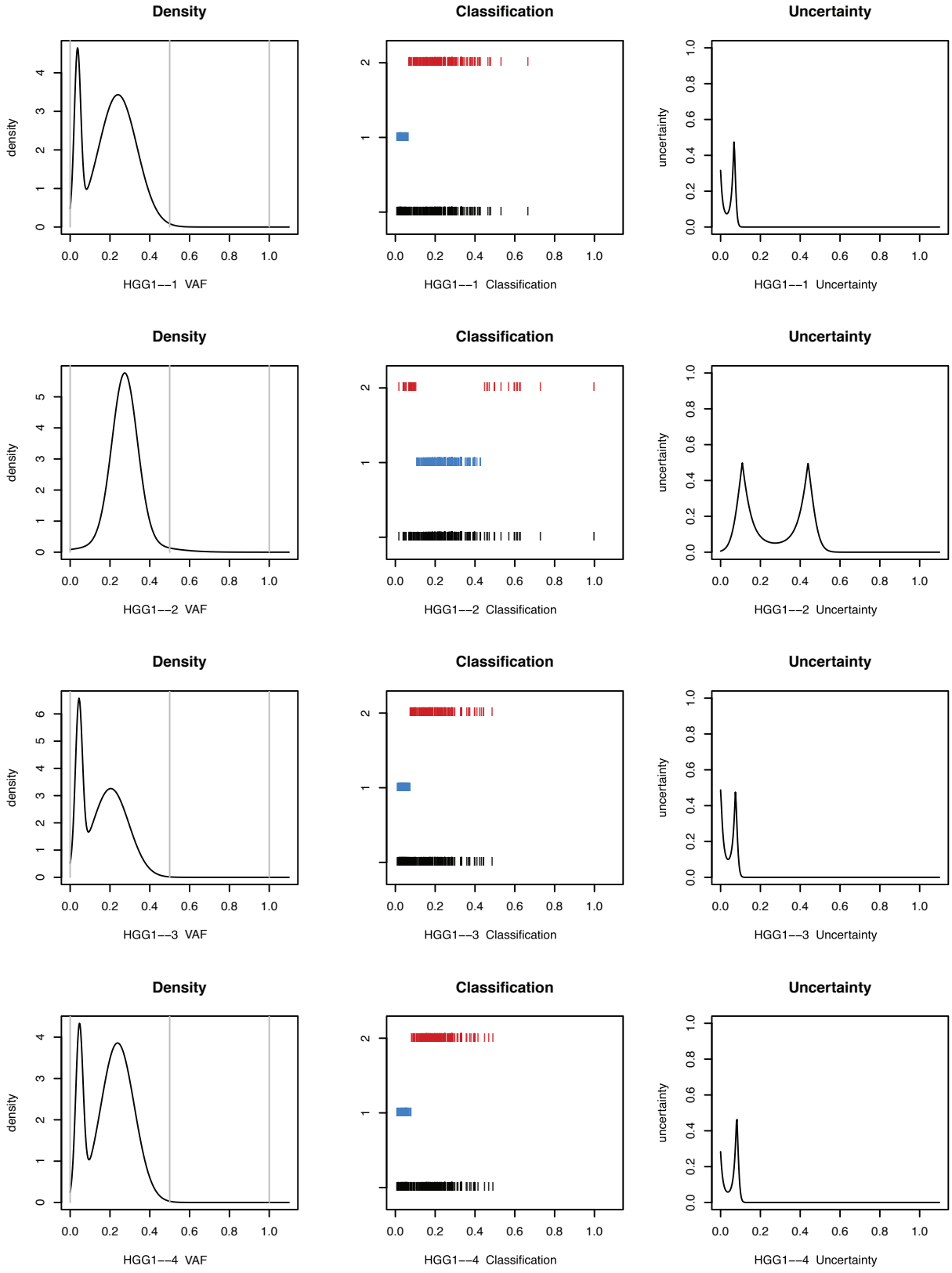

Supplementary Figure 11

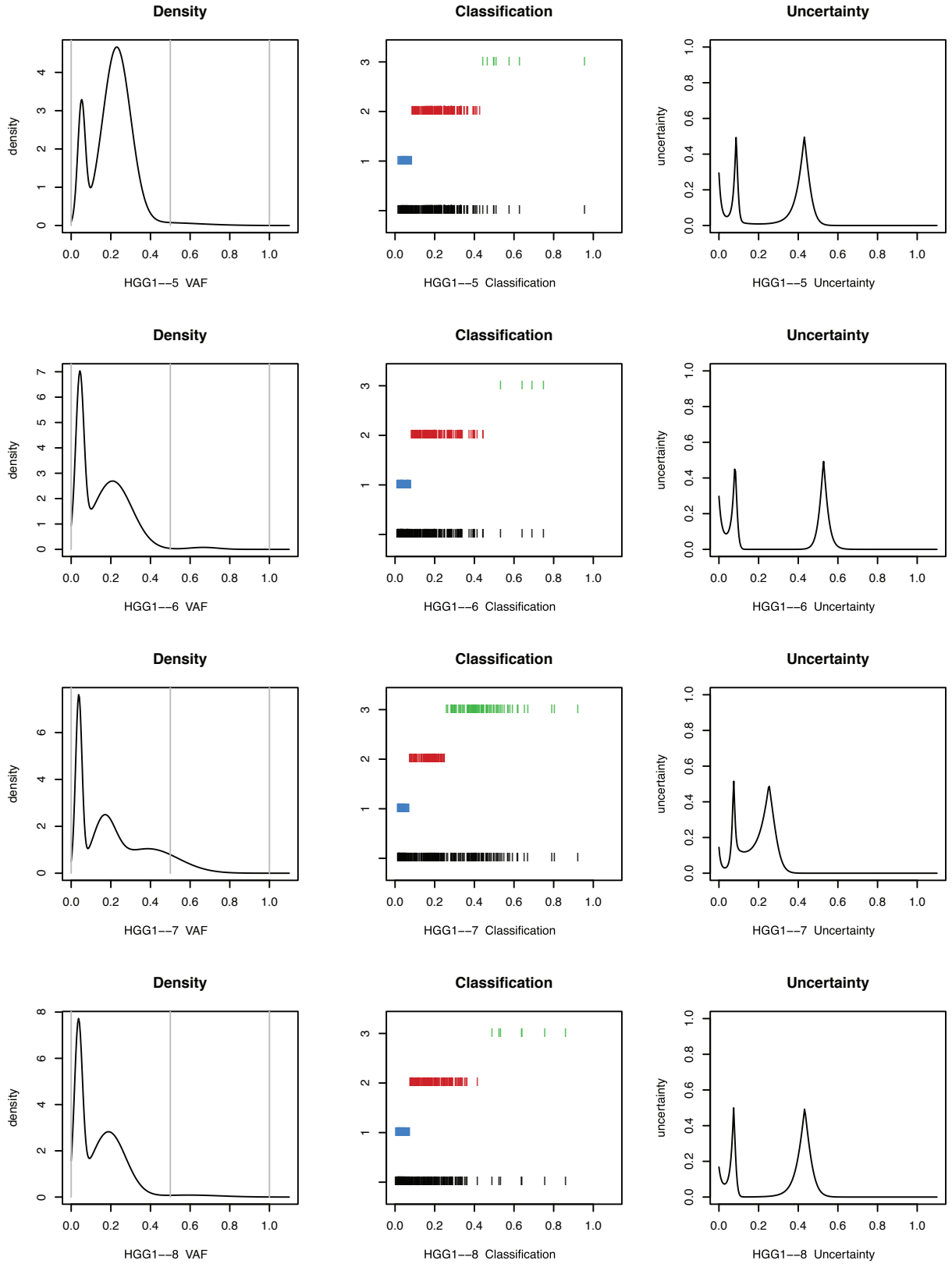

Supplementary Figure 11

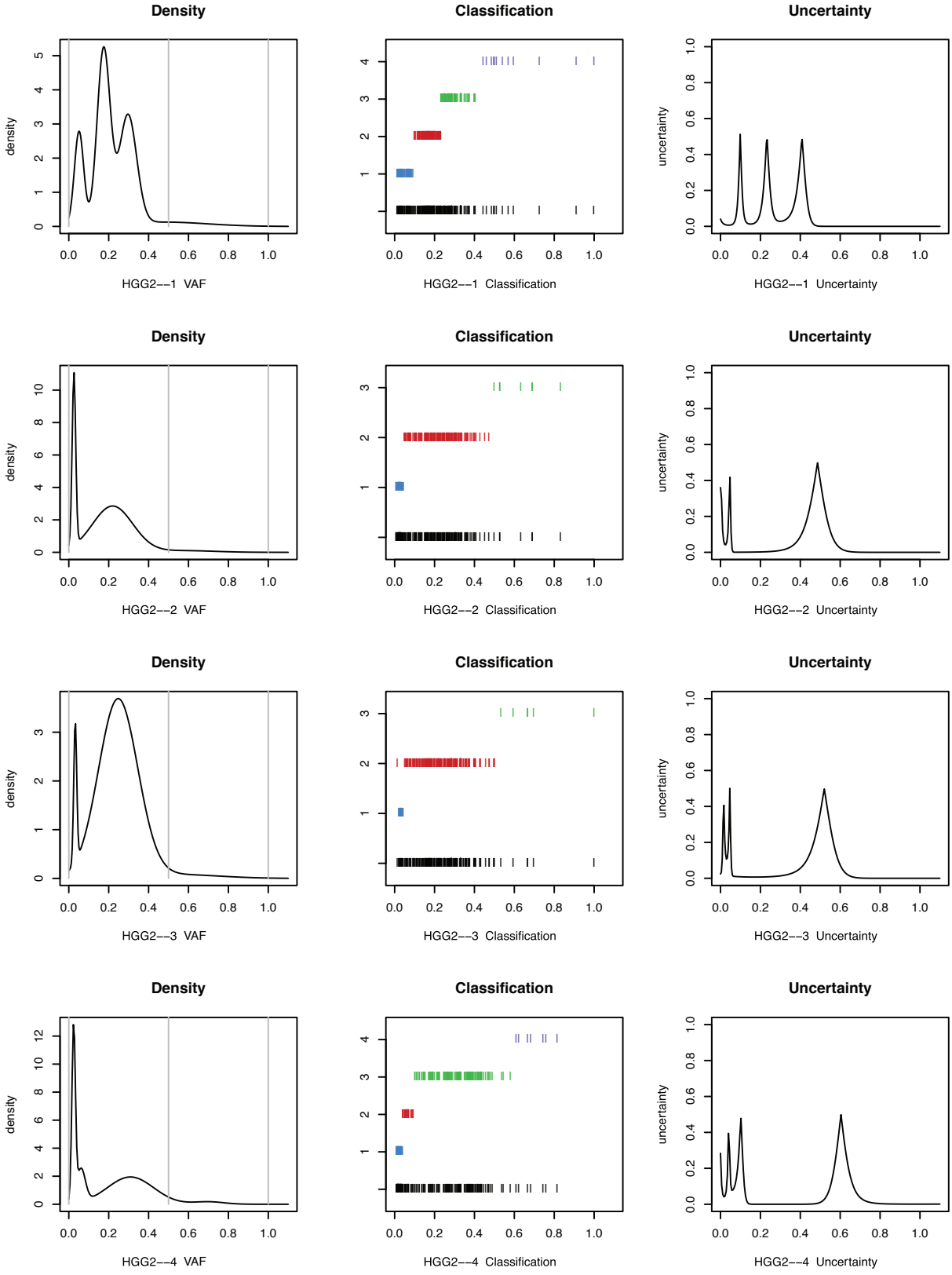

Supplementary Figure 11

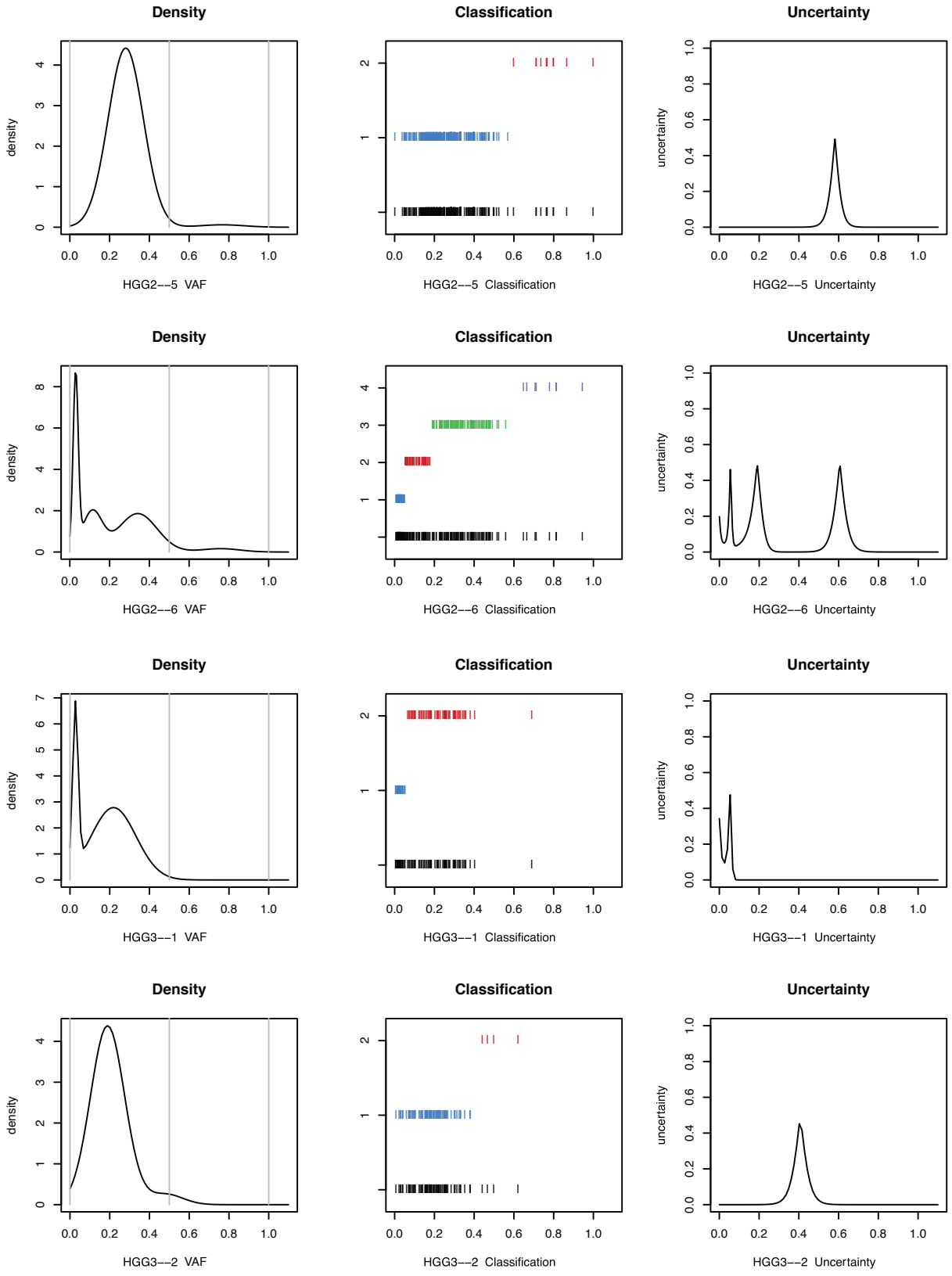

Supplementary Figure 11

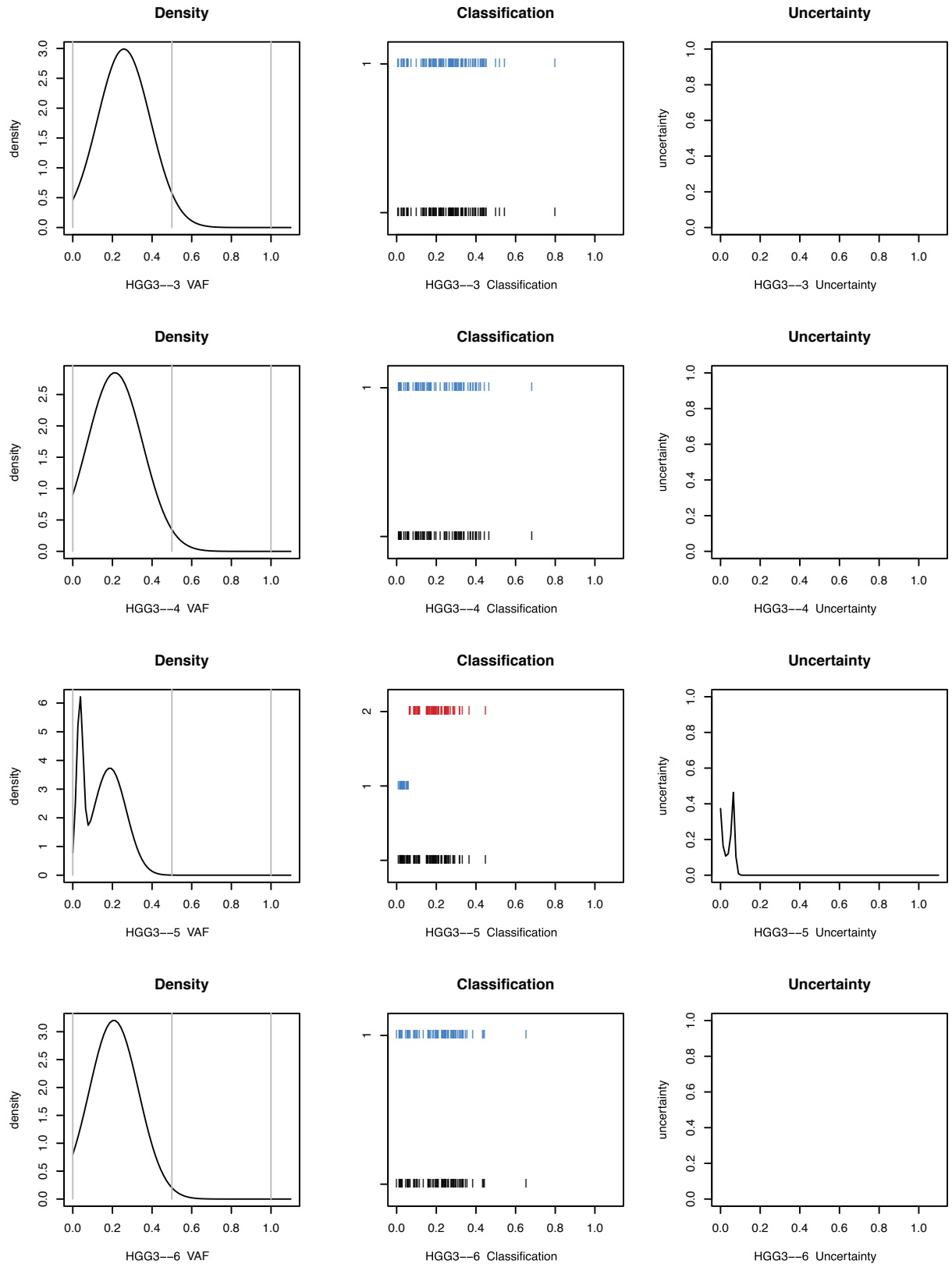

Supplementary Figure 11

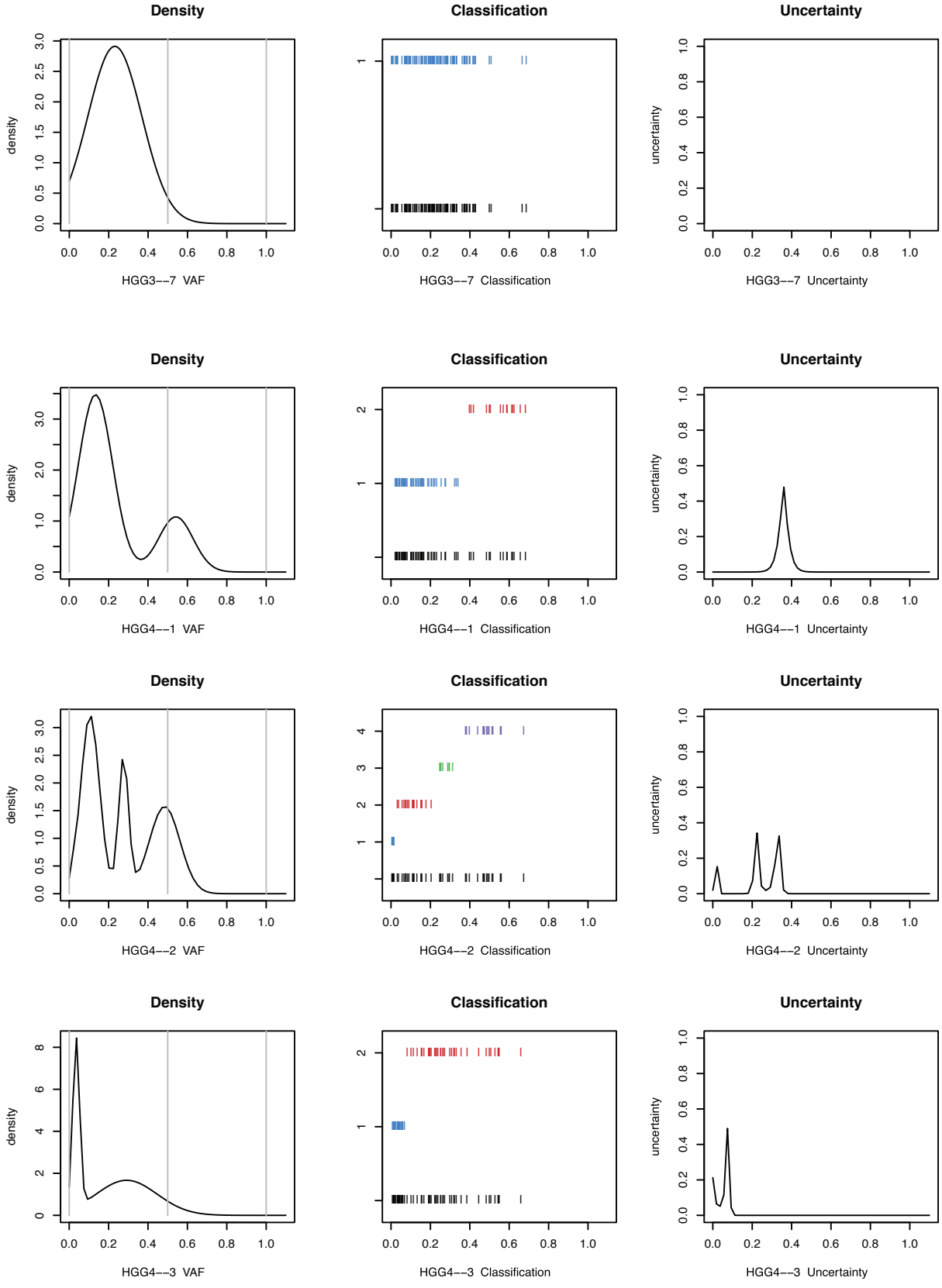

Supplementary Figure 11

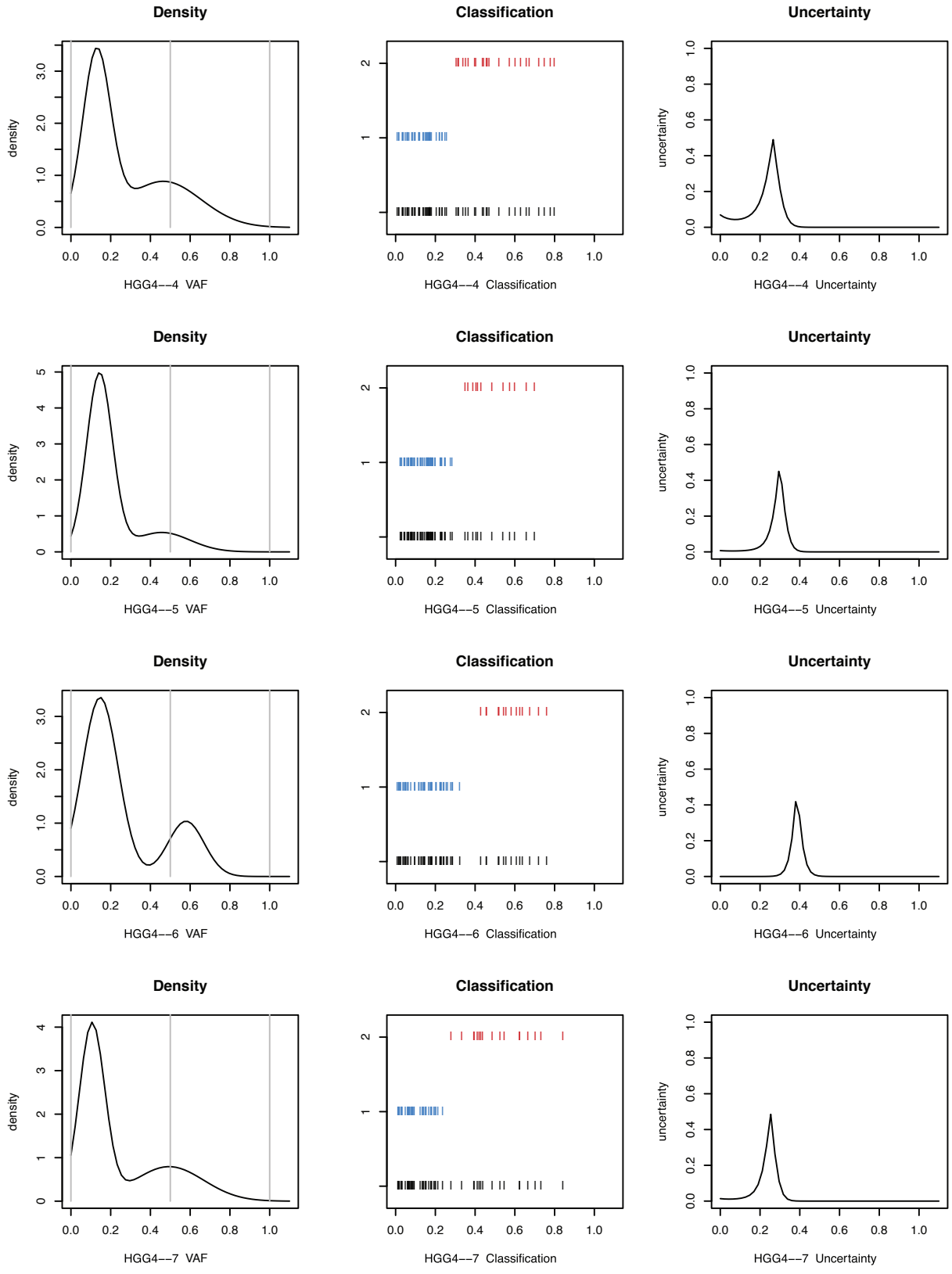

Supplementary Figure 11

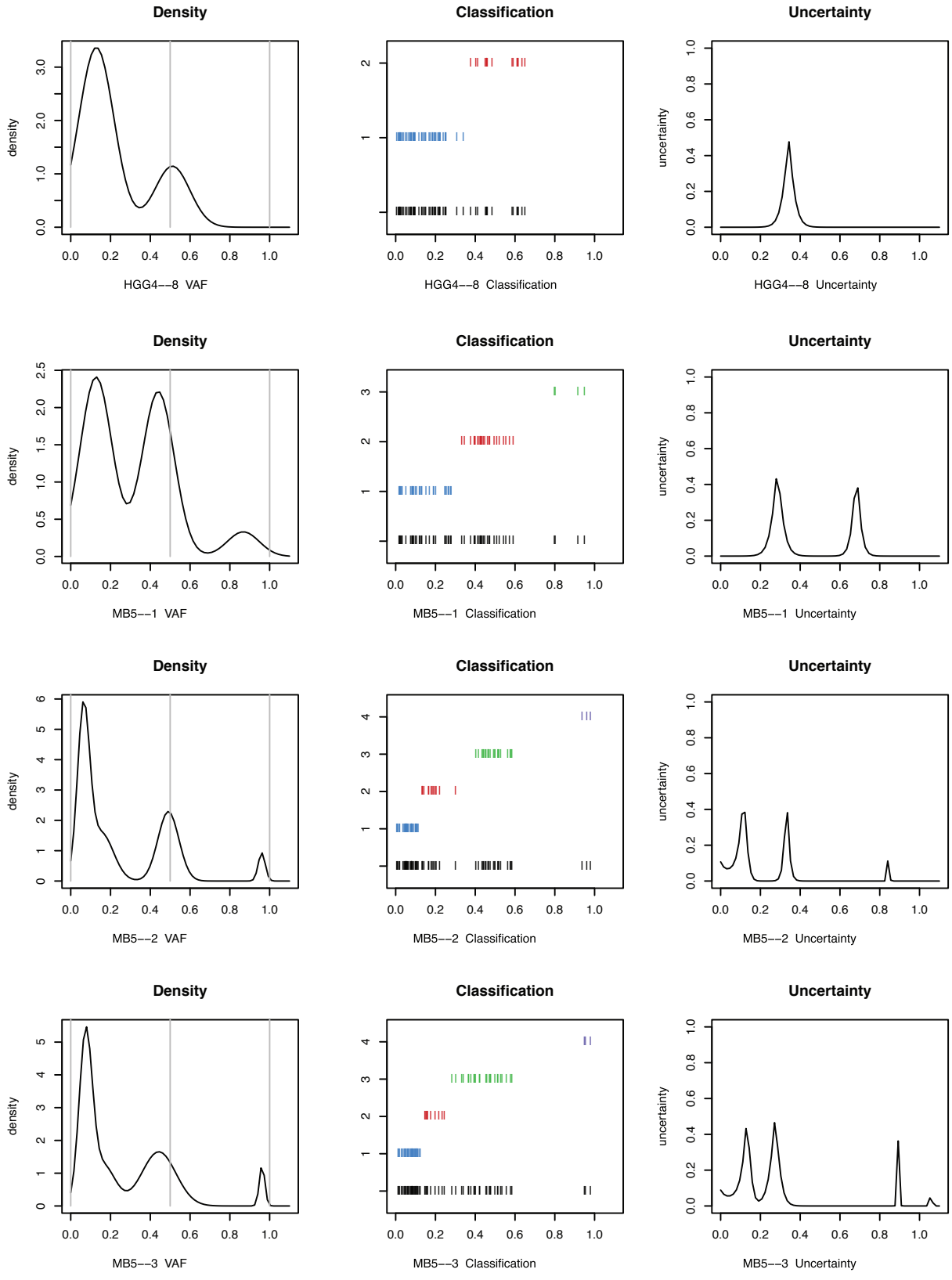

Supplementary Figure 11

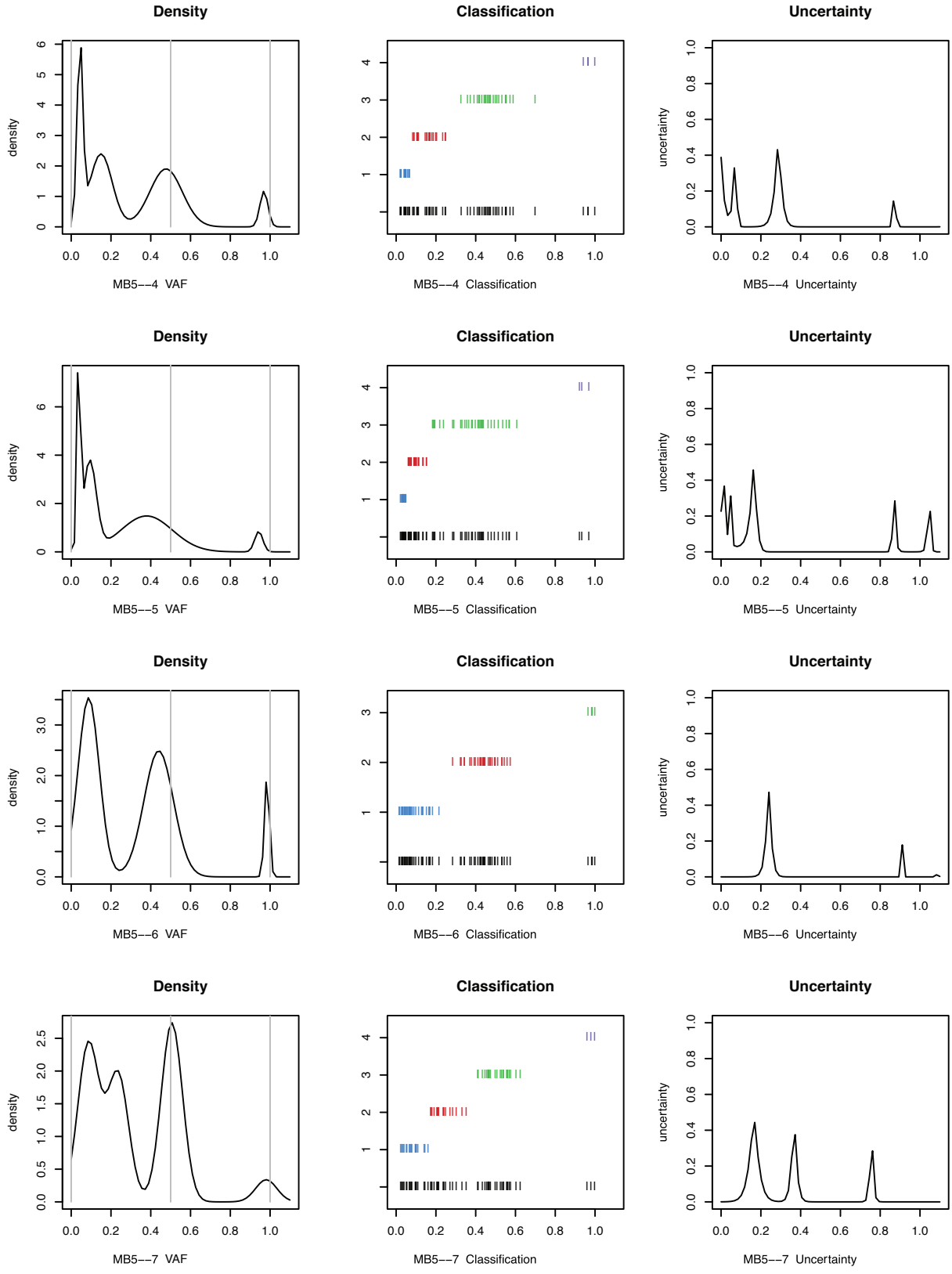

Supplementary Figure 11

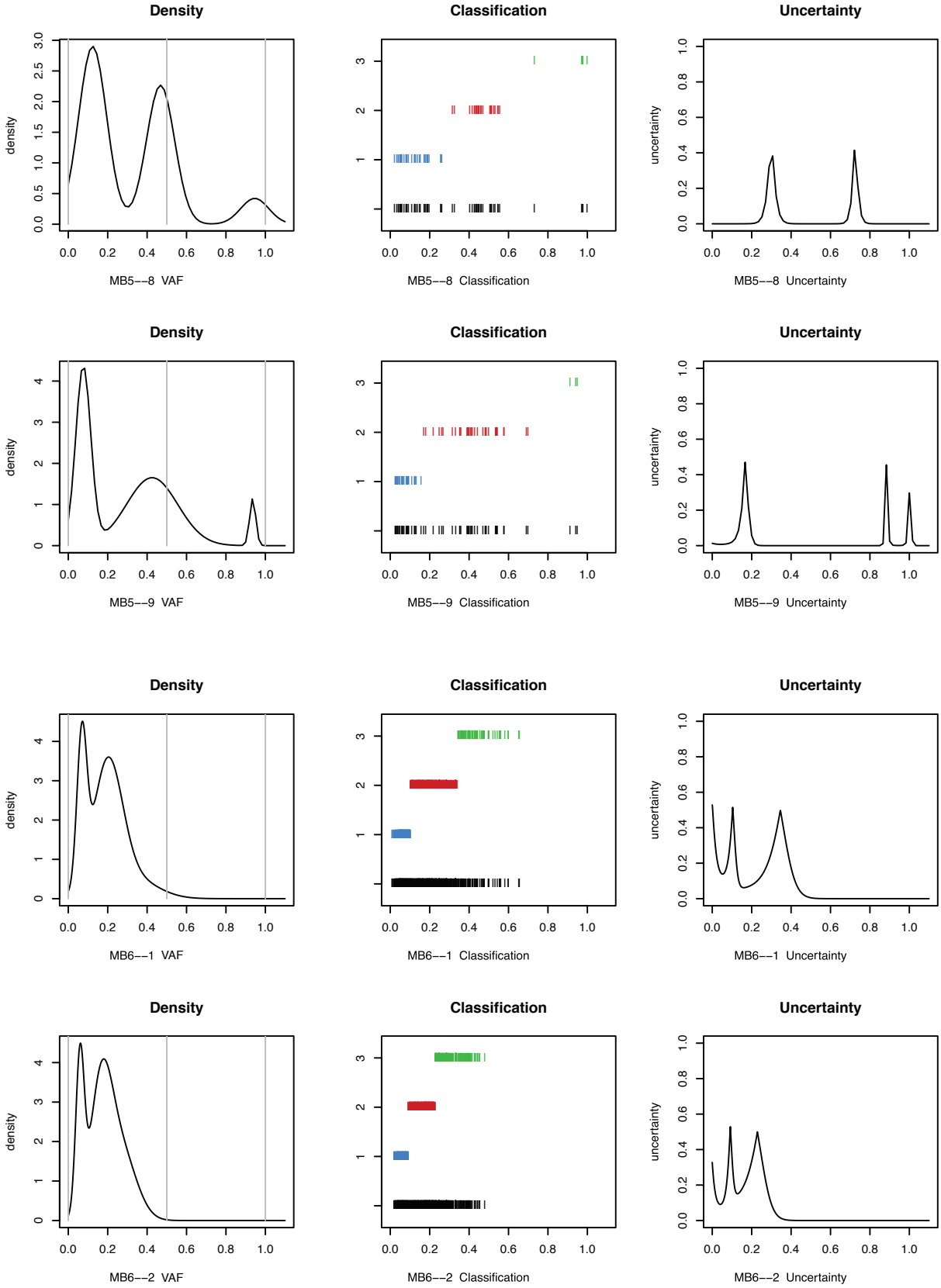

Supplementary Figure 11

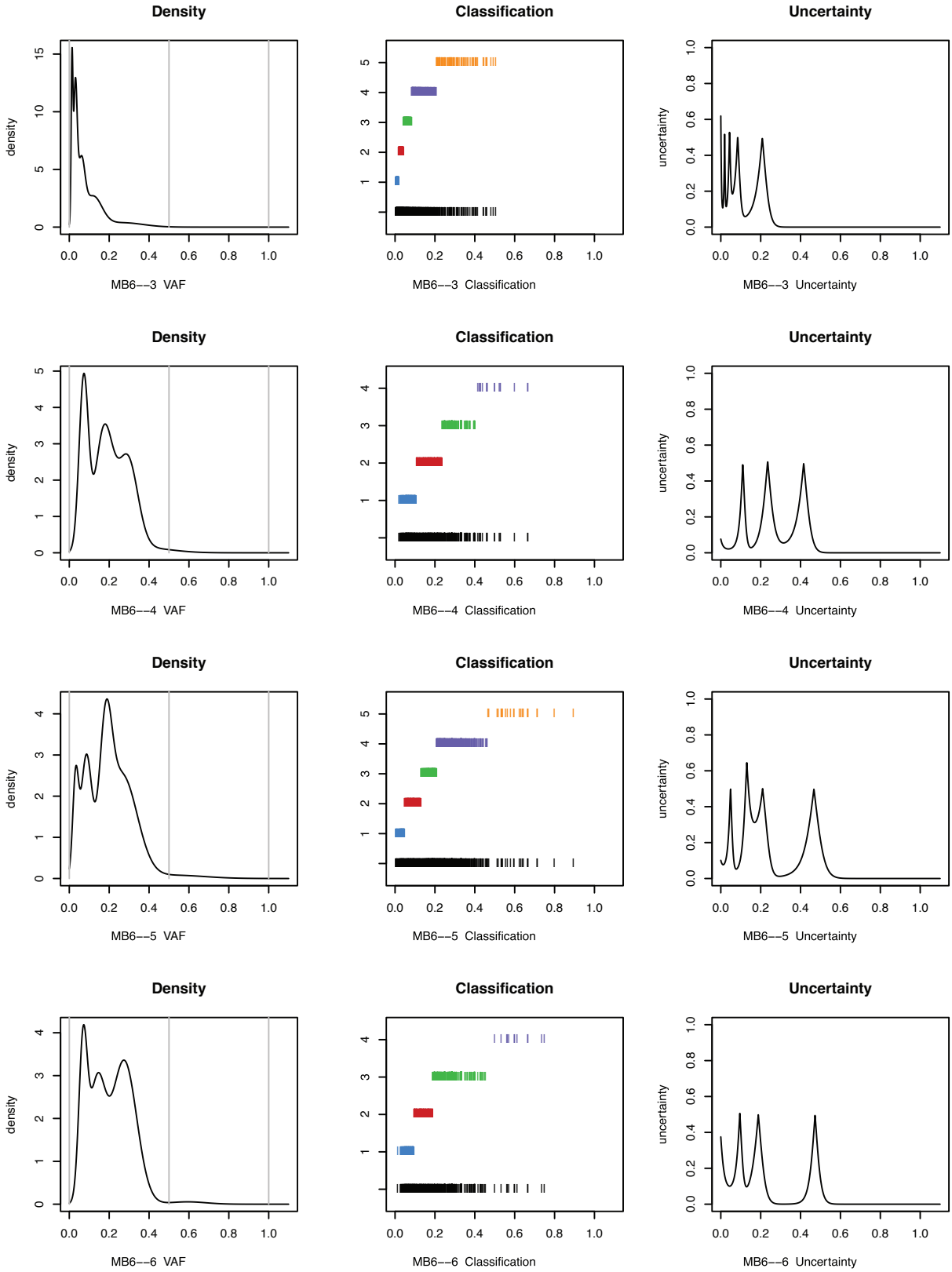

Supplementary Figure 11

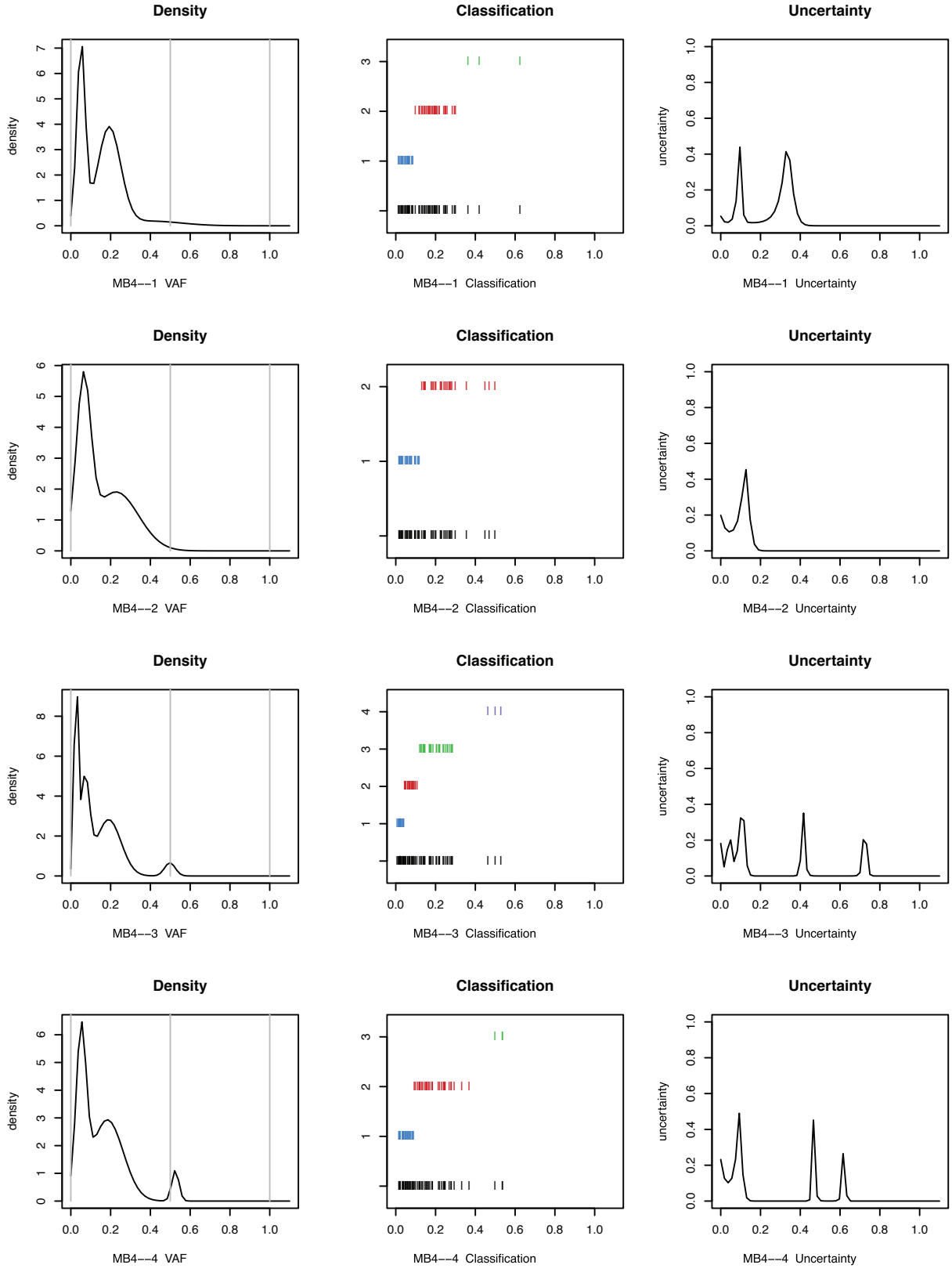

Supplementary Figure 11

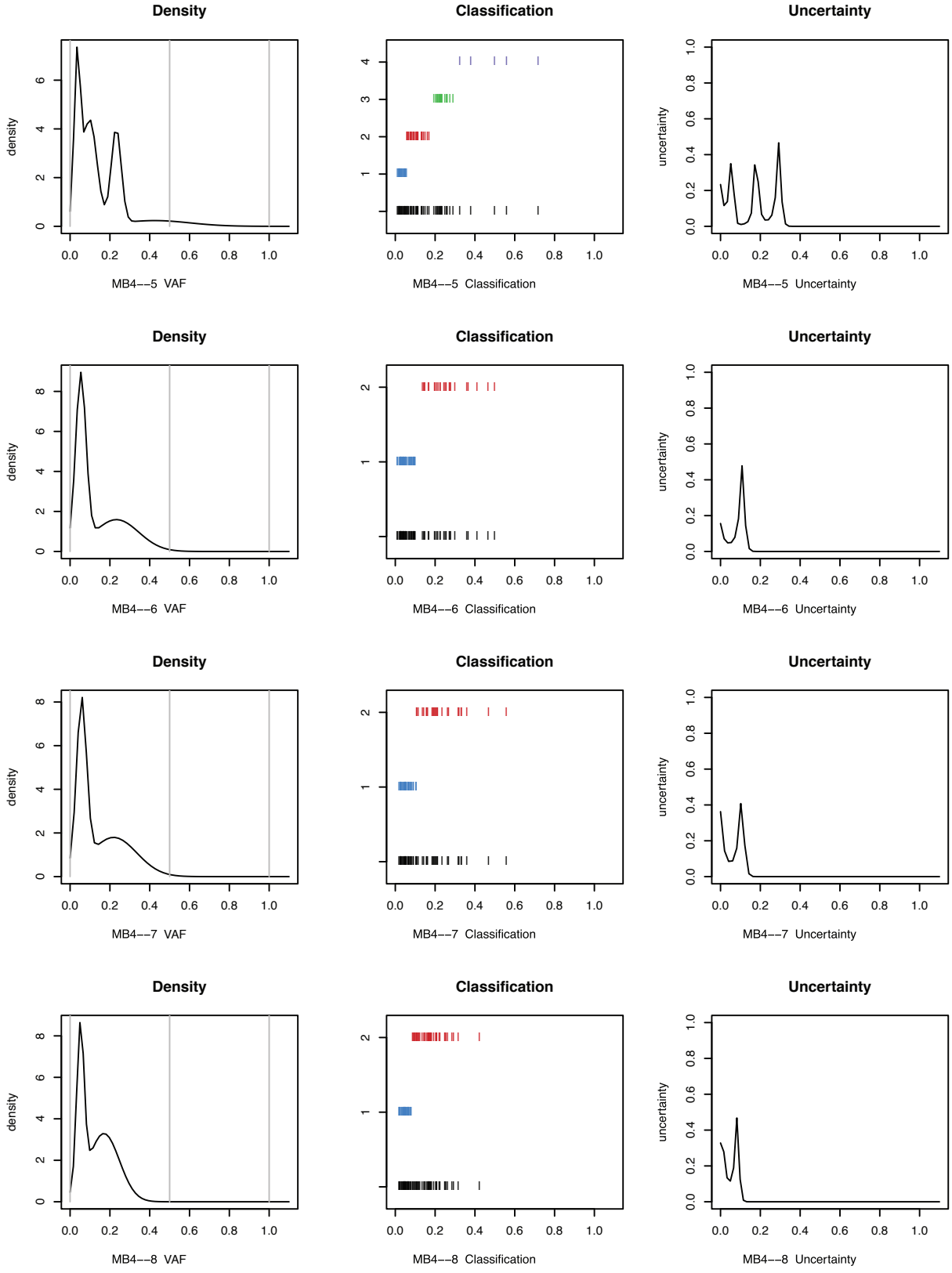

Supplementary Figure 11

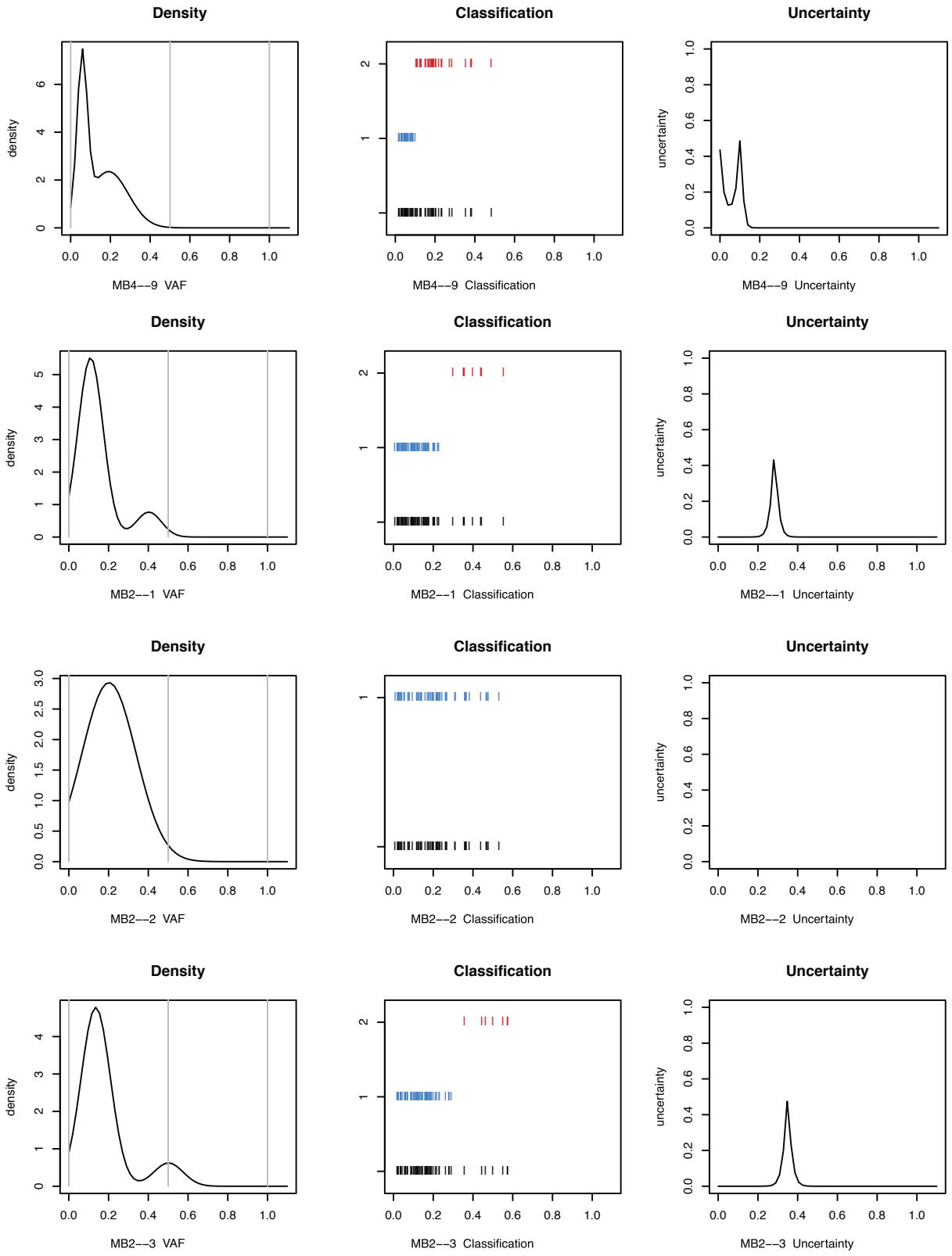

Supplementary Figure 11

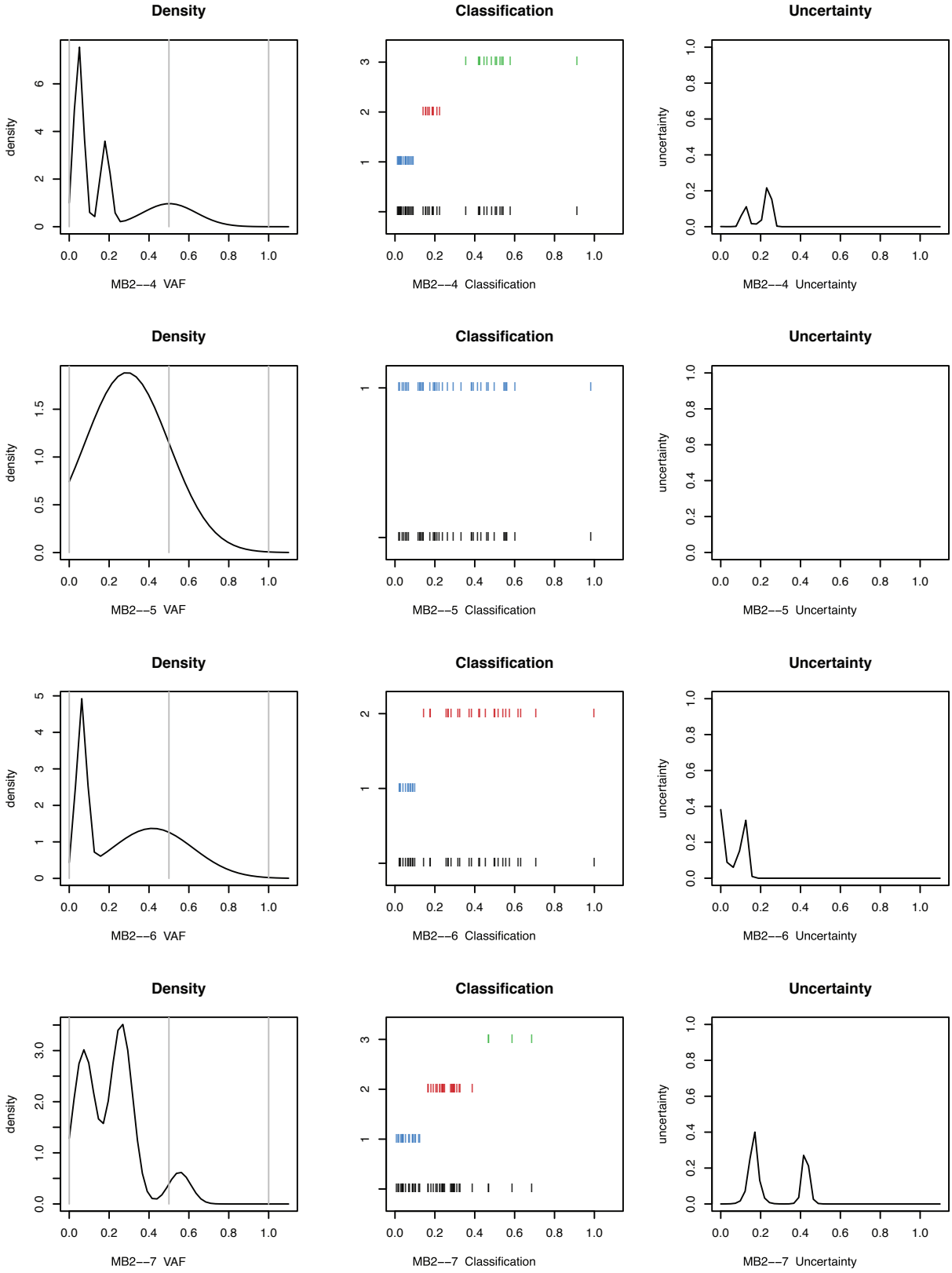

Supplementary Figure 11

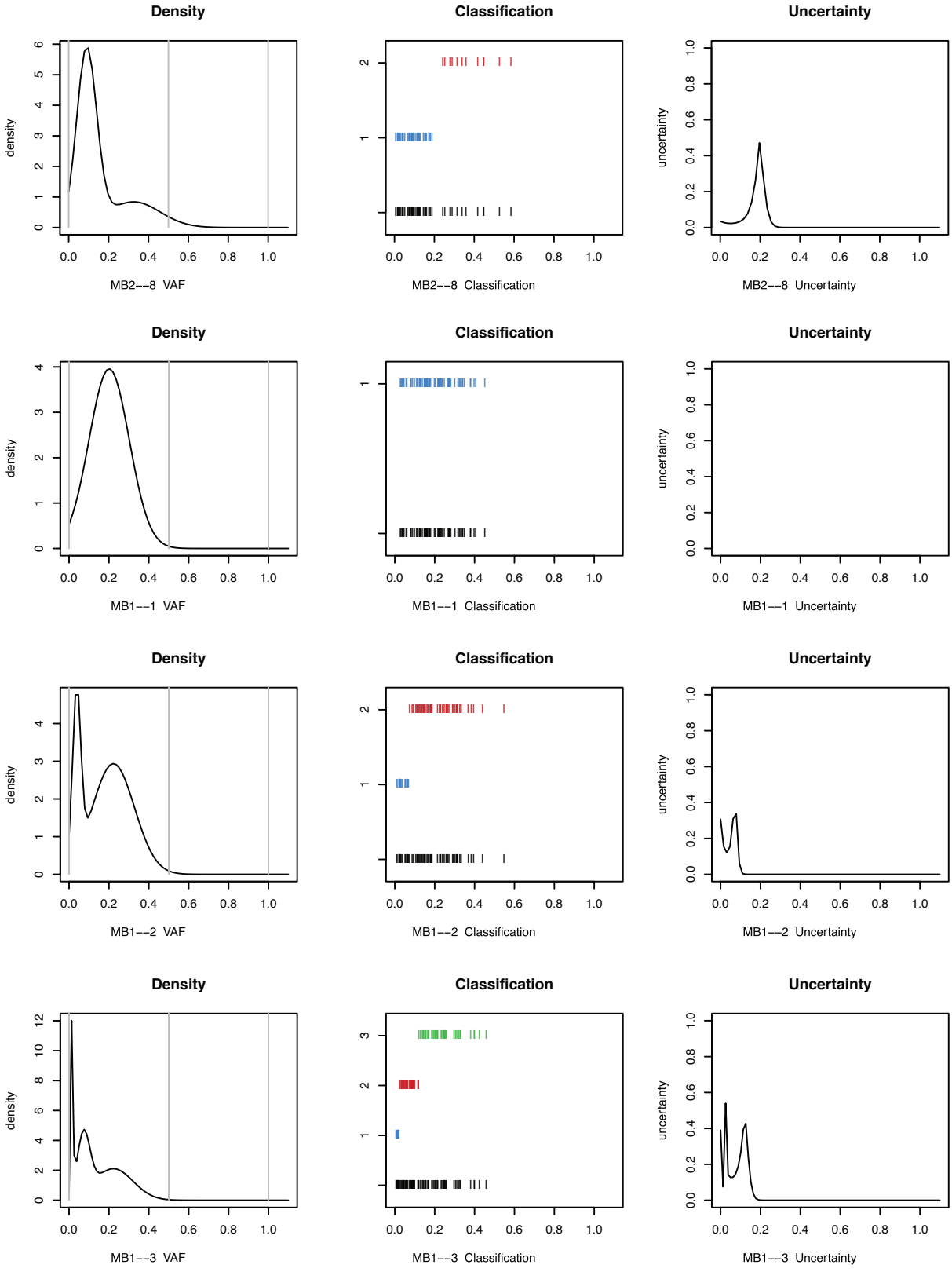

Supplementary Figure 11

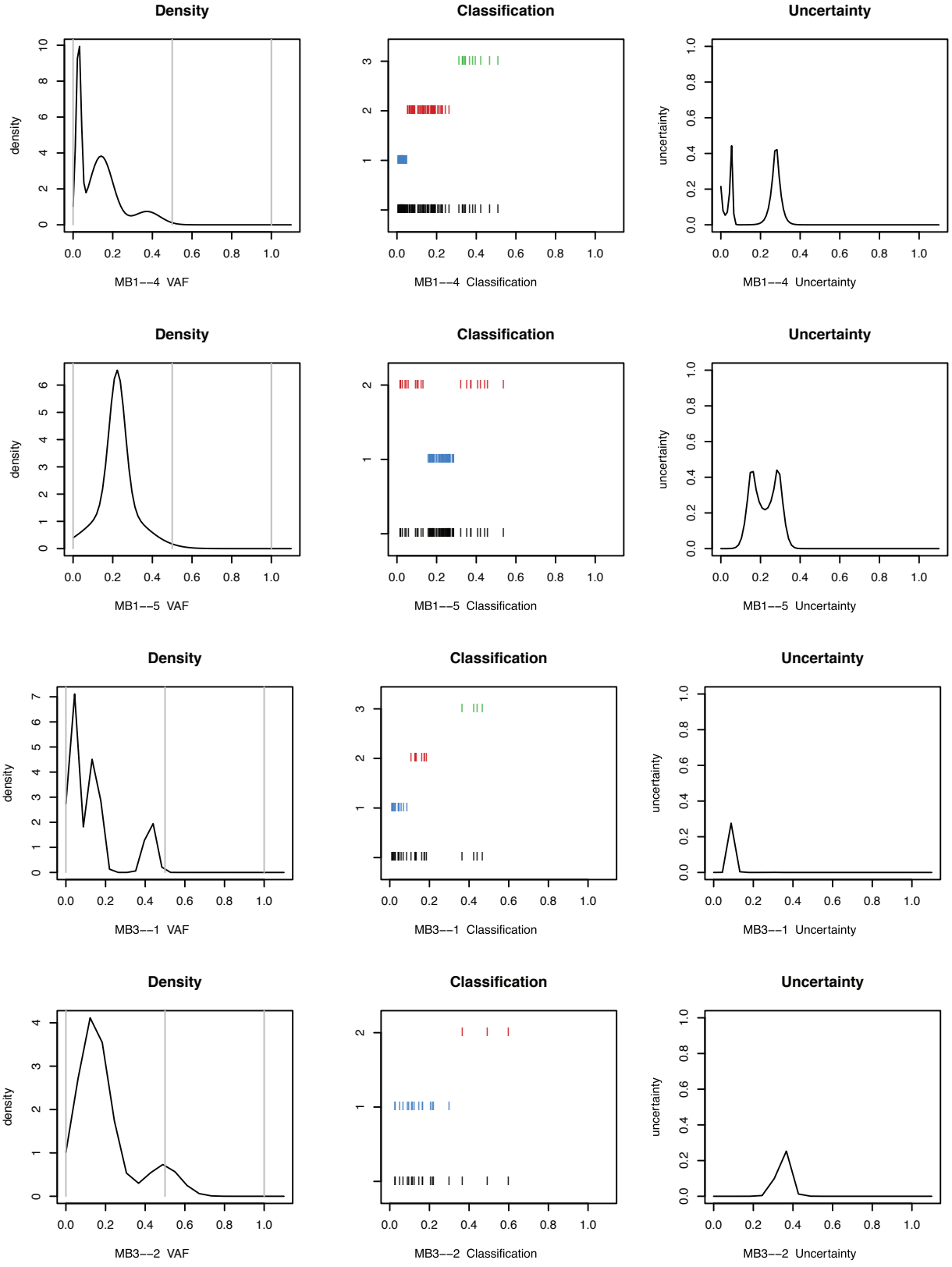

Supplementary Figure 11

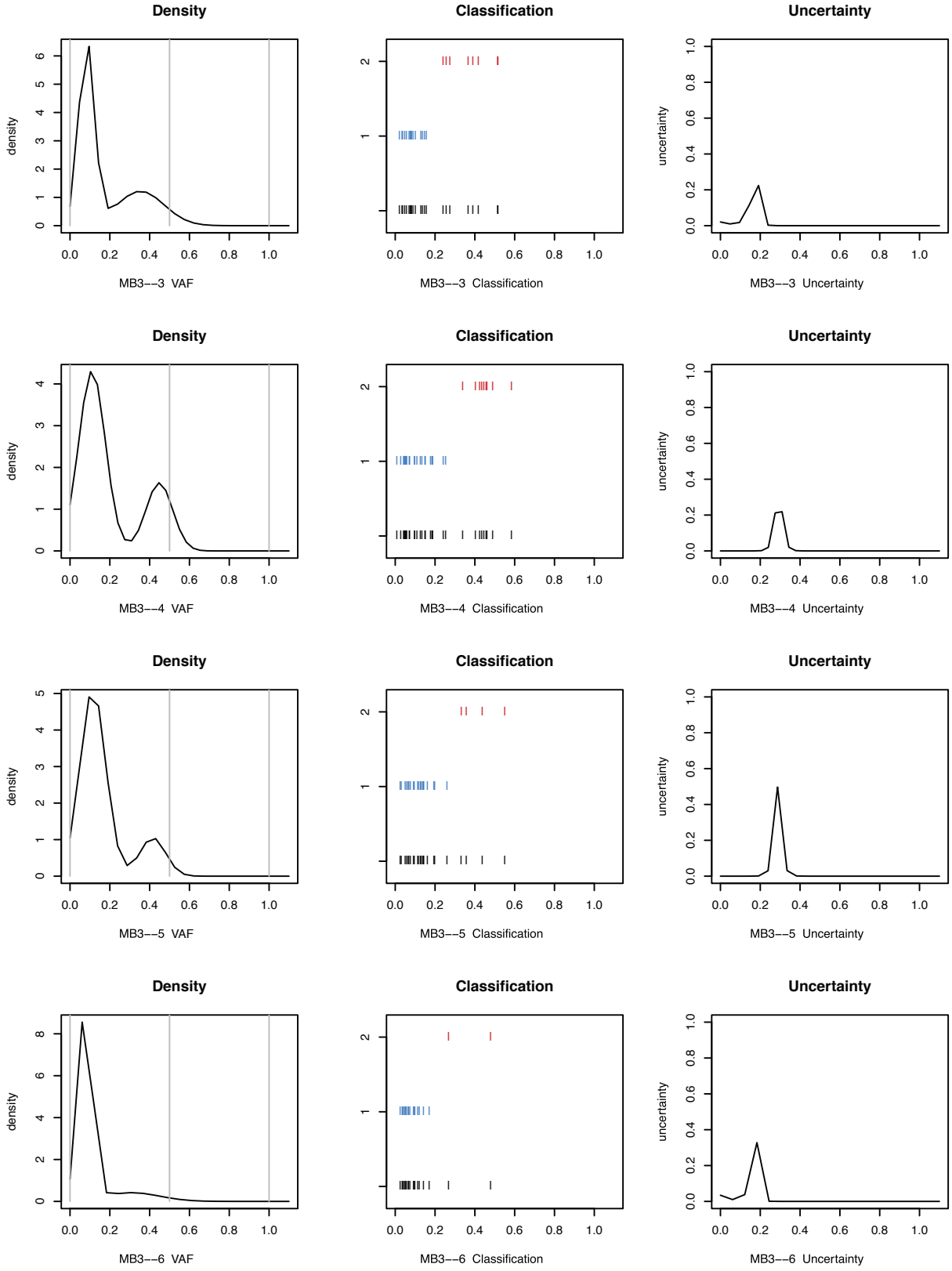

Supplementary Figure 11

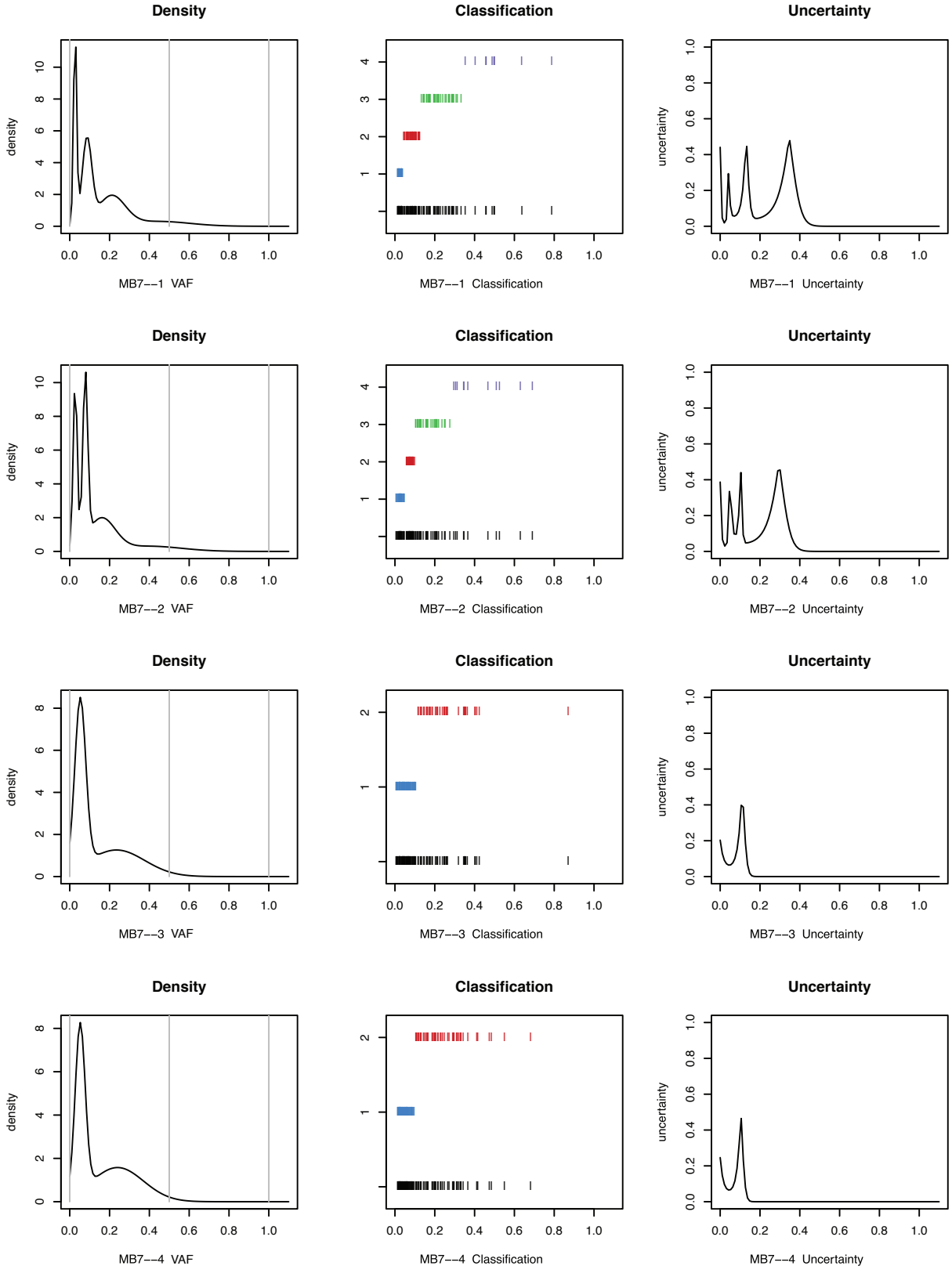

Supplementary Figure 11

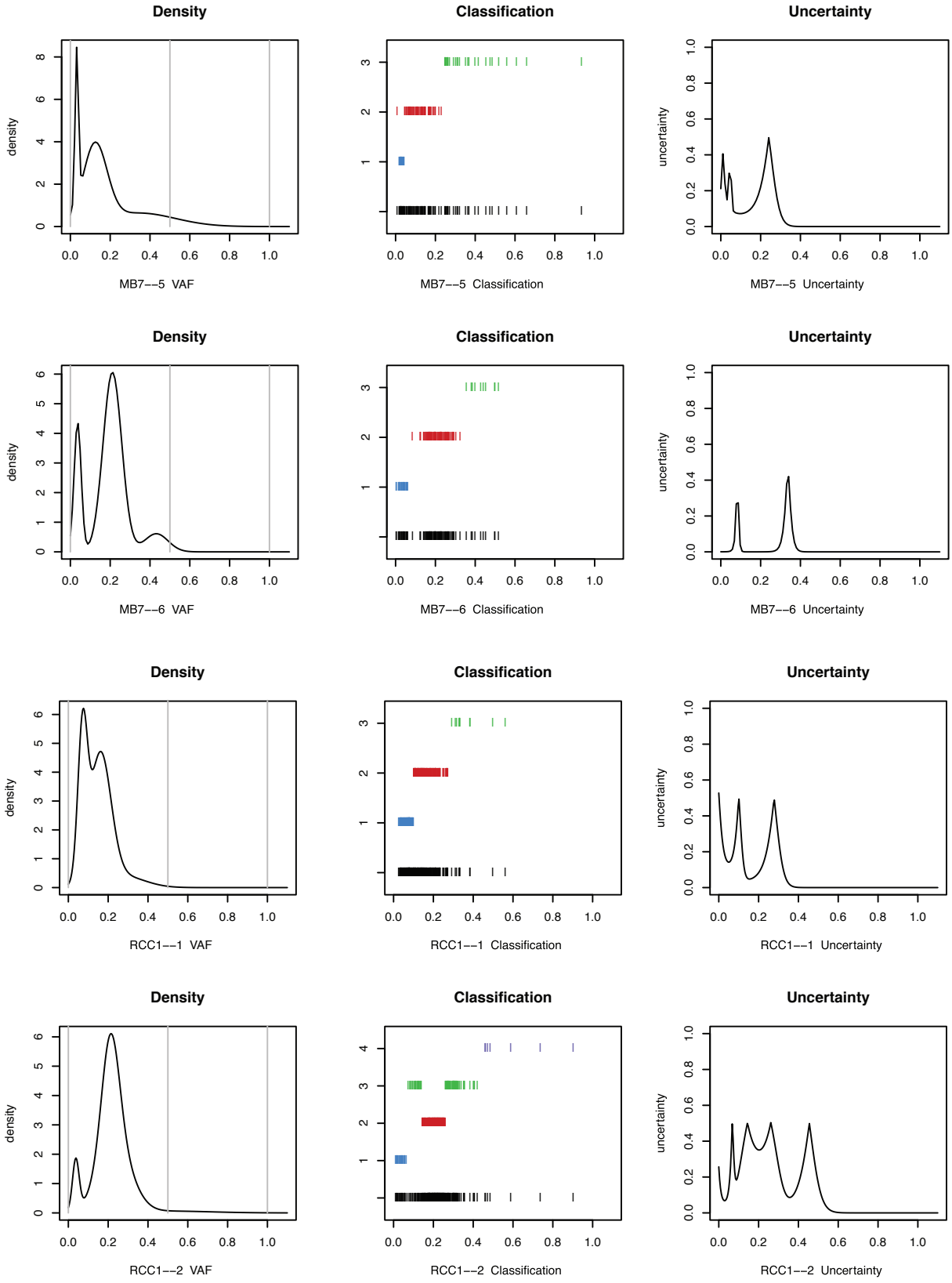

Supplementary Figure 11

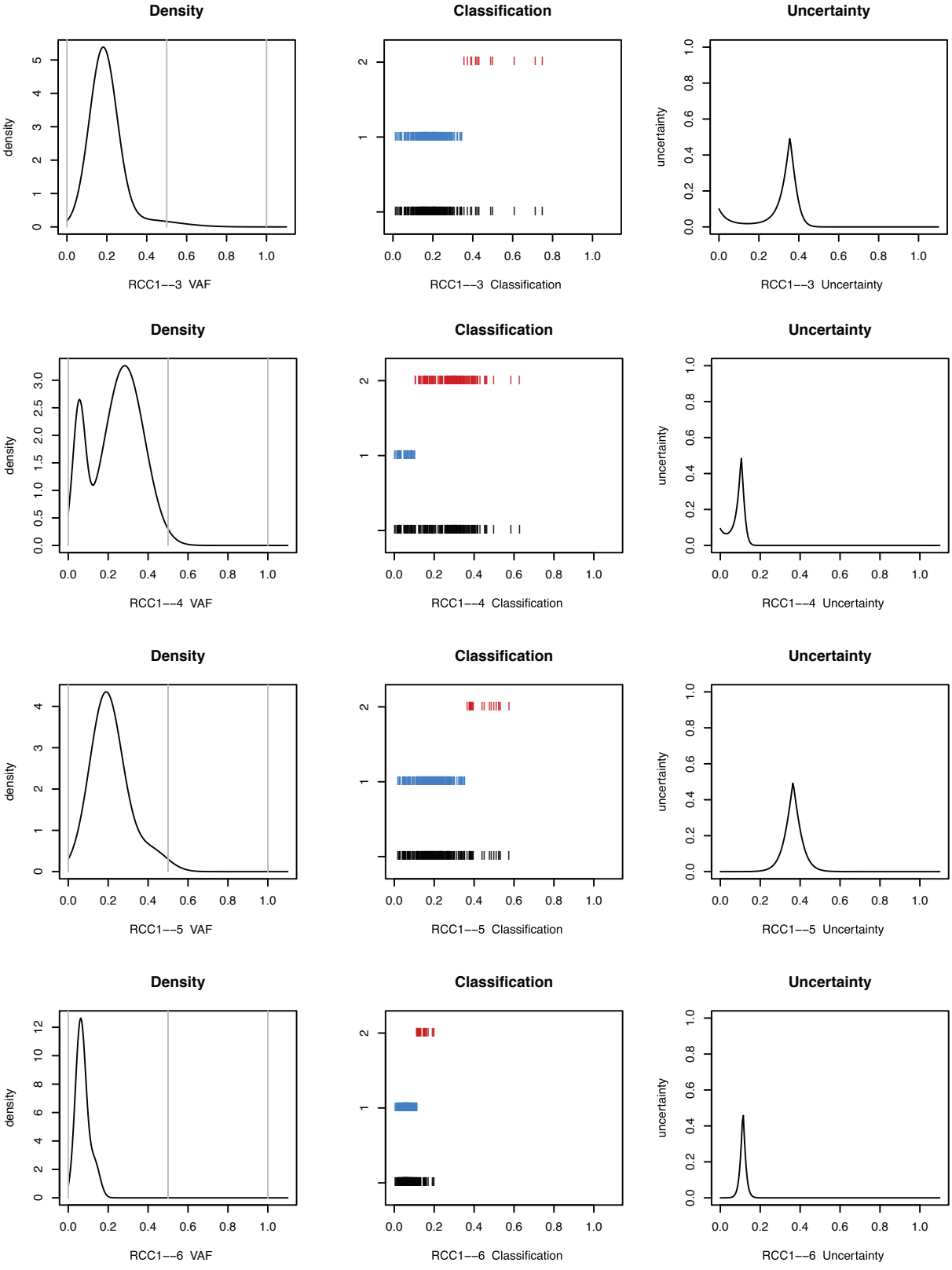

Supplementary Figure 11

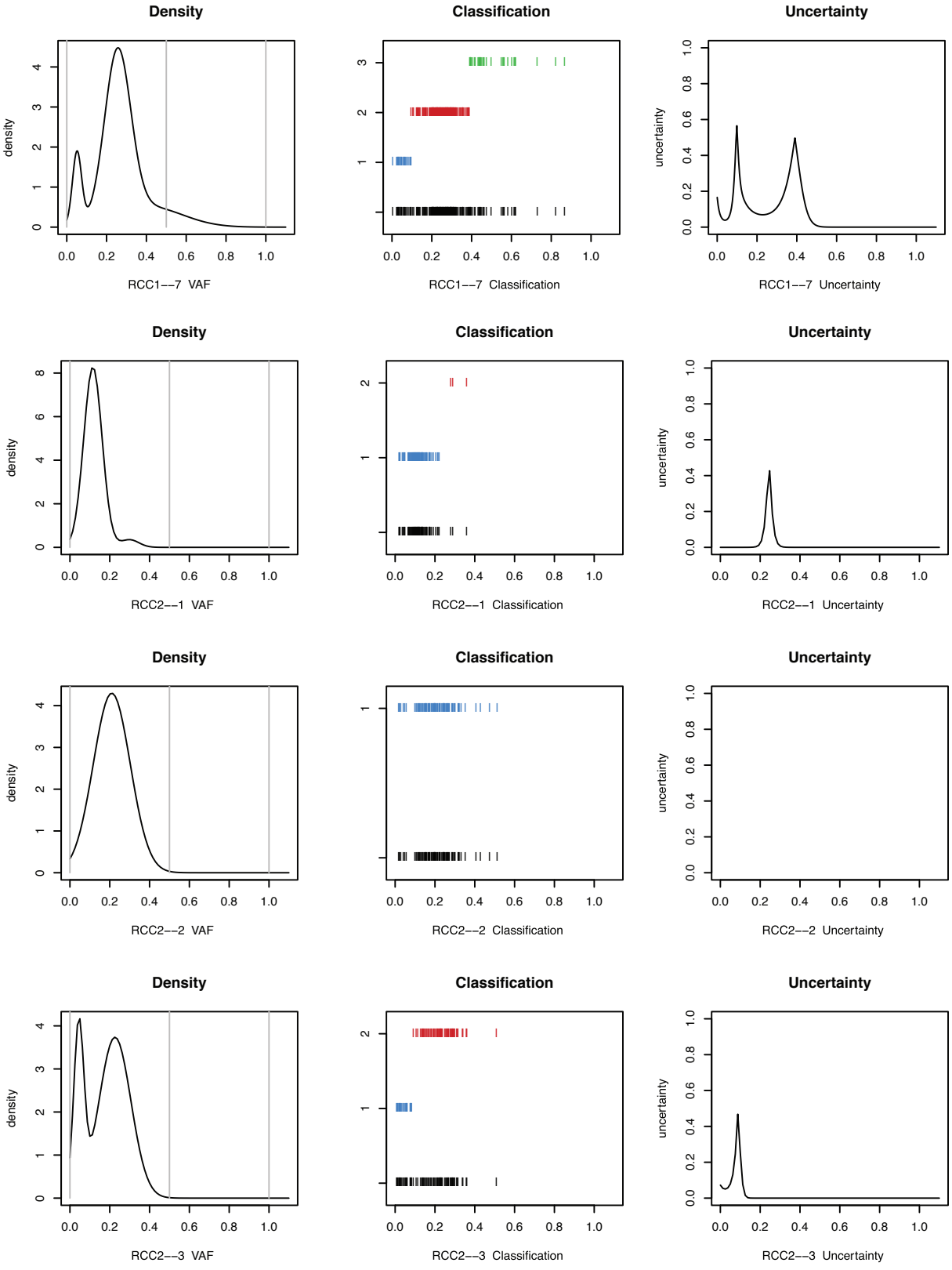

Supplementary Figure 11

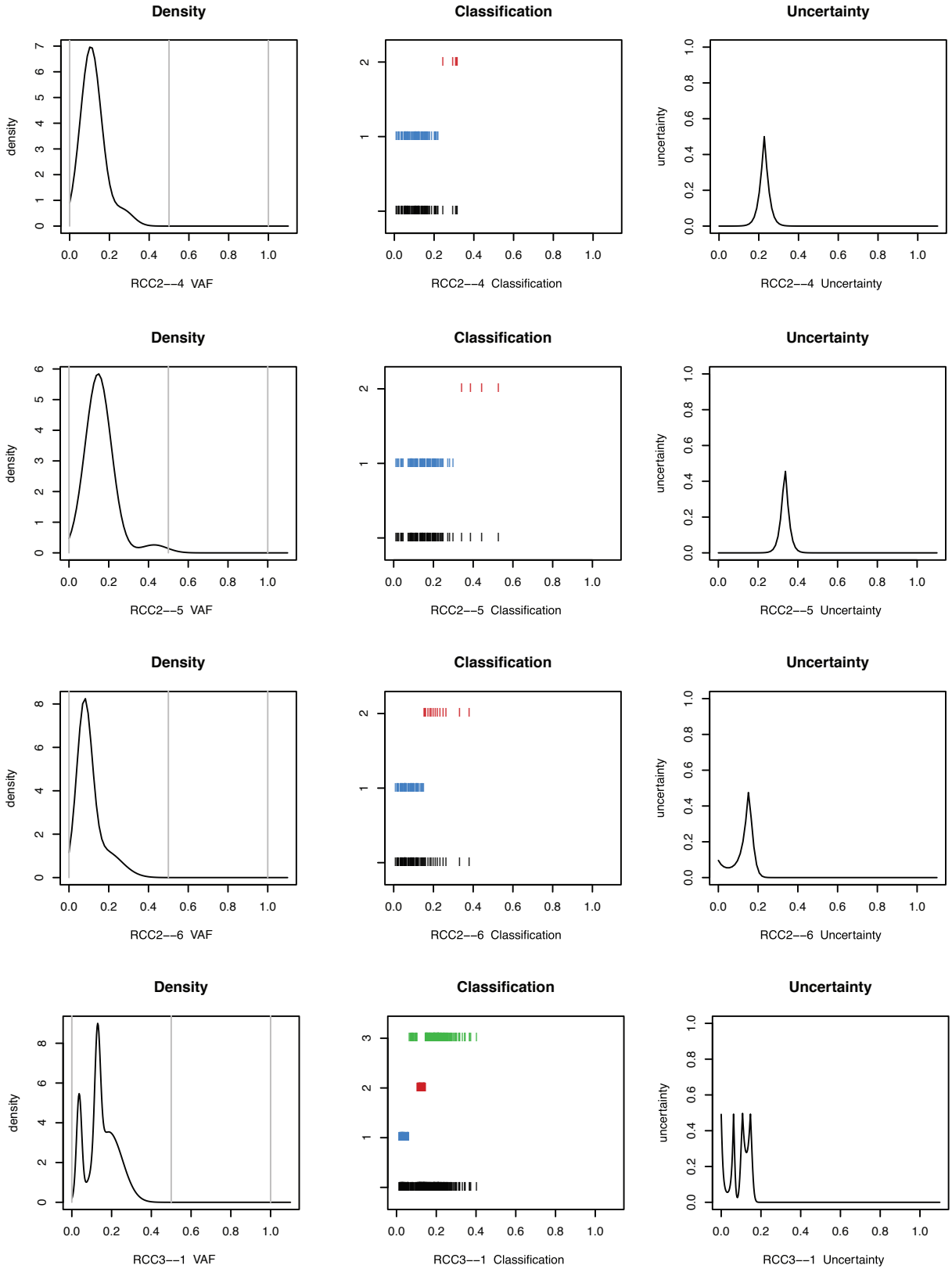

Supplementary Figure 11

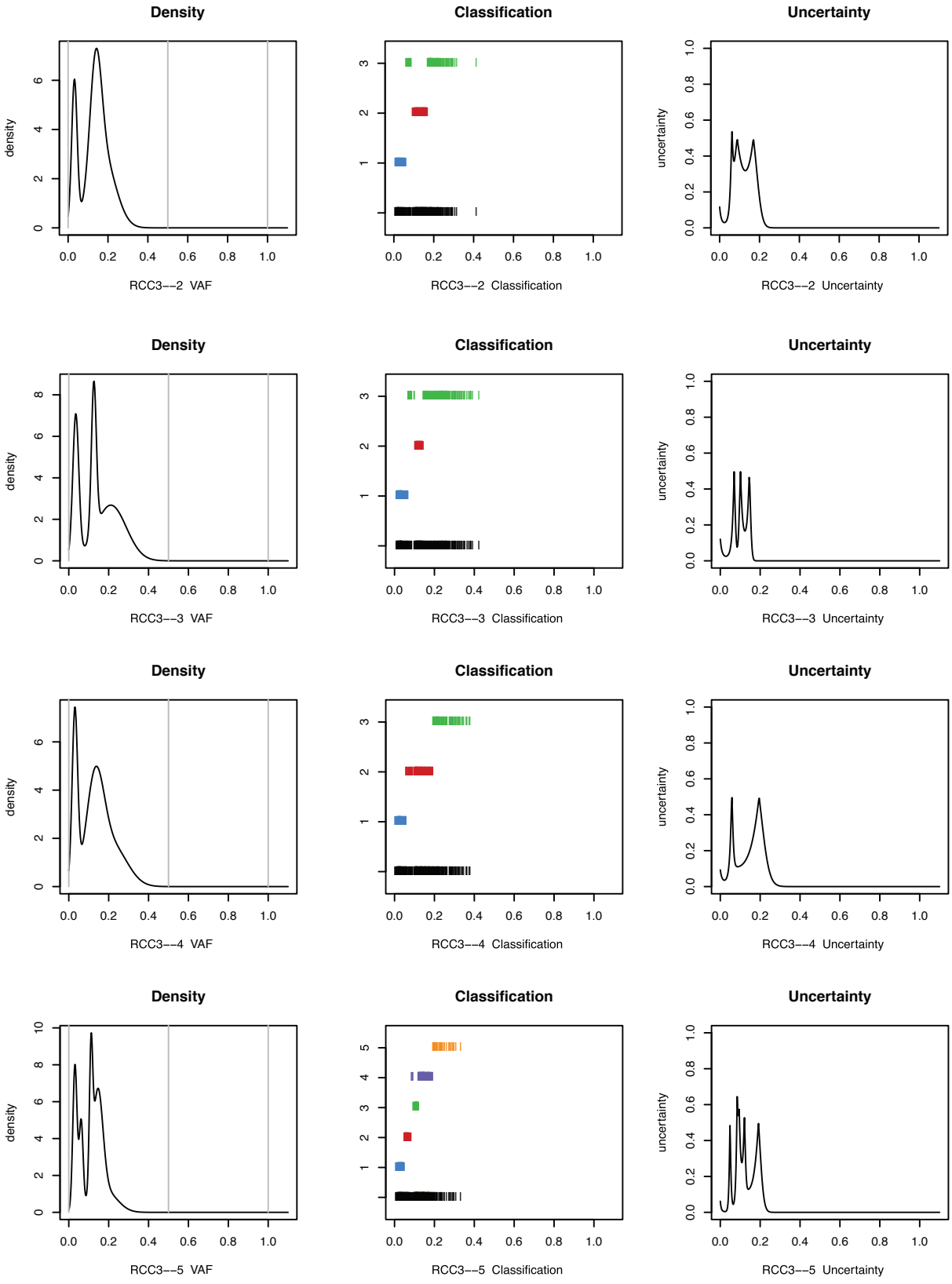

Supplementary Figure 11

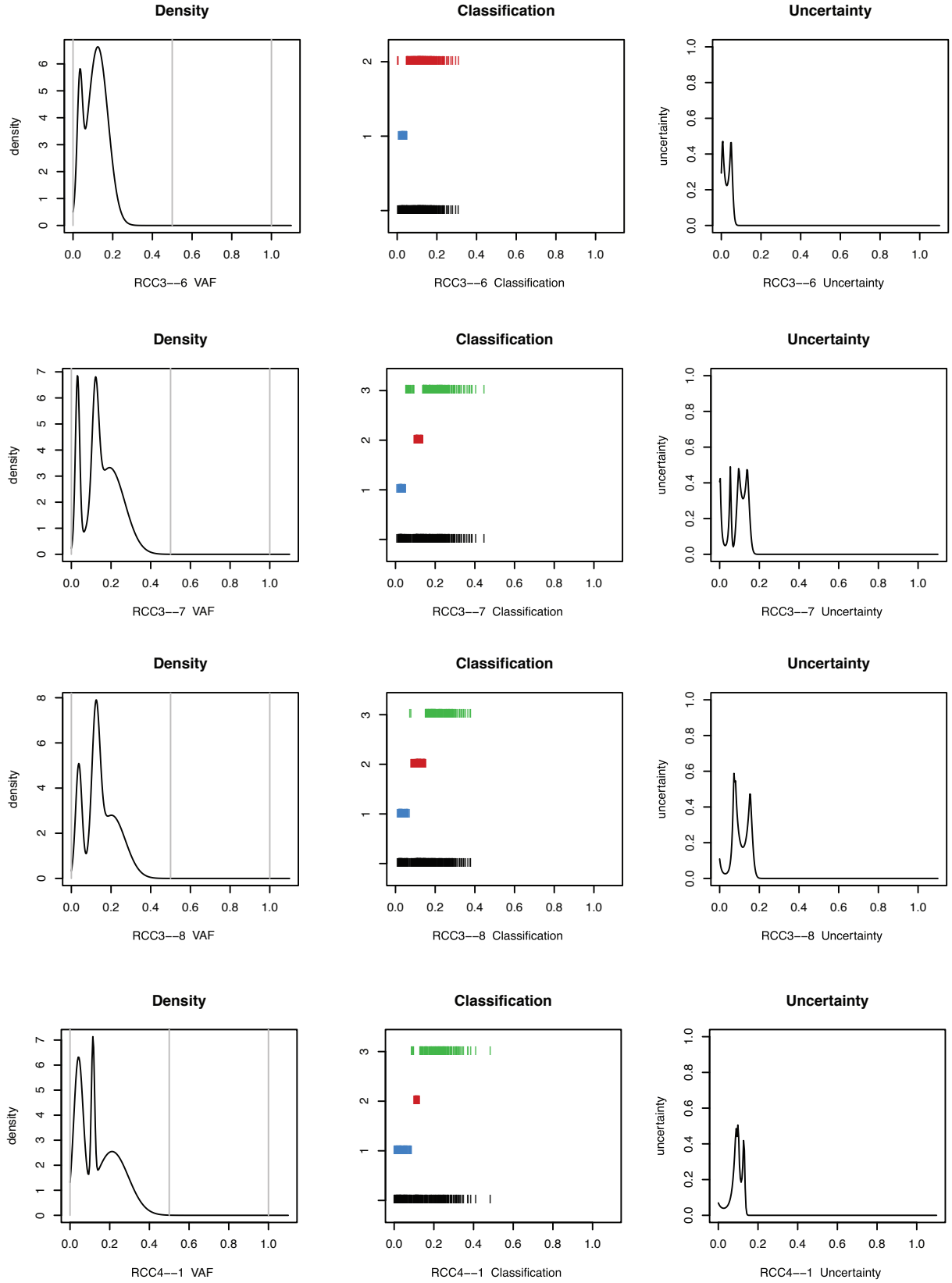

Supplementary Figure 11

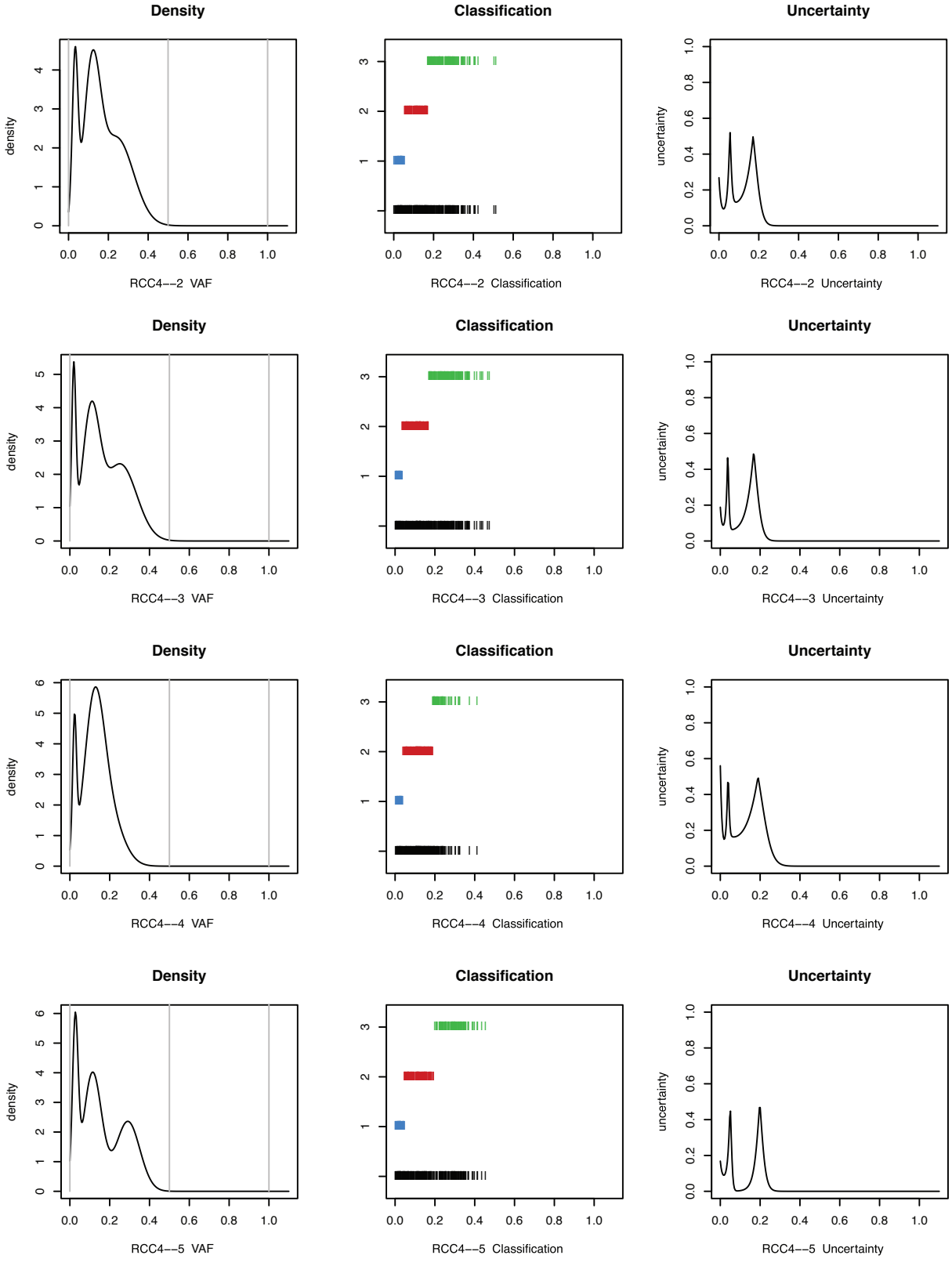

Supplementary Figure 11

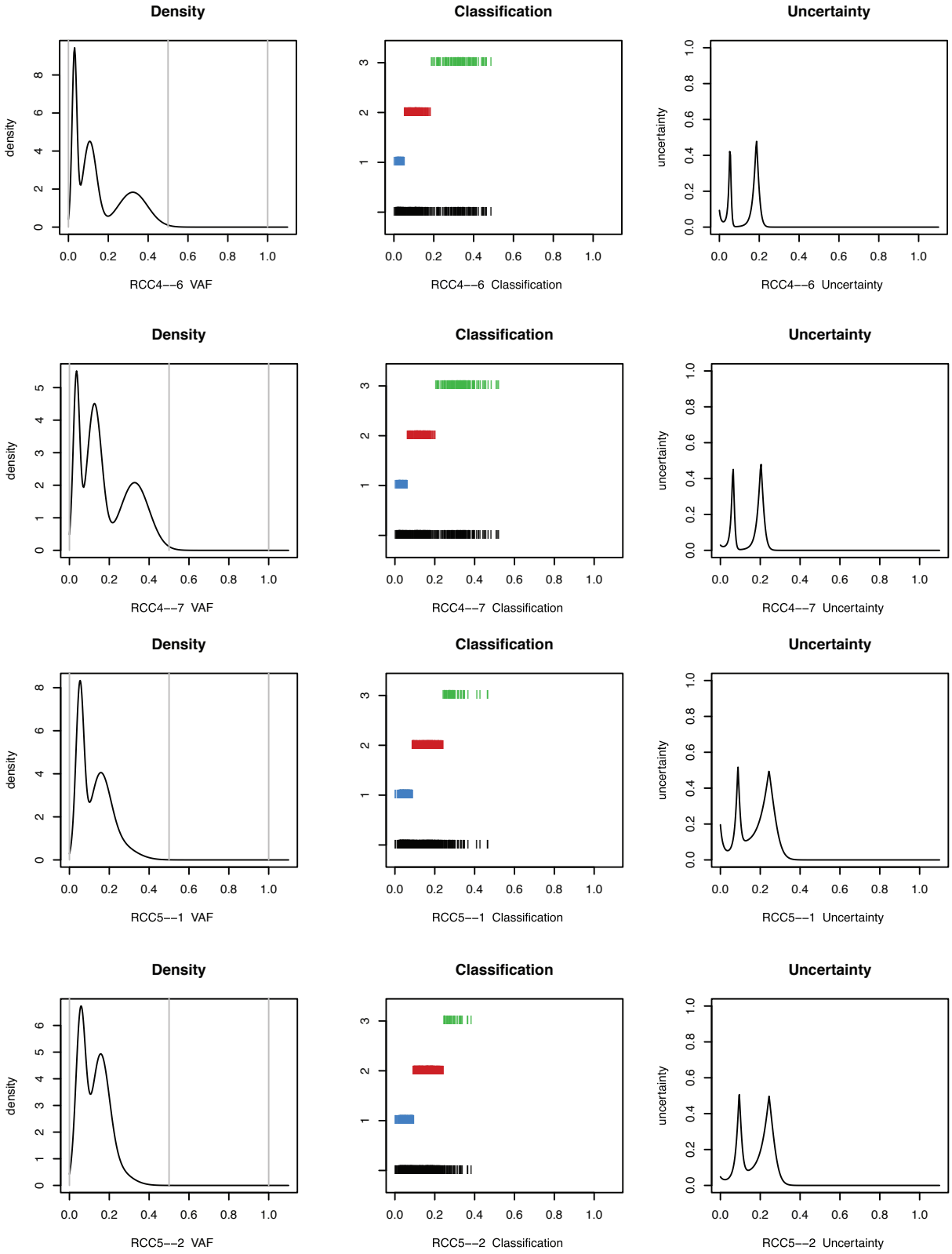

Supplementary Figure 11

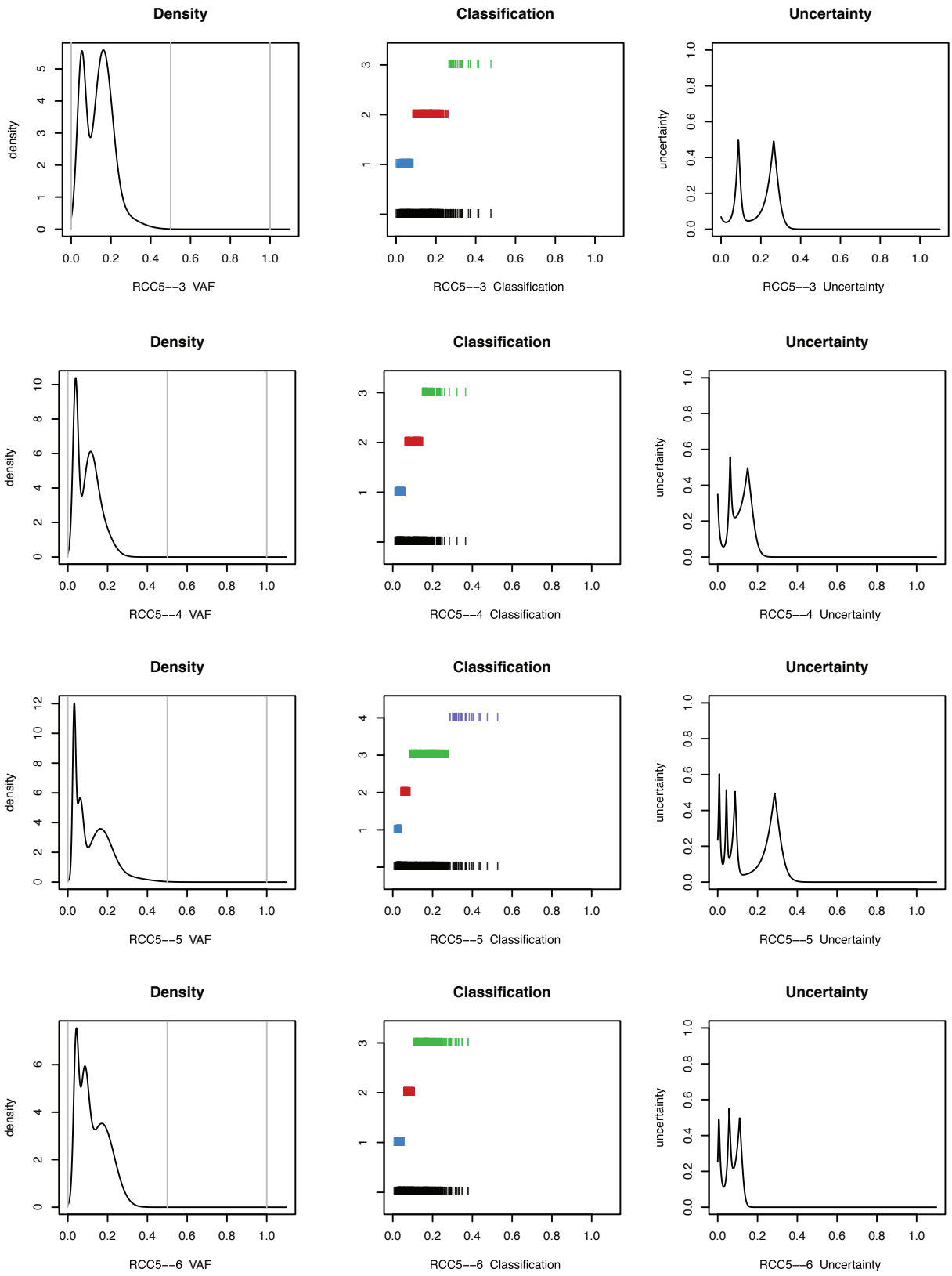

Supplementary Figure 11

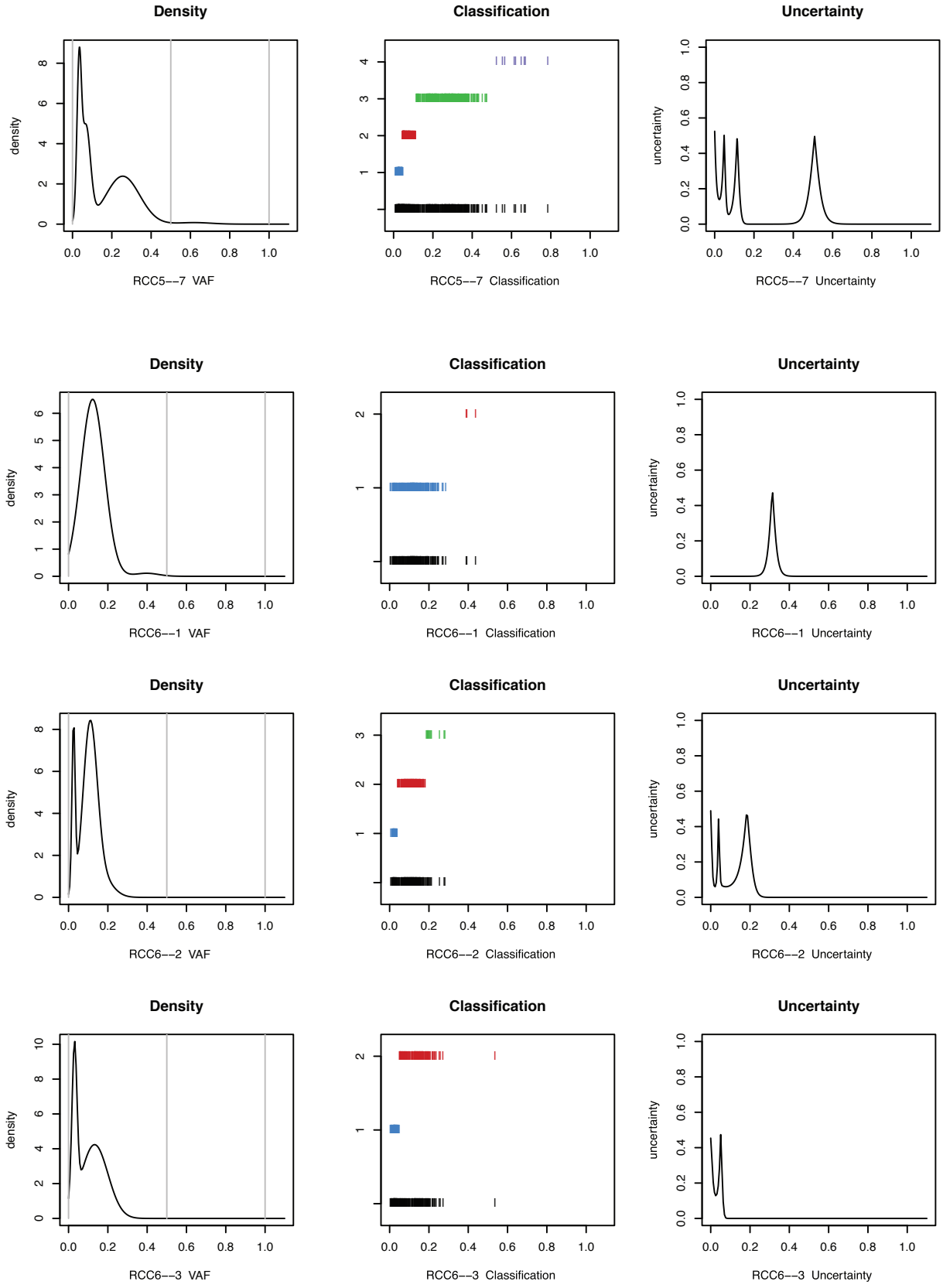

Supplementary Figure 11

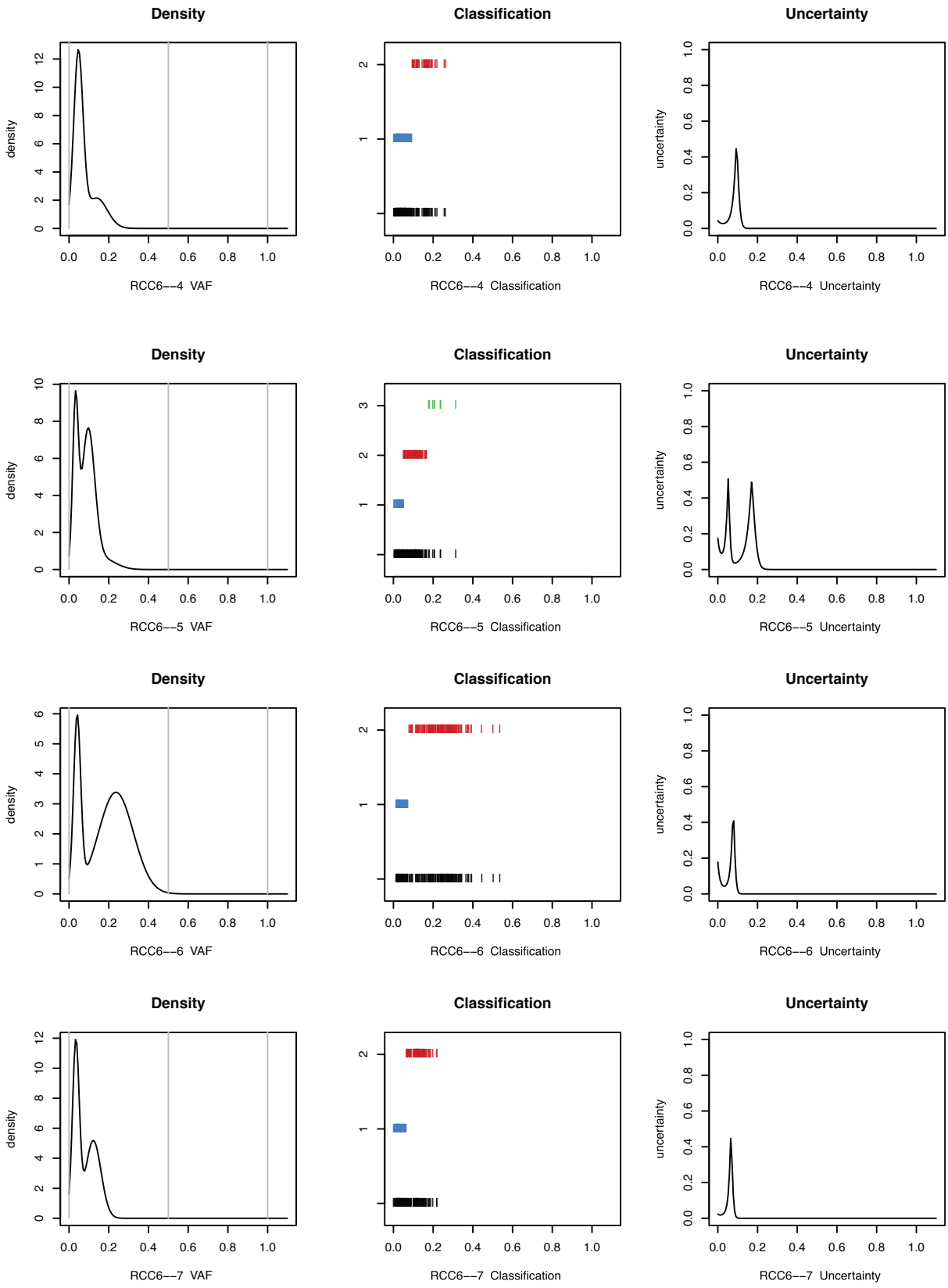

Supplementary Figure 11

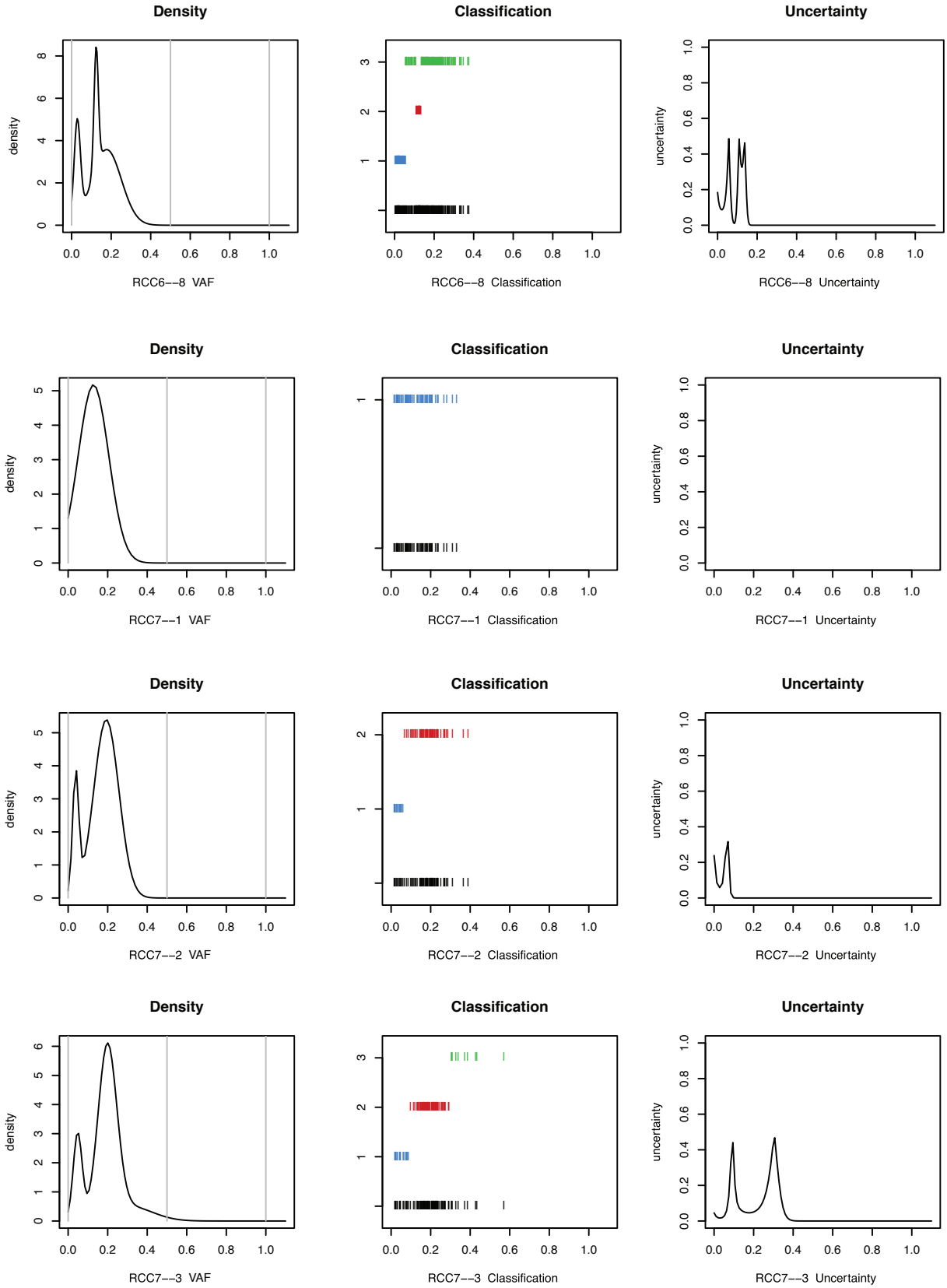

Supplementary Figure 11

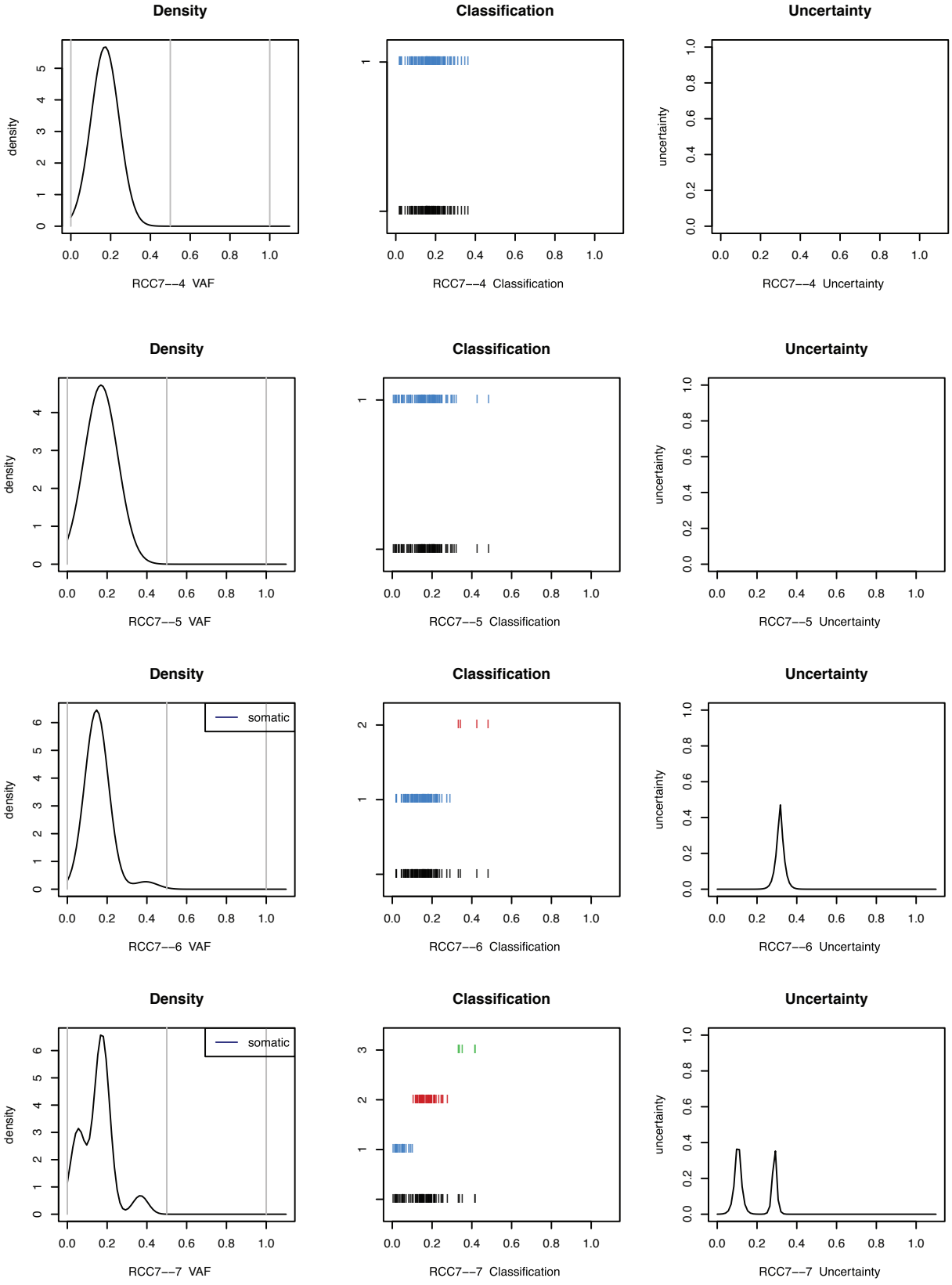

Supplementary Figure 11

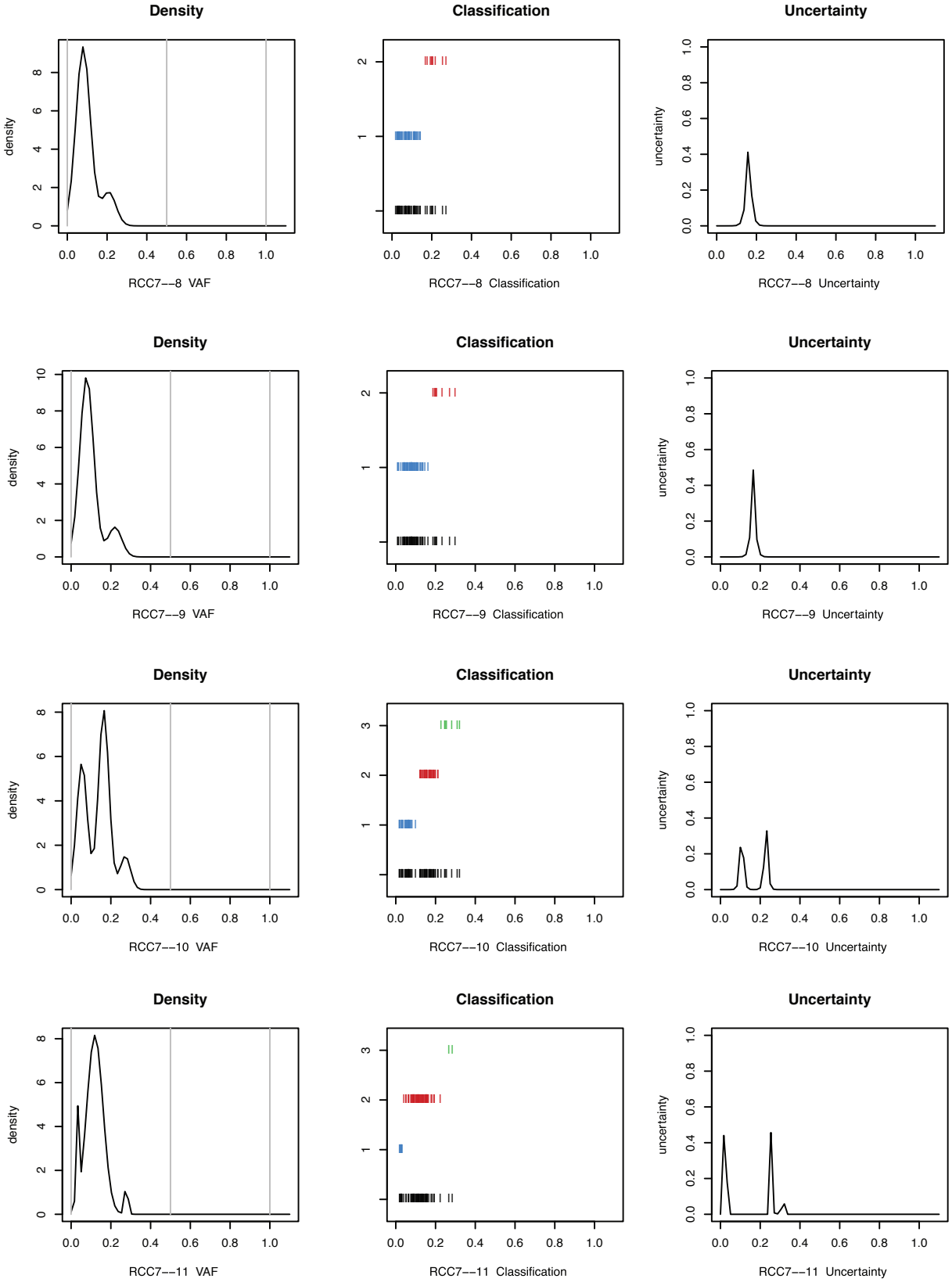

Supplementary Figure 11

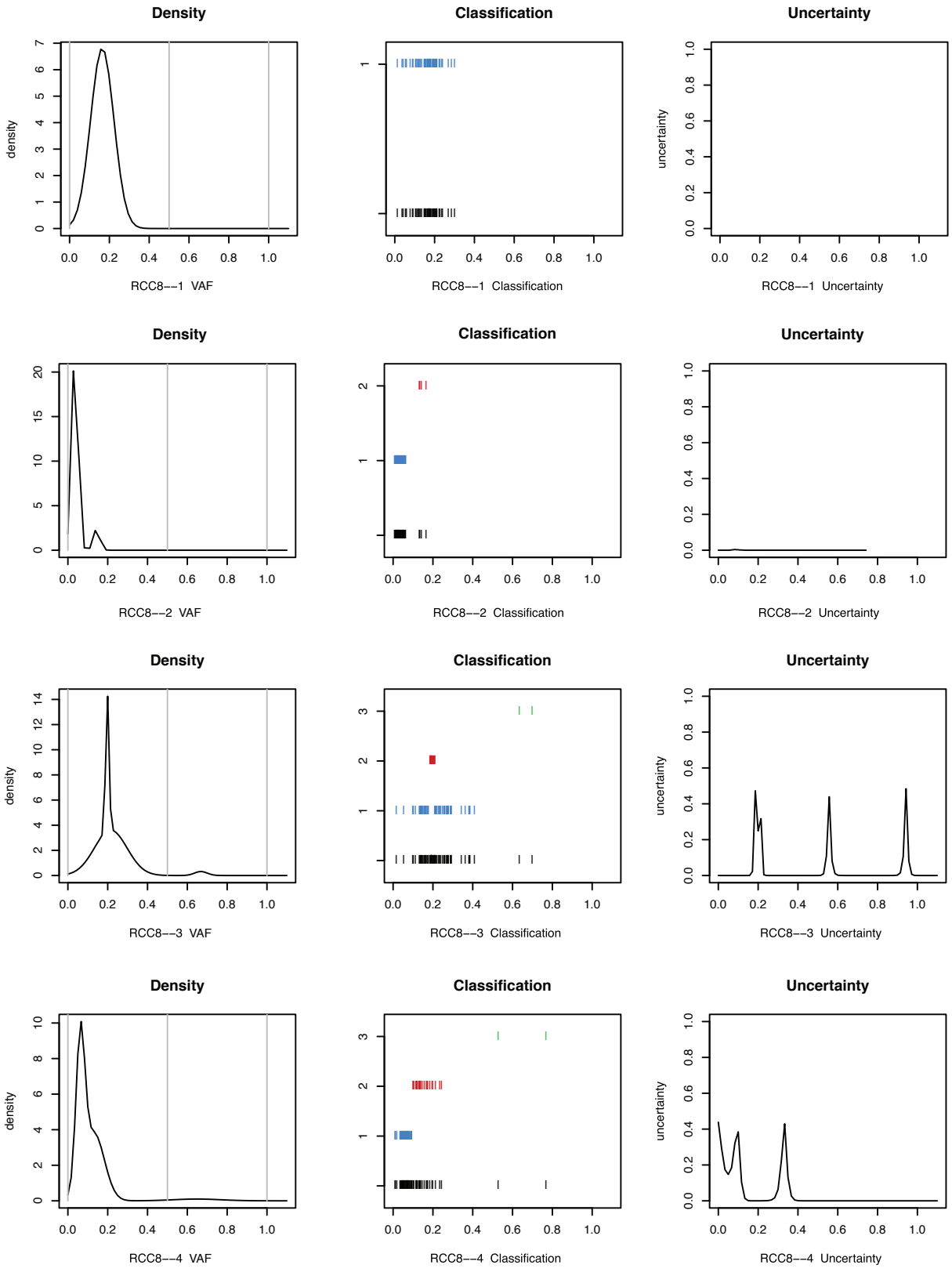

Supplementary Figure 11

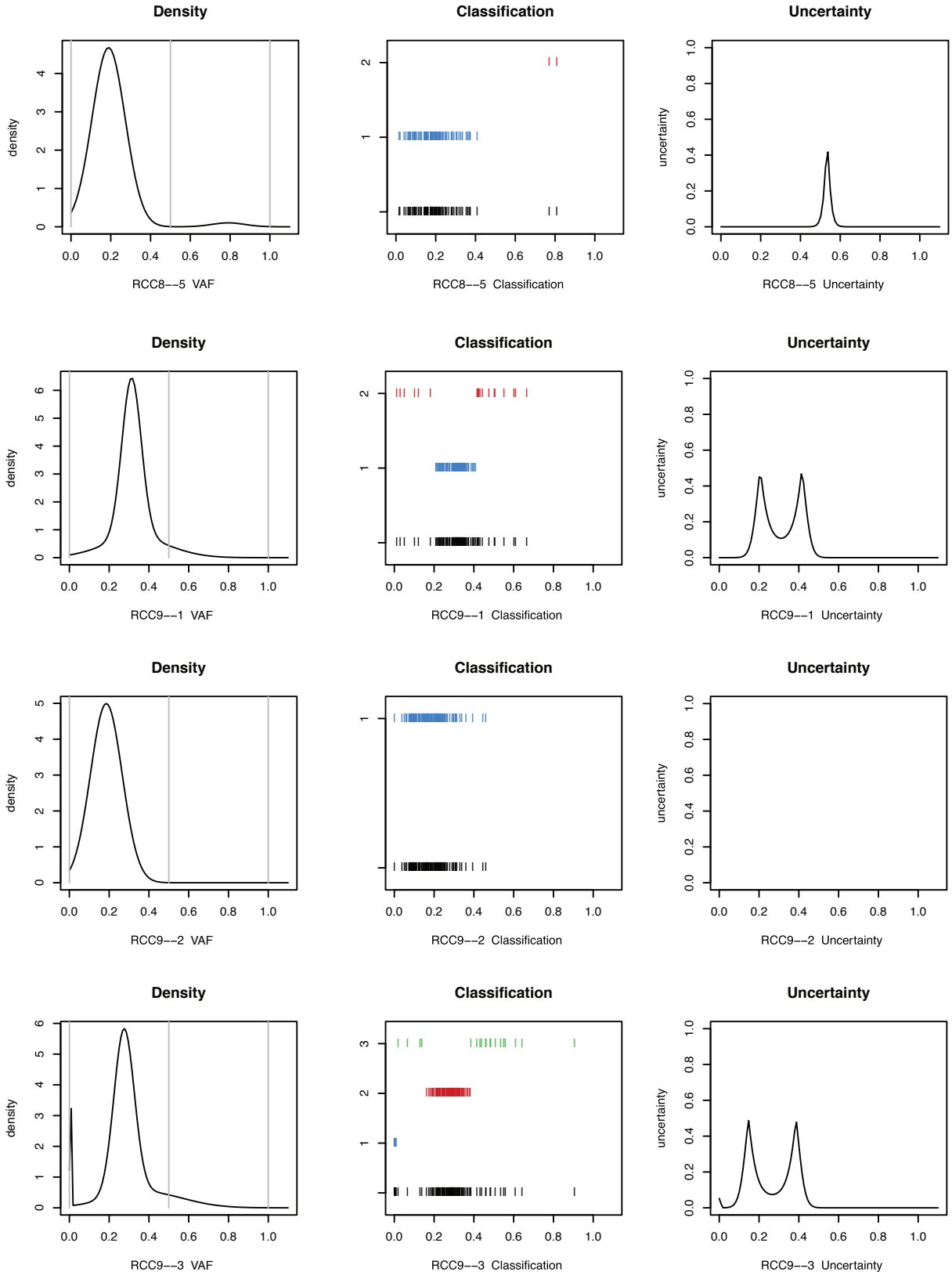

Supplementary Figure 11

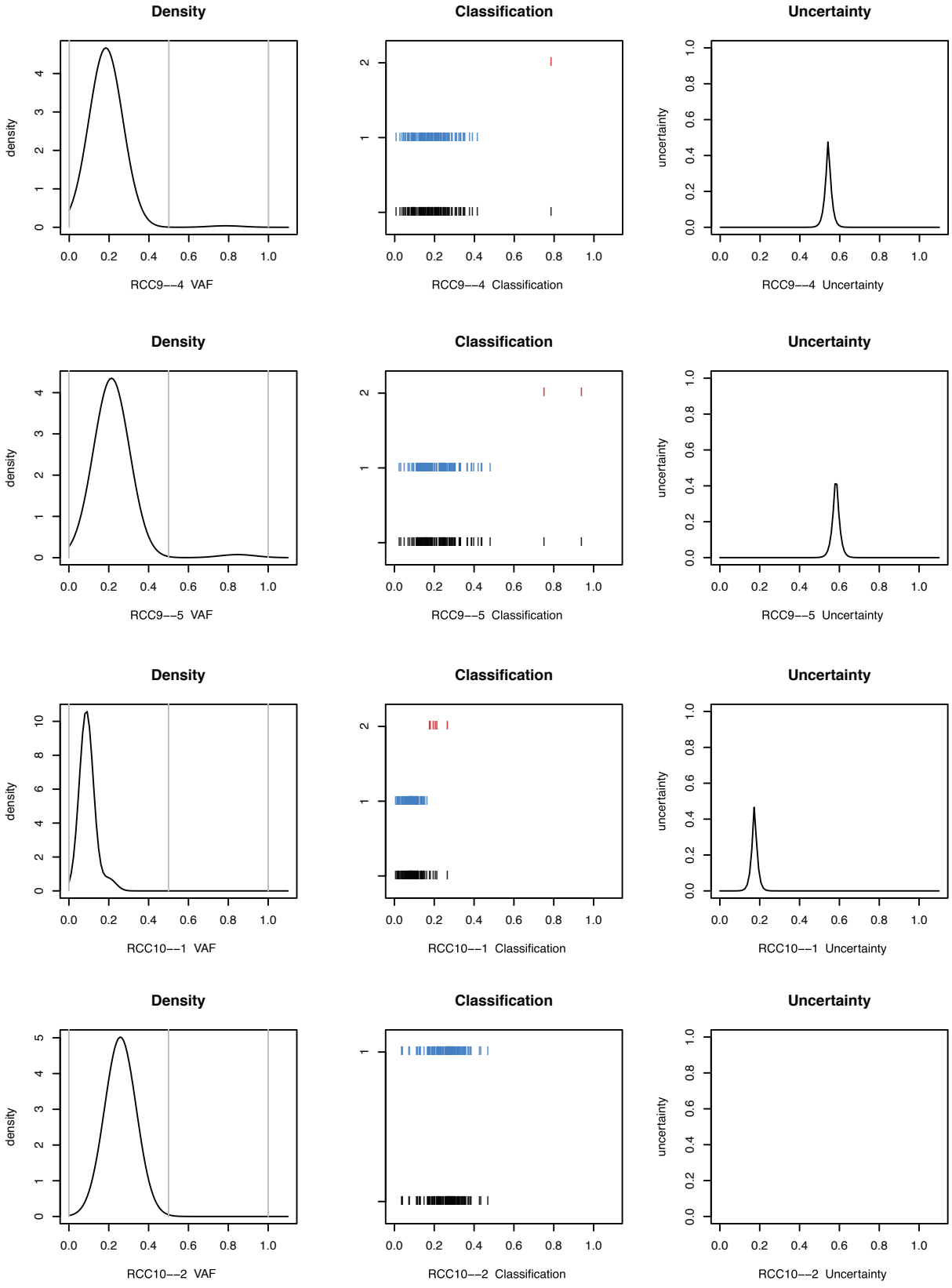

Supplementary Figure 11

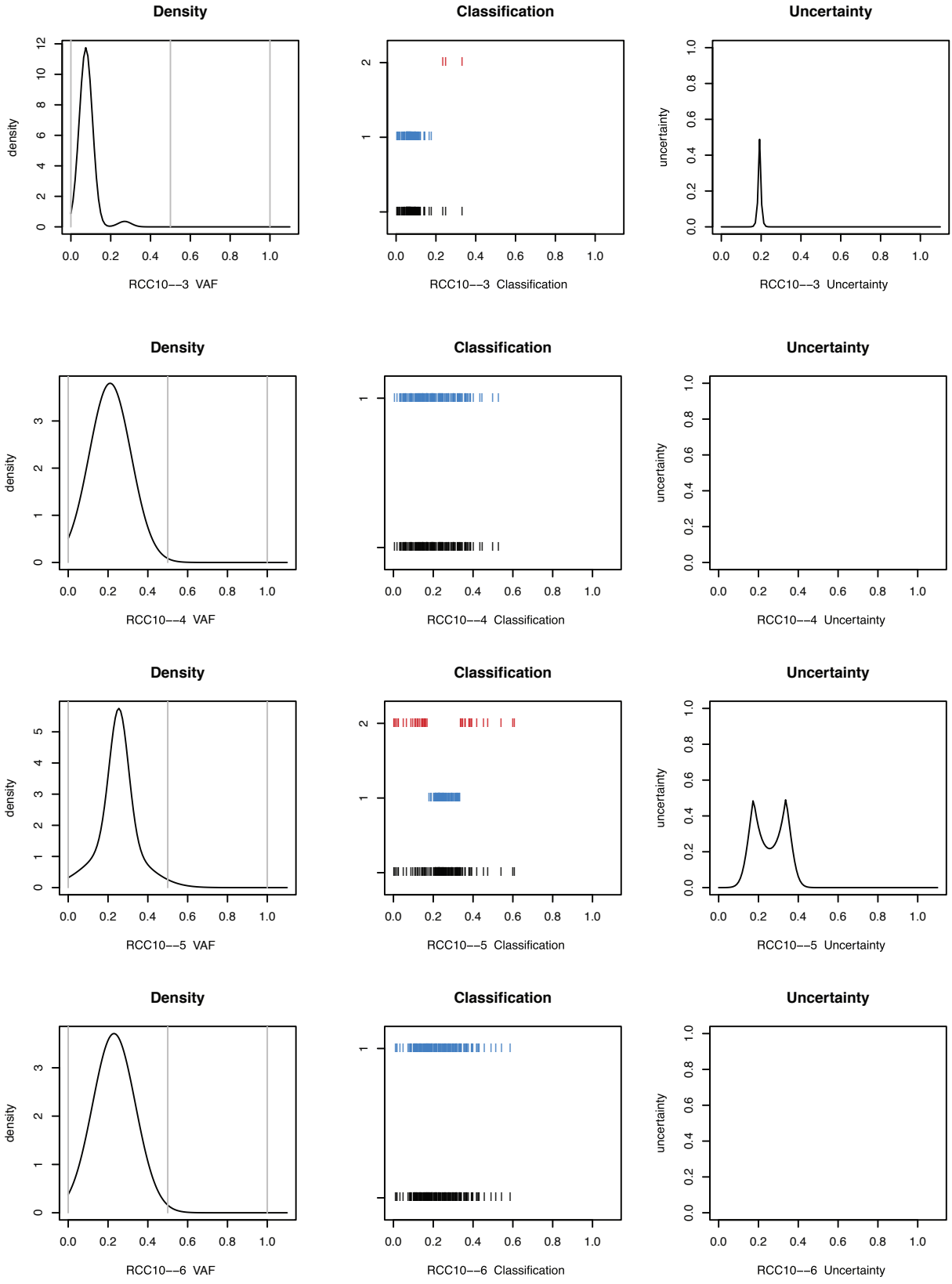

Supplementary Figure 11

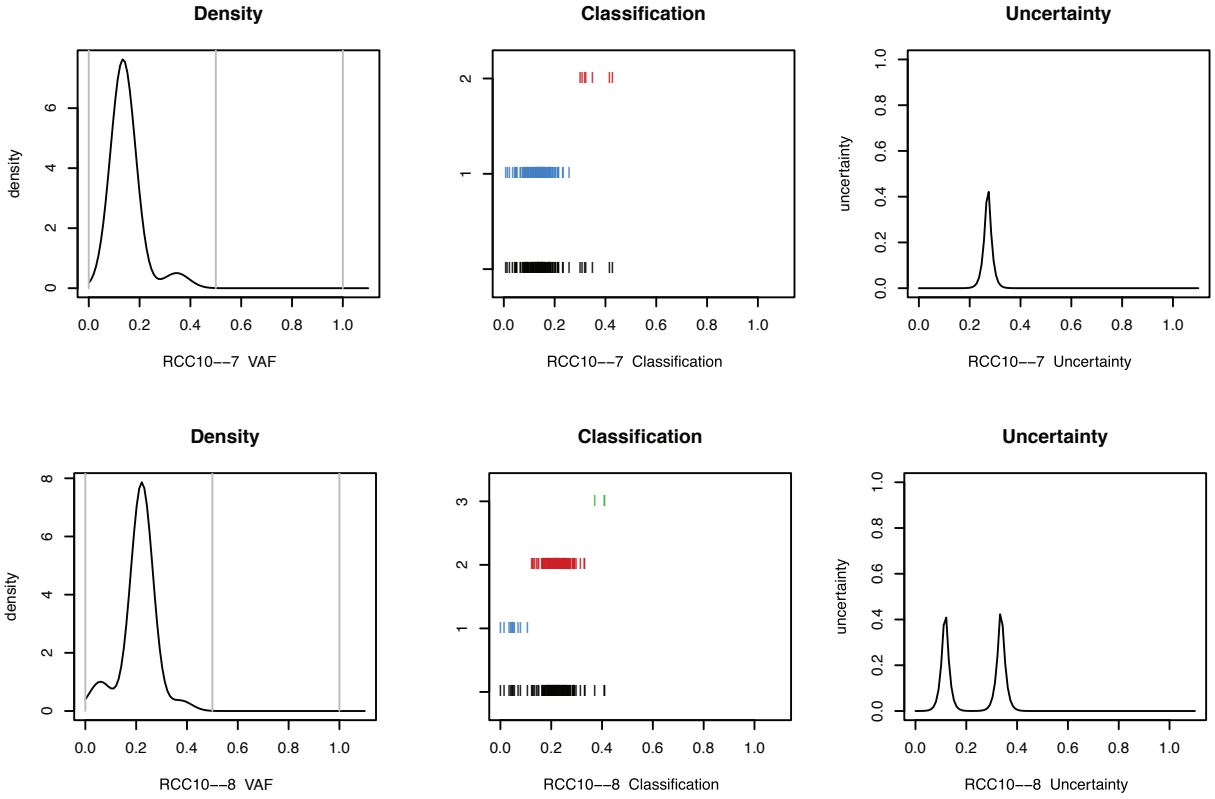

Supplementary Figure 11. Mutation classification. Classification results for somatic mutations in each biopsy include density plots of the variant allele frequency (VAF) of mutations in each sample, as well as the number of VAF populations (Classification), and classification uncertainty. Classification plot includes all mutations (black, lower track on y-axis), and mutations separated by population (numbered tracks on y-axis). Vertical grey lines are drawn at a VAF of 0.5 and 1.0 for reference. Classification results are tabulated in **Supplementary Table 1g**.

Supplementary Figure 12

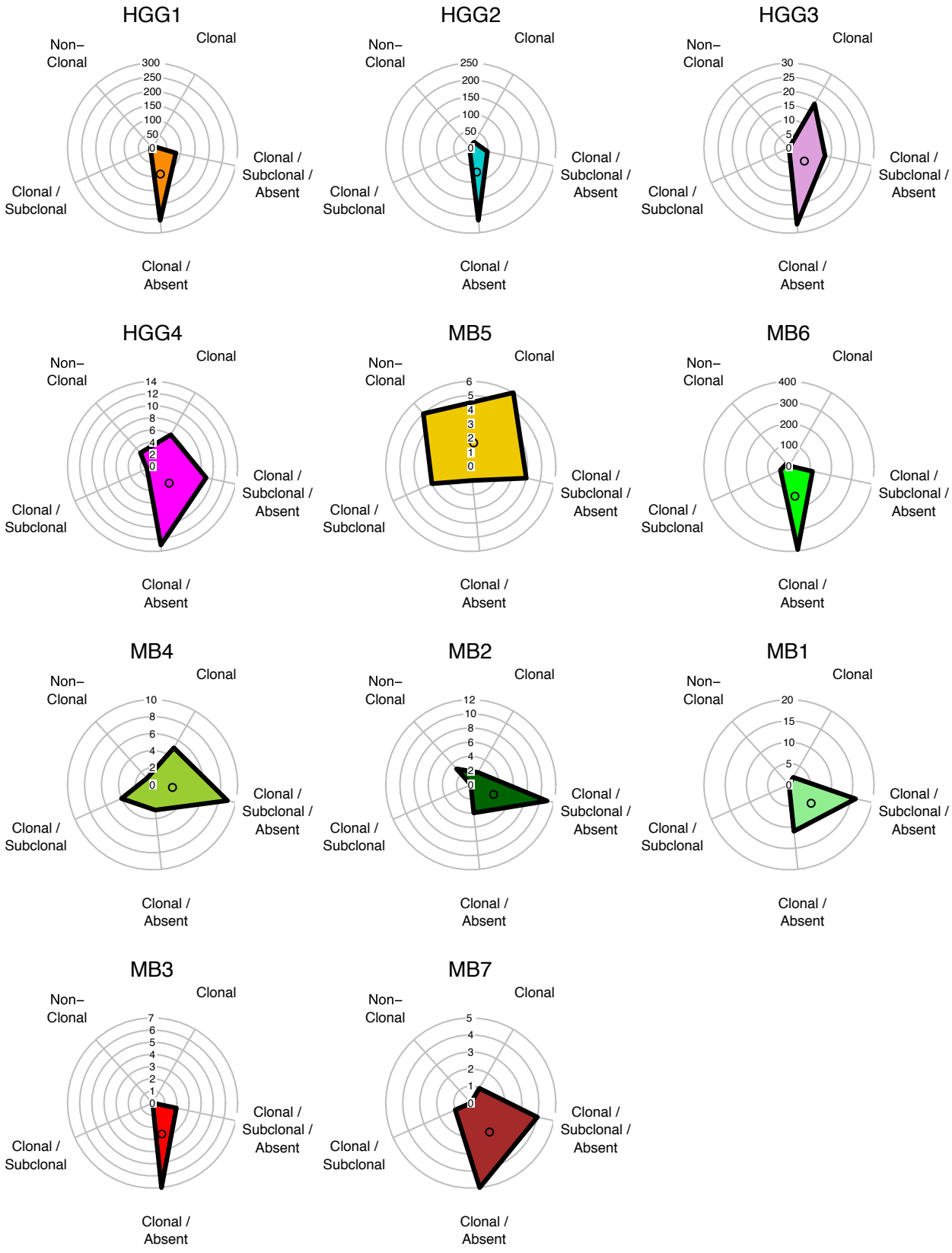

Supplementary Figure 12

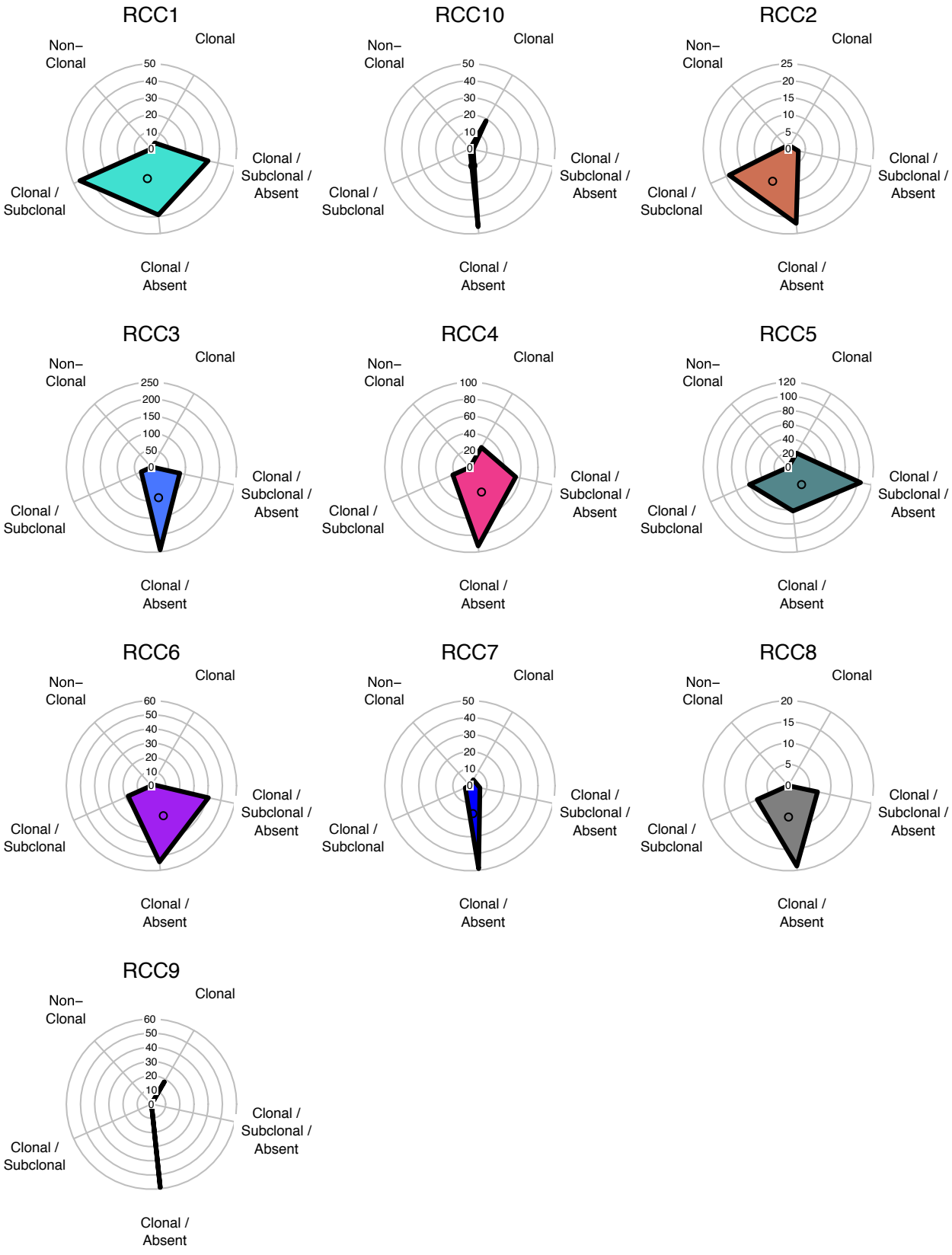

Supplementary Figure 12. ON/OFF mutation patterns across biopsies. Non-synonymous mutations in each tumor were binned into 5 categories: clonal in all biopsies (Clonal); clonal in some biopsies and sub-clonal in others (Clonal/Subclonal); clonal in some biopsies and completely absent in others (Clonal/Absent); clonal in some biopsies, sub-clonal in others, and absent in others (Clonal/Subclonal/Absent); and those never detected as clonal (Non-Clonal). Polygons on radial plots indicate the number of mutations on each of the 5 axes, with polygon centers marked by a black circle representing the trend per patient.

Supplementary Figure 13

a

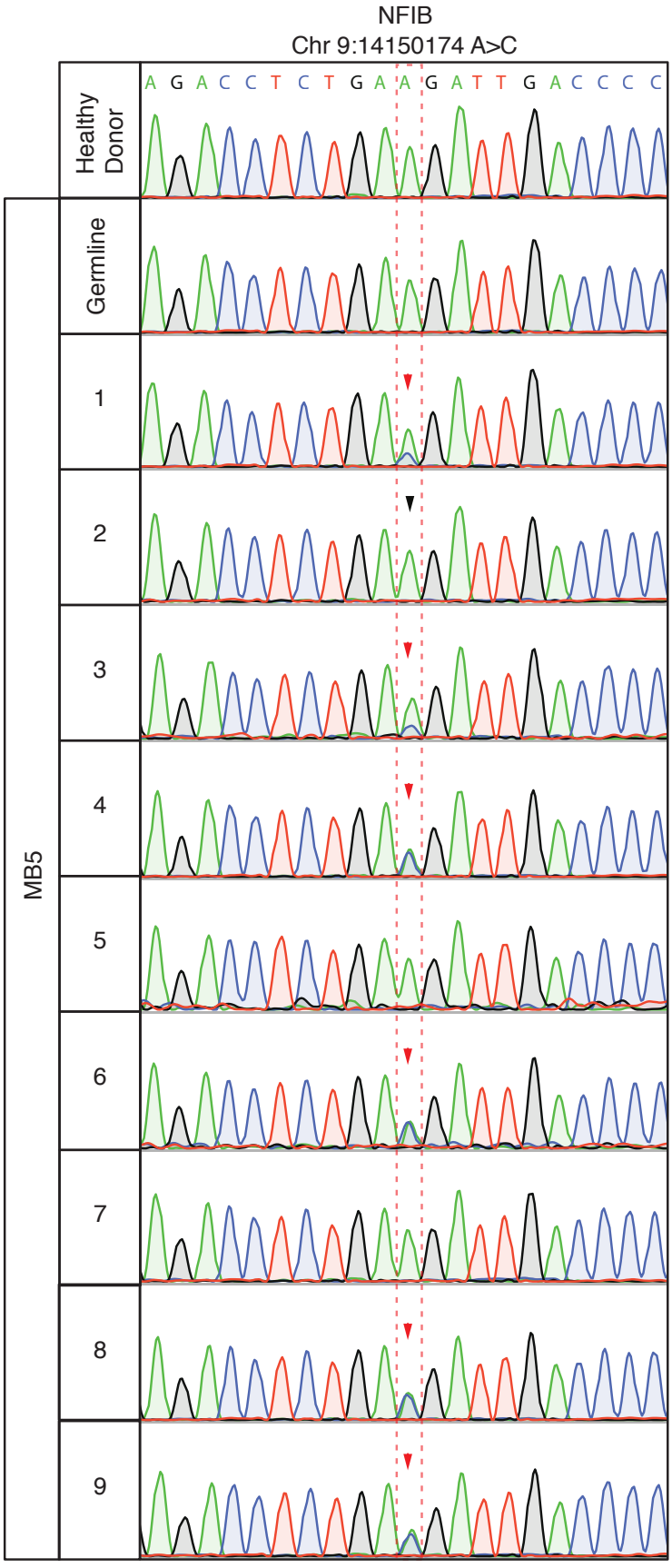

Supplementary Figure 13

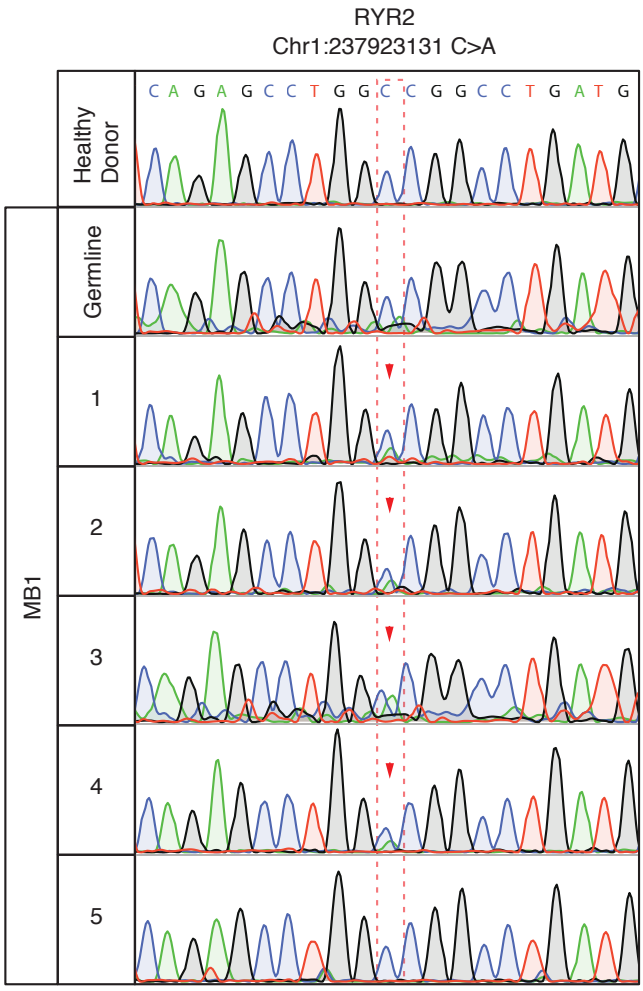

Supplementary Figure 13

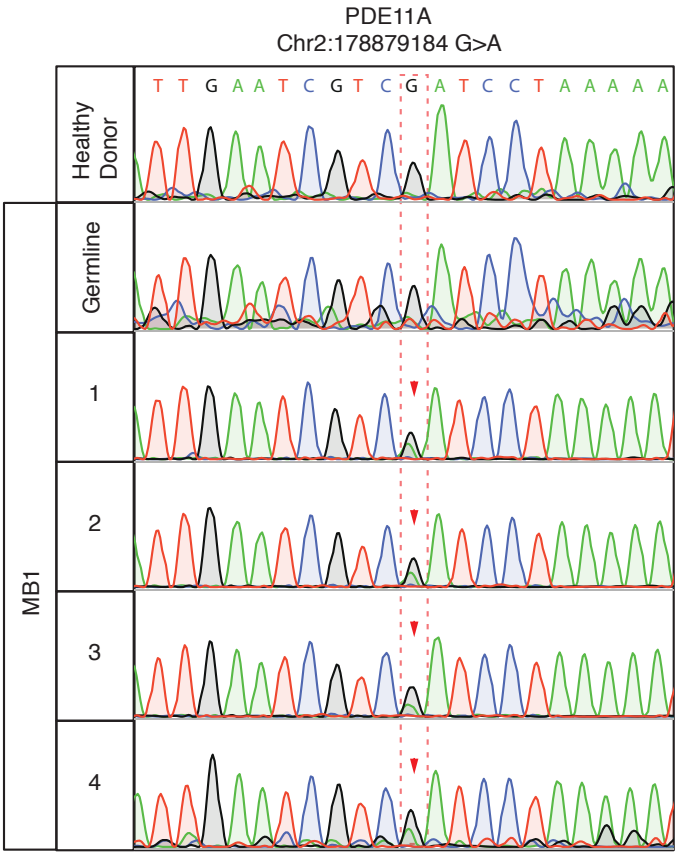

Supplementary Figure 13

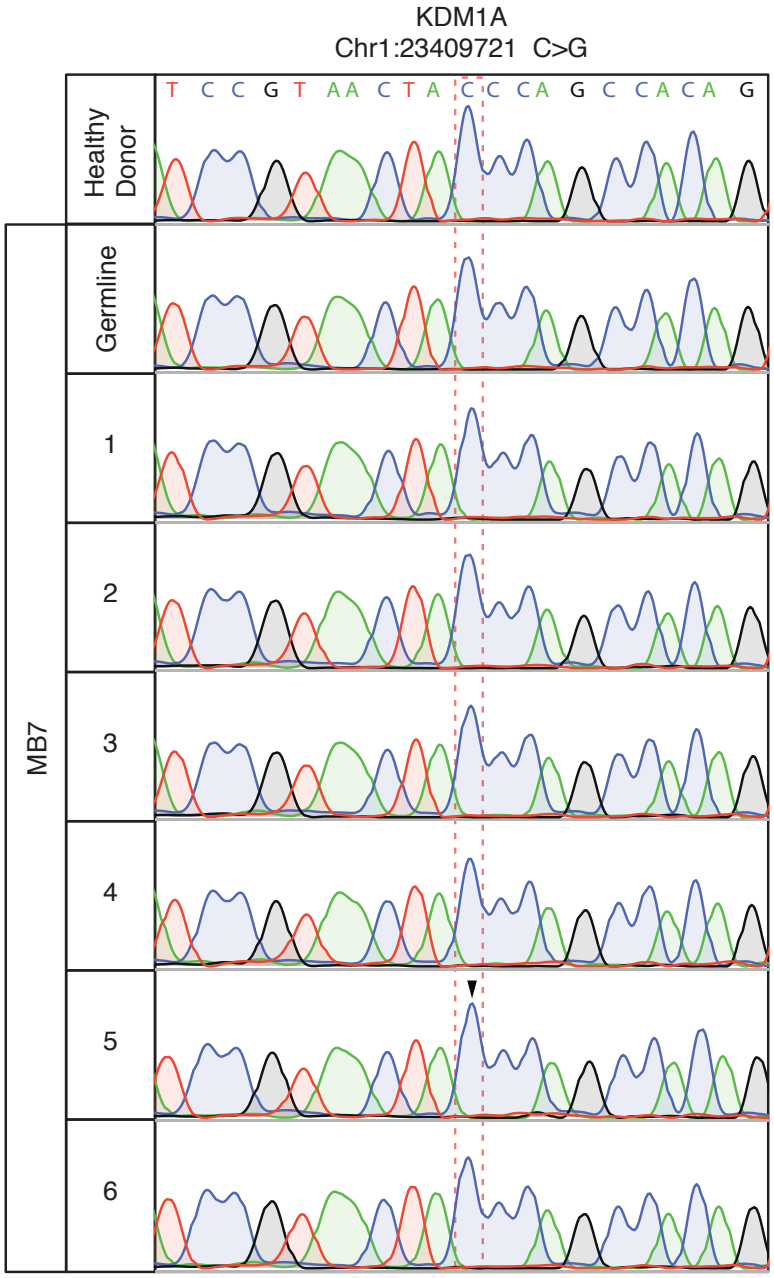

Supplementary Figure 13

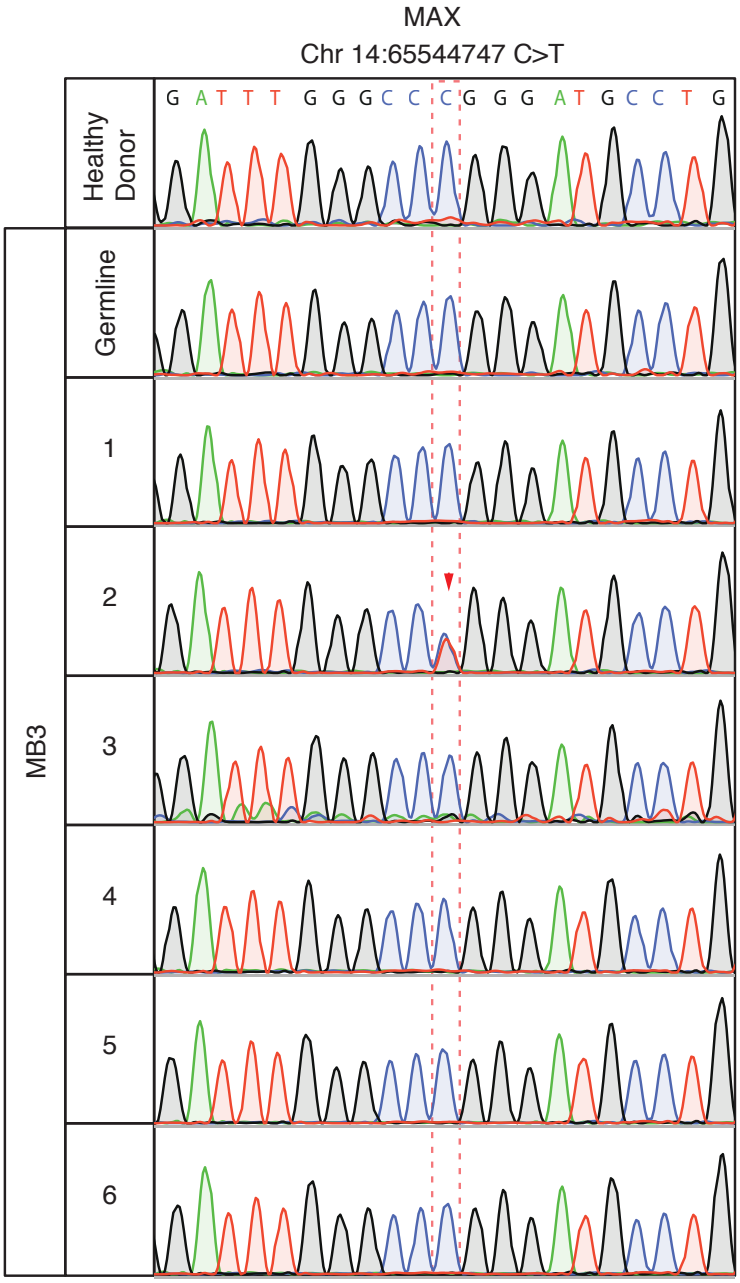

Supplementary Figure 13

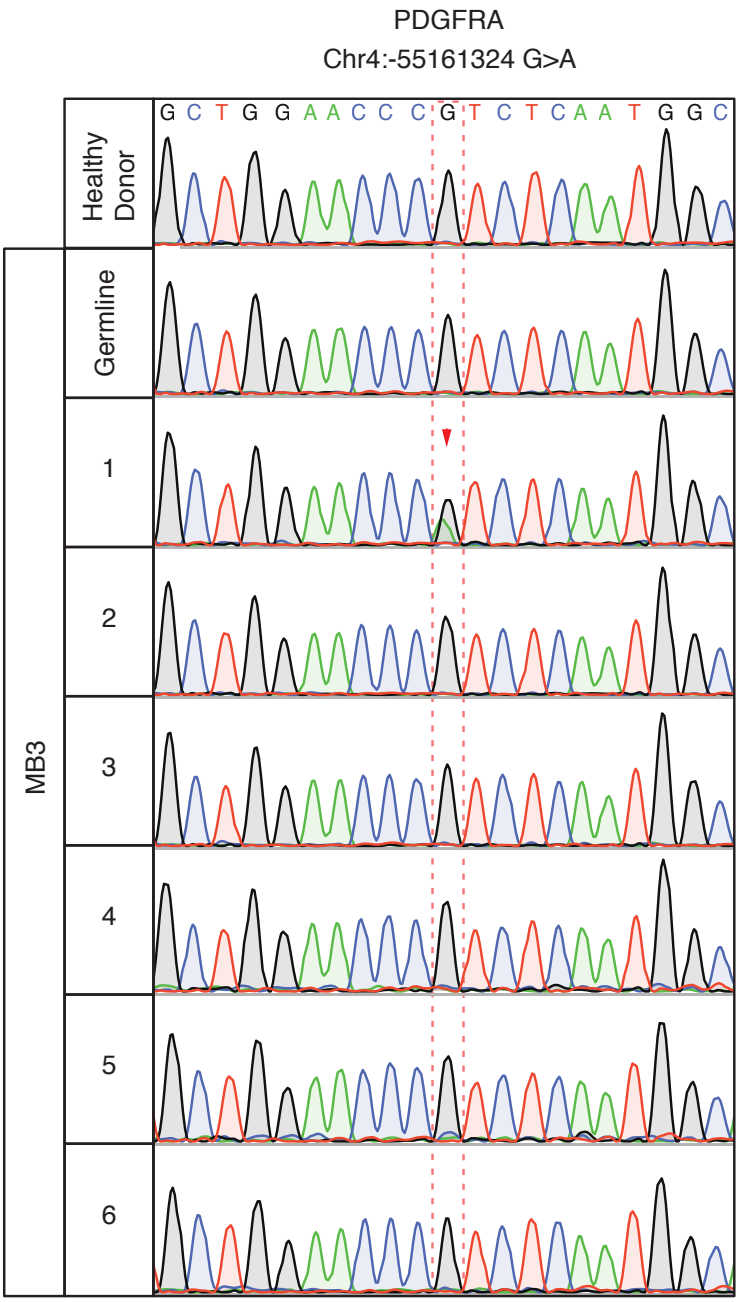

Supplementary Figure 13

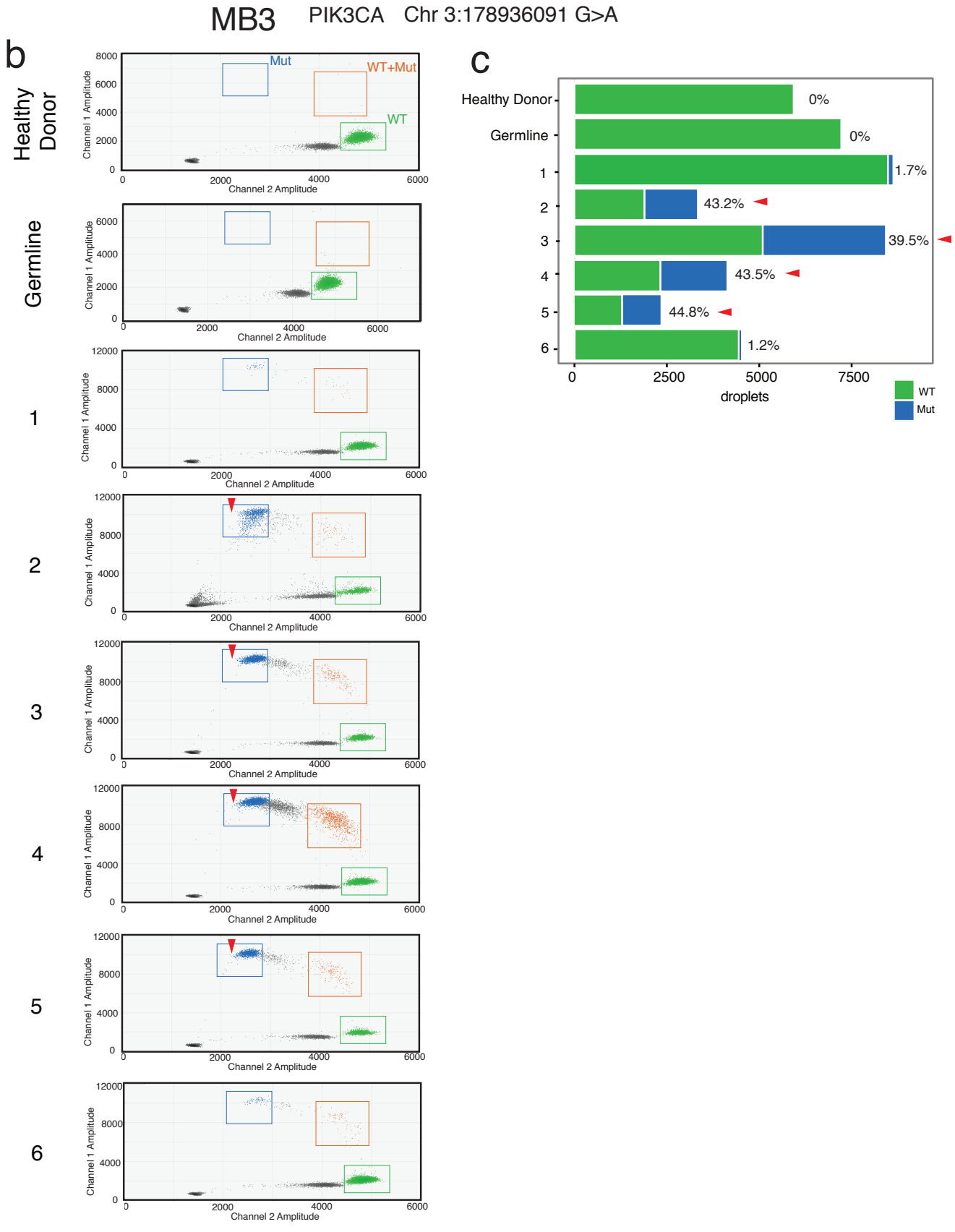

Supplementary Figure 13. Validation results for selected mutations. (a) PCR amplification and Sanger sequencing of a select set of mutations are presented. Panels show a manual alignment of Sanger Sequencing chromatograms from different geographically distinct biopsies from the same tumor (biopsy labels on the left) as well as matched germline and healthy donor sample controls samples. The top part of each panel provides the Gene symbol, genomic coordinates, nucleotide variation, and reference sequence. Dashed red boxes highlight the peaks corresponding to the nucleotide of interest in the chromatogram and red arrowheads highlight cases where the presence of the SNV was confirmed. Black arrowheads indicate biopsies where an expected SNV was not confirmed, All chromatograms show sequencing on the positive strand with the exception of PDGFRA, which shows the sequencing on the negative strand. **(b)** Validation by droplet digital PCR (ddPCR) of the presence of the PIK3CA mutation (chr 3:178936091 G>A) in six biopsies of tumor MB3 as well as matched germline and a control sample. In each assay, the sample is partitioned into droplets that will act as independent PCR reactions (dots). The use of fluorescently labeled and allele specific probes allow the simultaneous detection of each allele present in the droplets. Green dots: droplets that contain the wild type (WT) allele; blue dots: mutant allele droplets; orange dots: both mutant and WT. Red arrowheads annotate biopsies where SNV was confirmed **(c)** Stacked barplot of PIK3CA mutant allele frequency quantification from b. Green: WT; Blue: mutation. Percentages are presented to the right of each bar. Red arrowheads annotate biopsies where SNV was confirmed. The depth of sampling in ddPCR allows sensitive detection of low frequency events in biopsies 1 and 6 (<2%).

Supplementary Figure 14

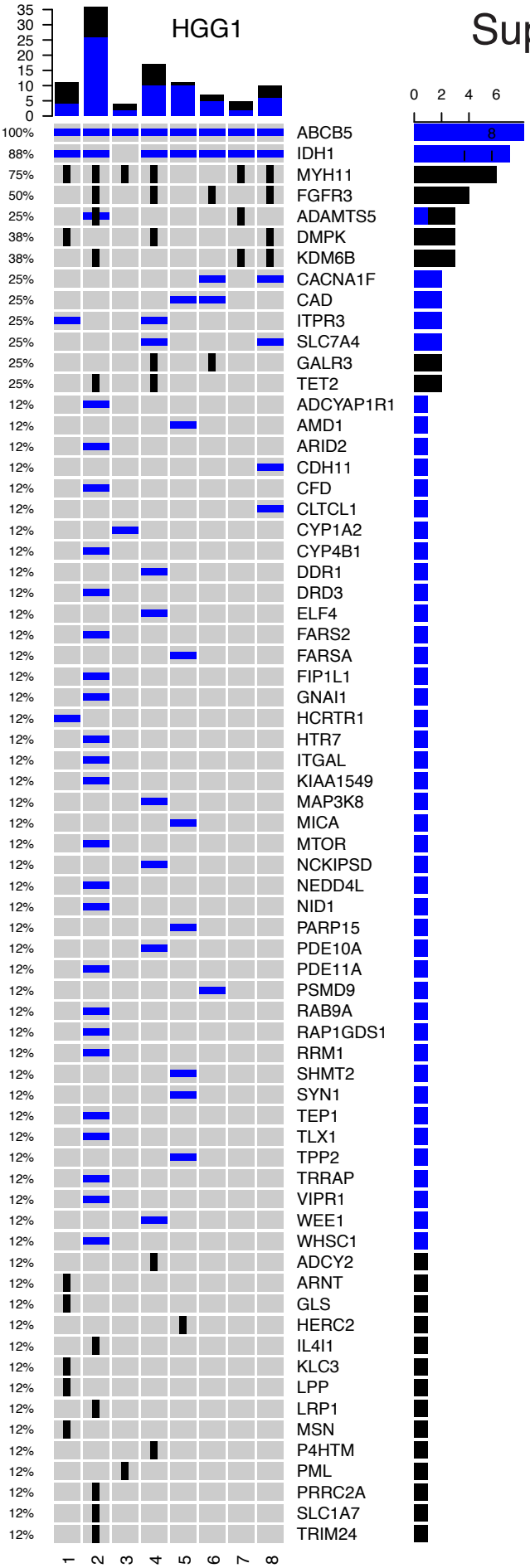

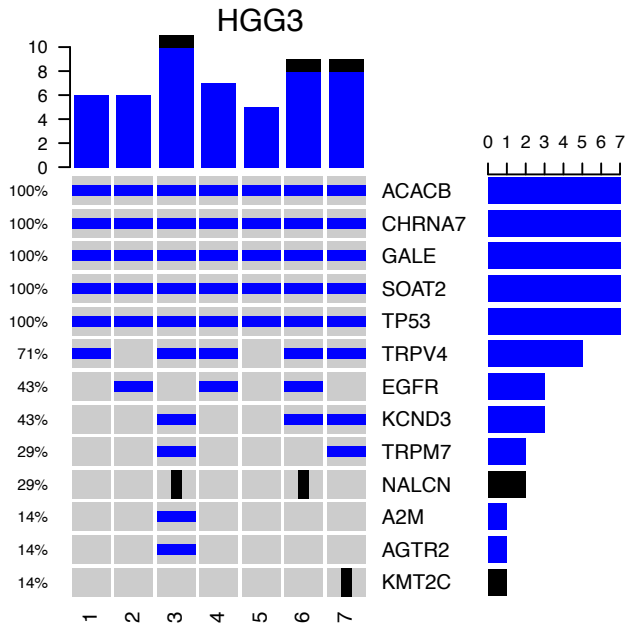

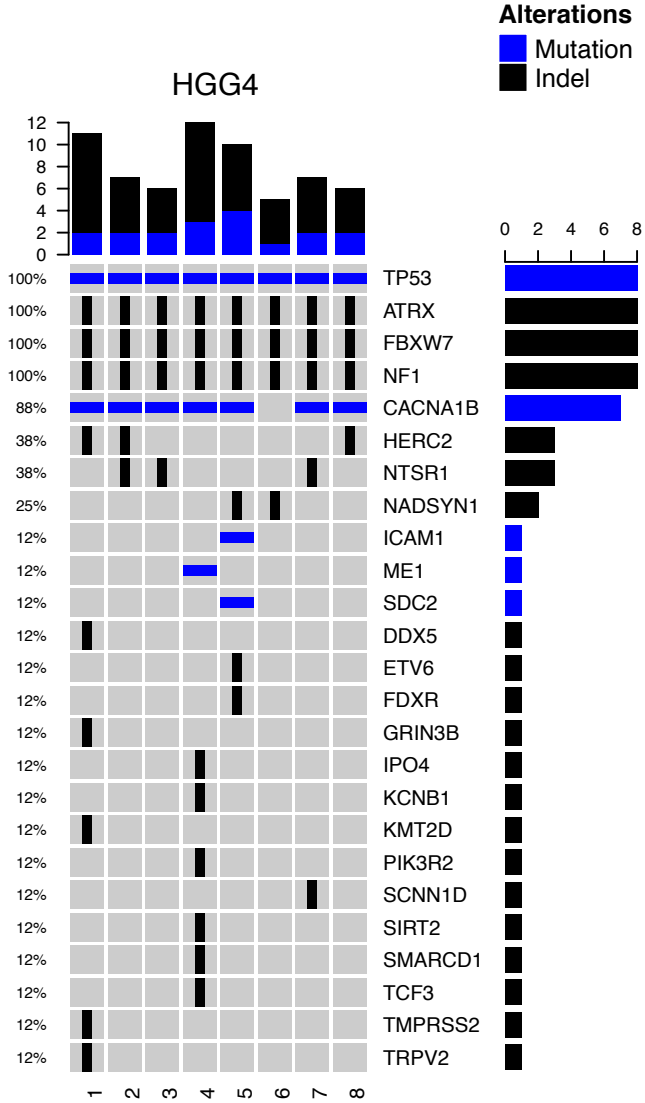

Alterations

Mutation

Indel

Supplementary Figure 14

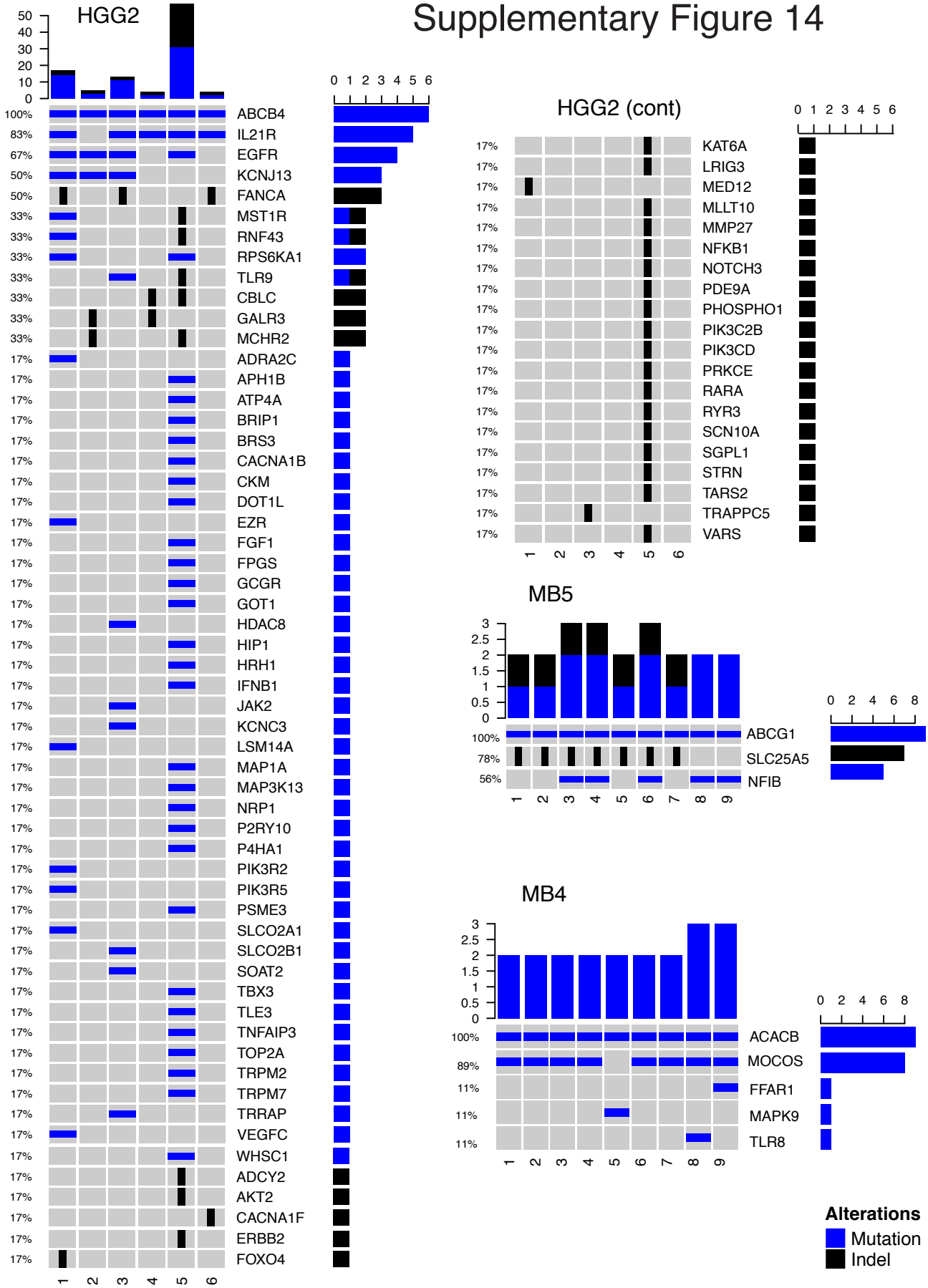

Supplementary Figure 14

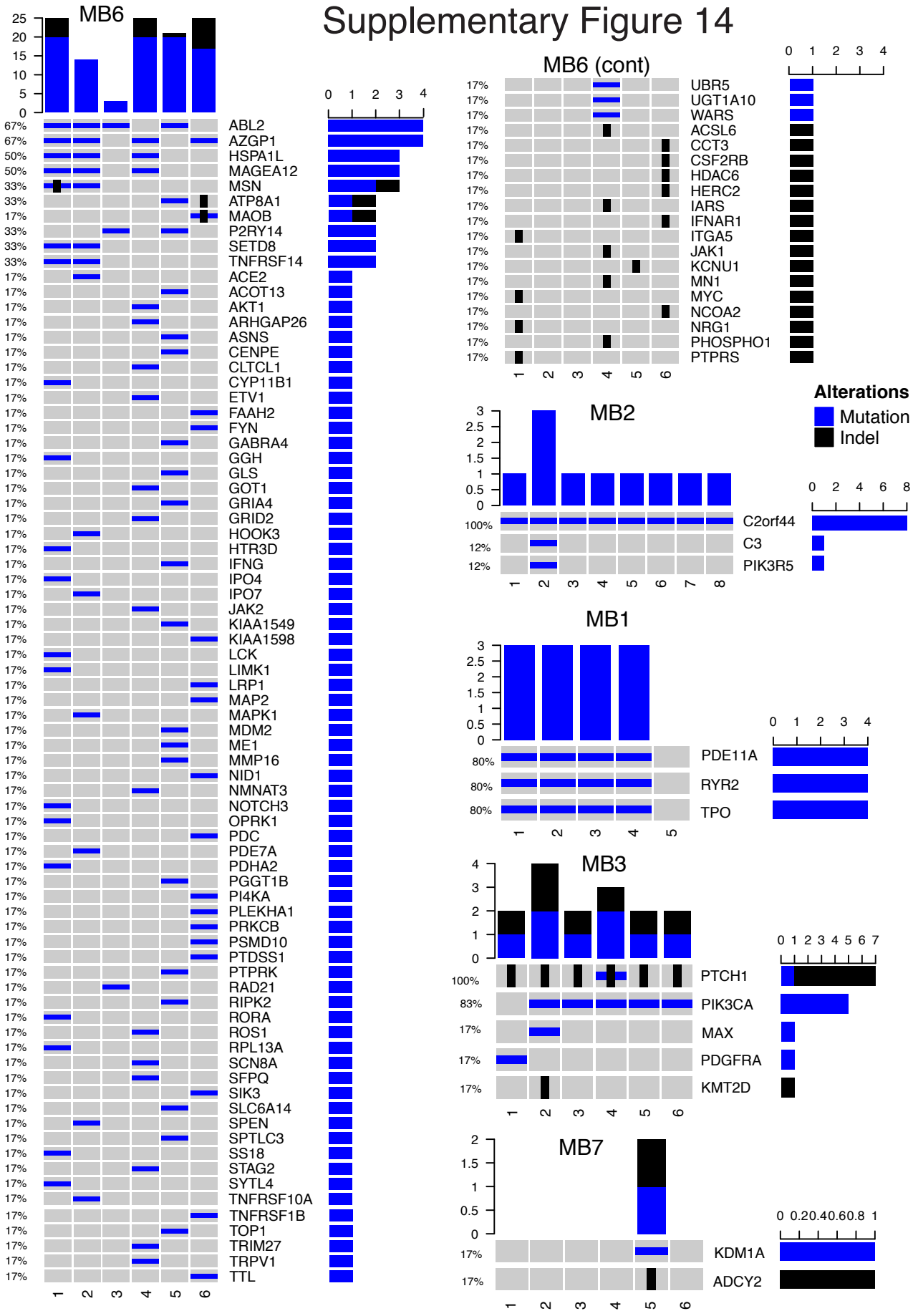

Supplementary Figure 14

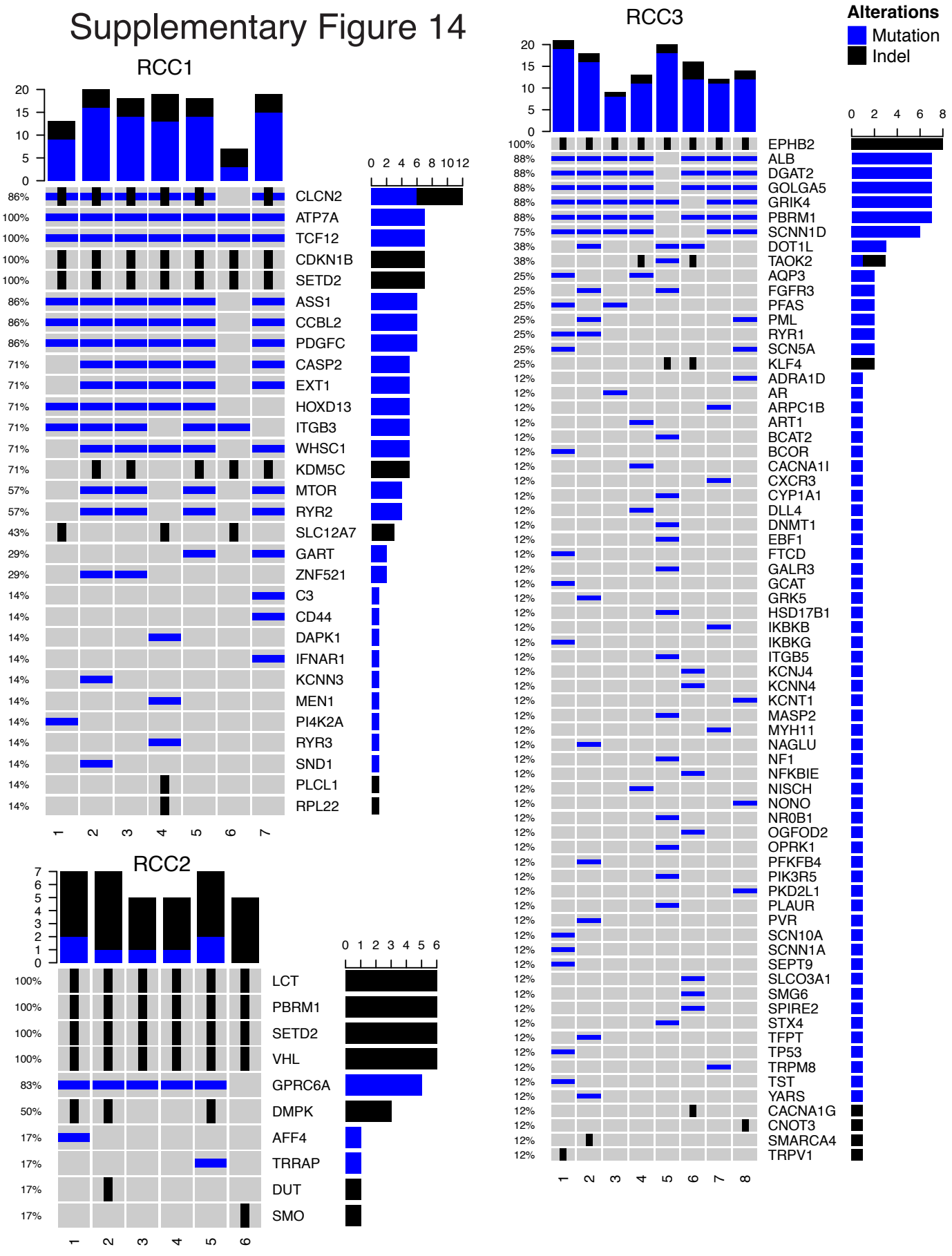

Supplementary Figure 14

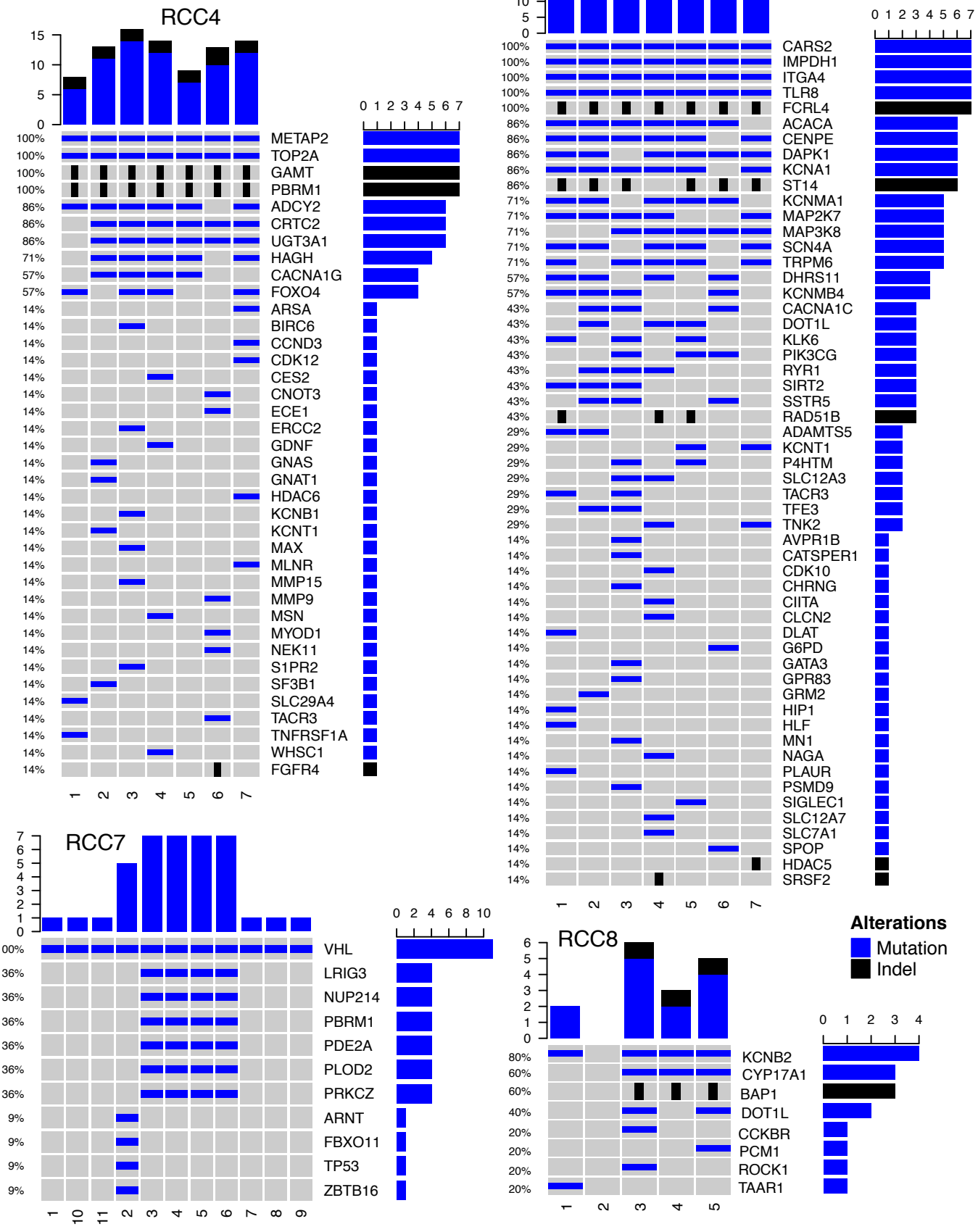

Supplementary Figure 14

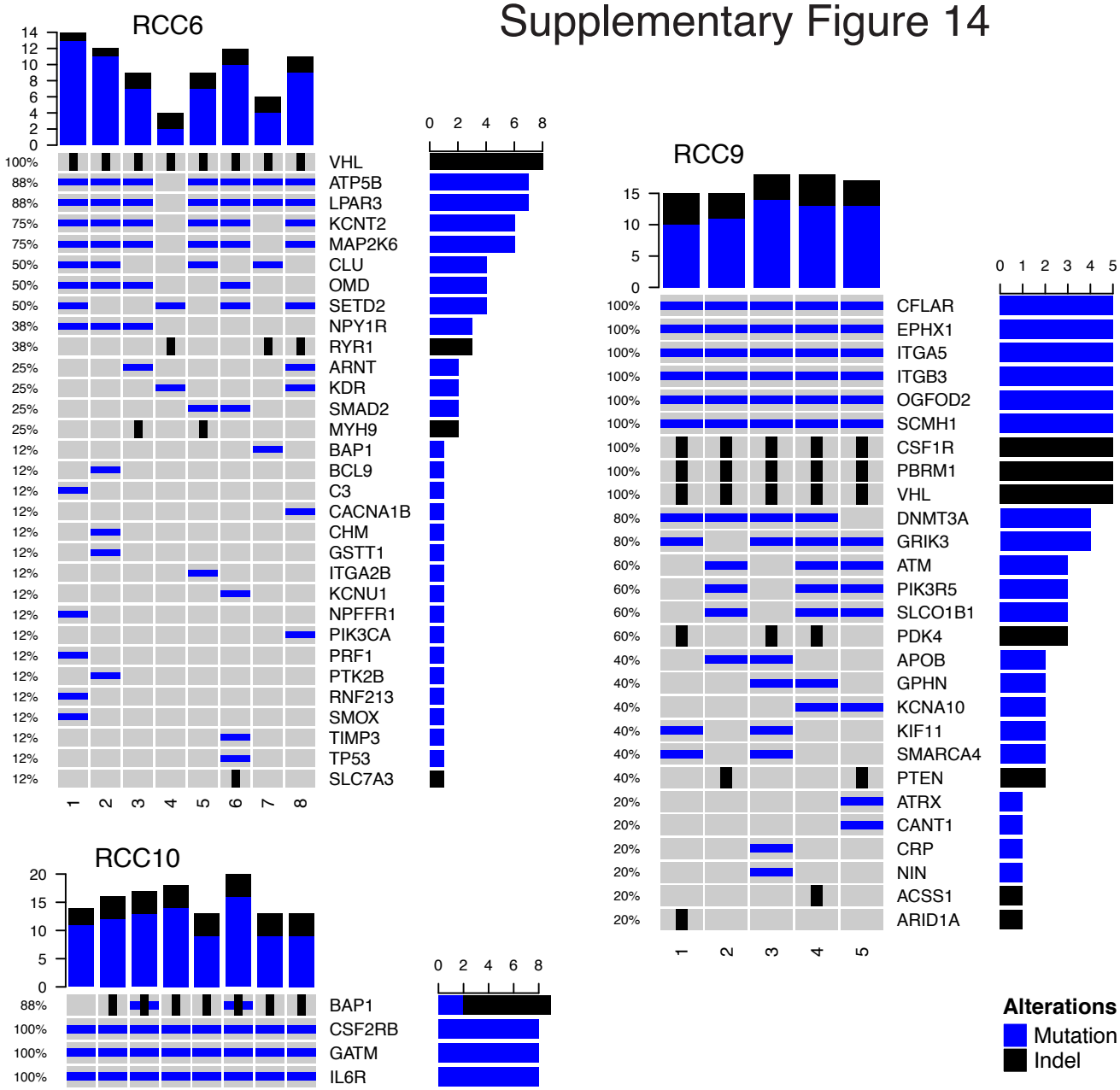

Supplementary Figure 14. Oncoprints of clonal candidate actionable and driver mutations (SNVs / indels). Patient-specific oncoprints of candidate driver and actionable mutations and indels in genes from the Cancer Gene Census and the Drug-Gene Interaction Database. Columns correspond to data from individual biopsies, and rows correspond to genes with alterations. The percent of biopsies with clonal alterations in individual genes is shown on the left, and the total number of individual alterations is presented by a barplot on the right of each gene. Barplots above each biopsy column indicate the number and type of alteration identified.

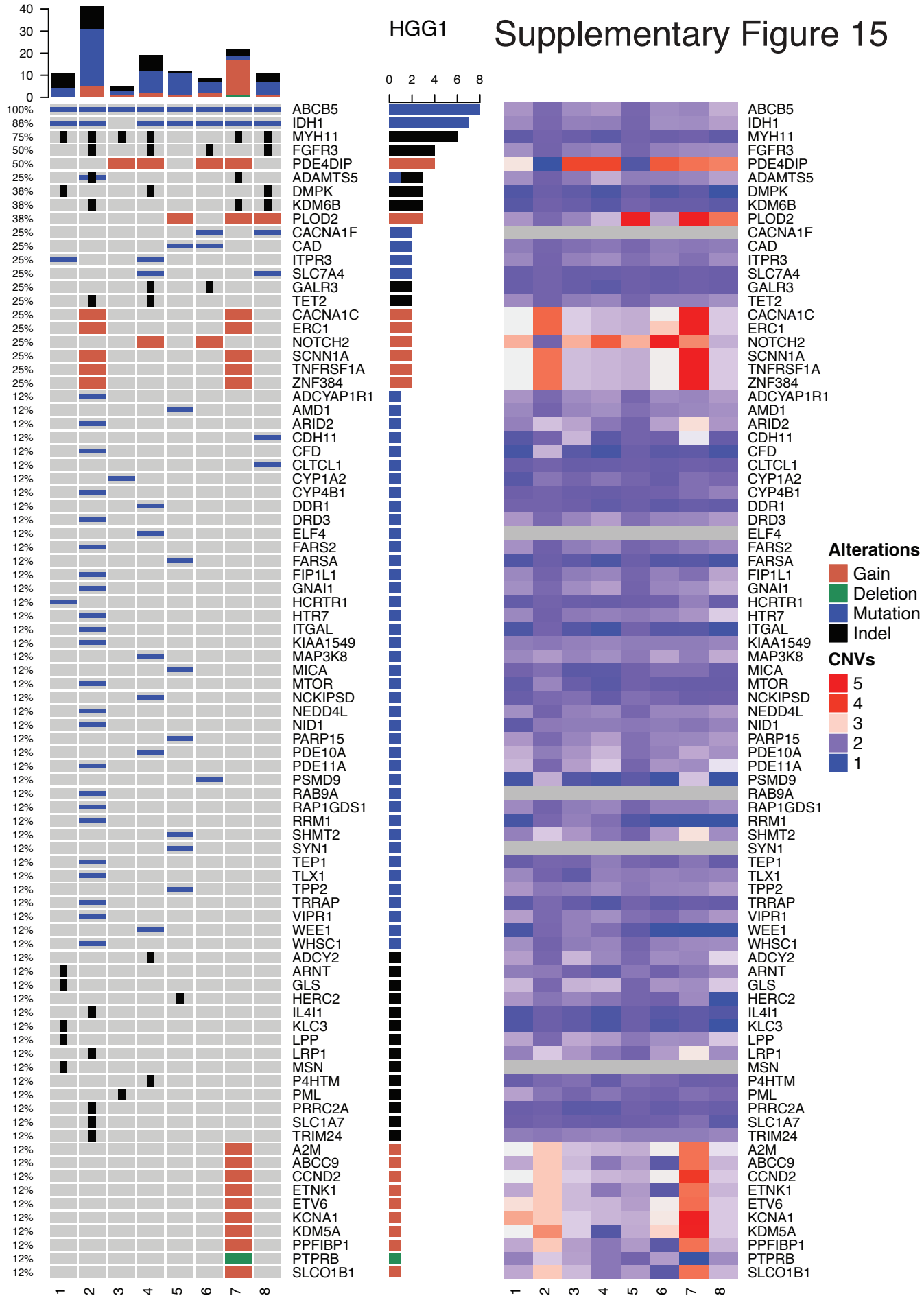
HGG1
Supplementary Figure 15
Alterations
Gain
Deletion
Mutation
Indel
CNVs
5
4
3
2
1

Supplementary Figure 15

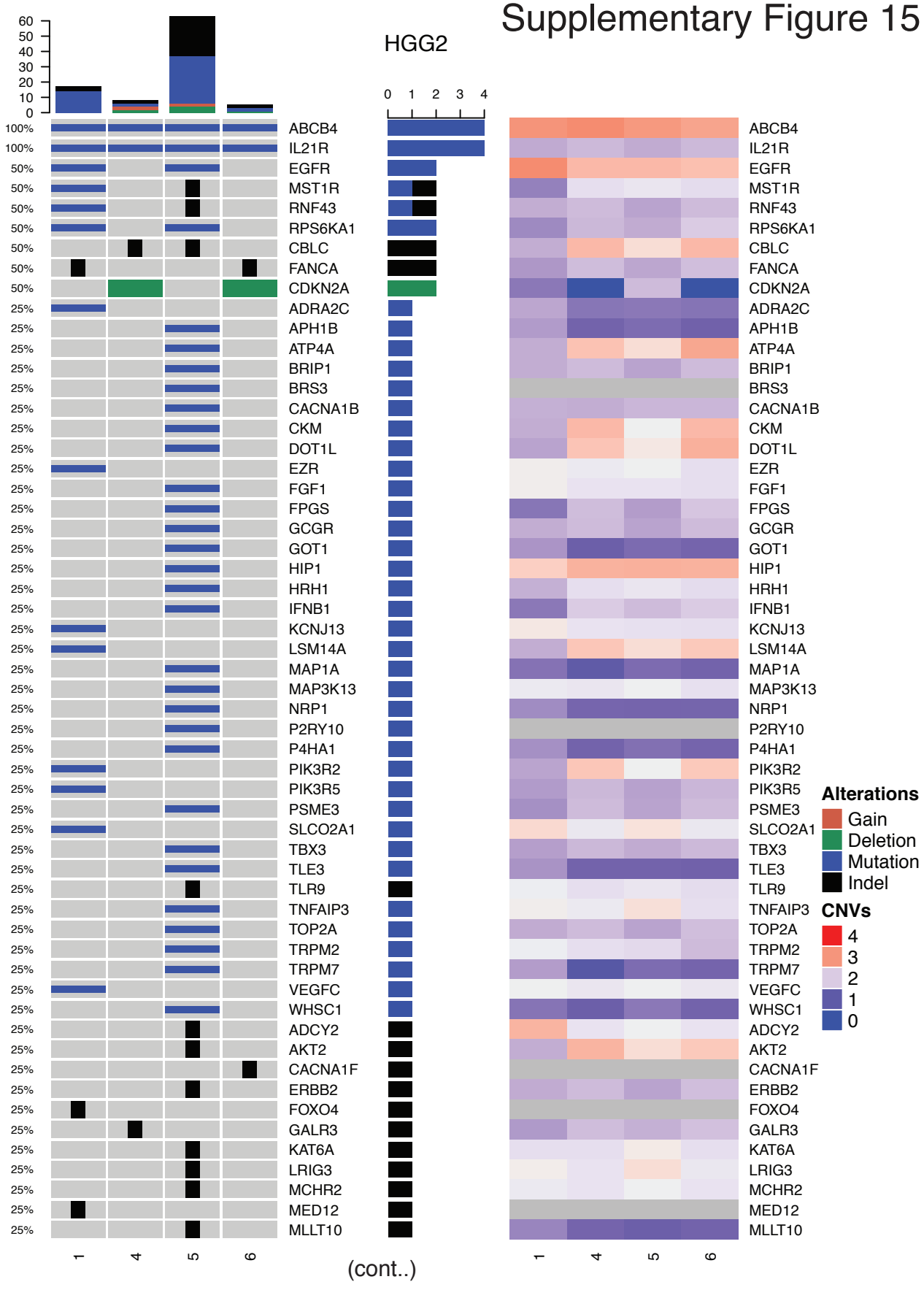

(cont..)

Supplementary Figure 15

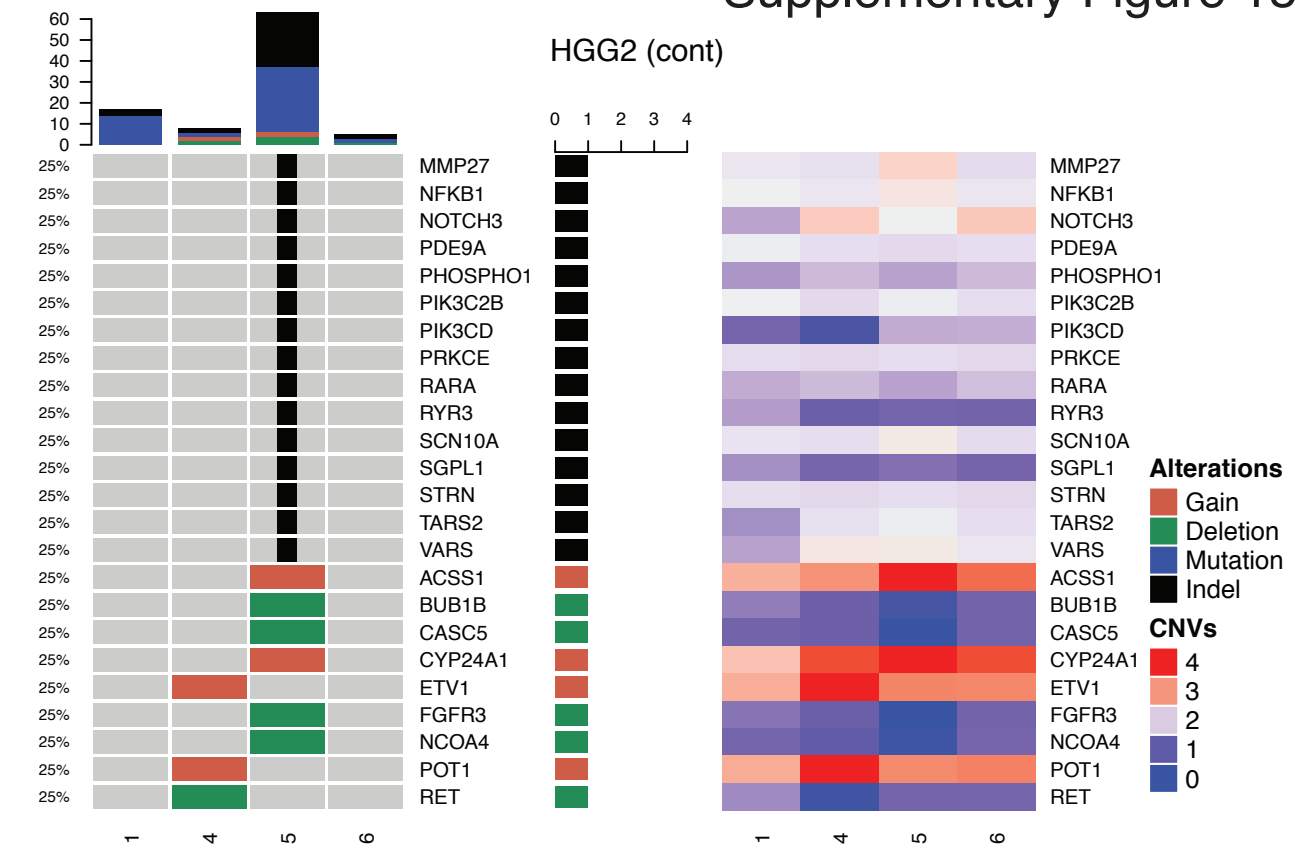

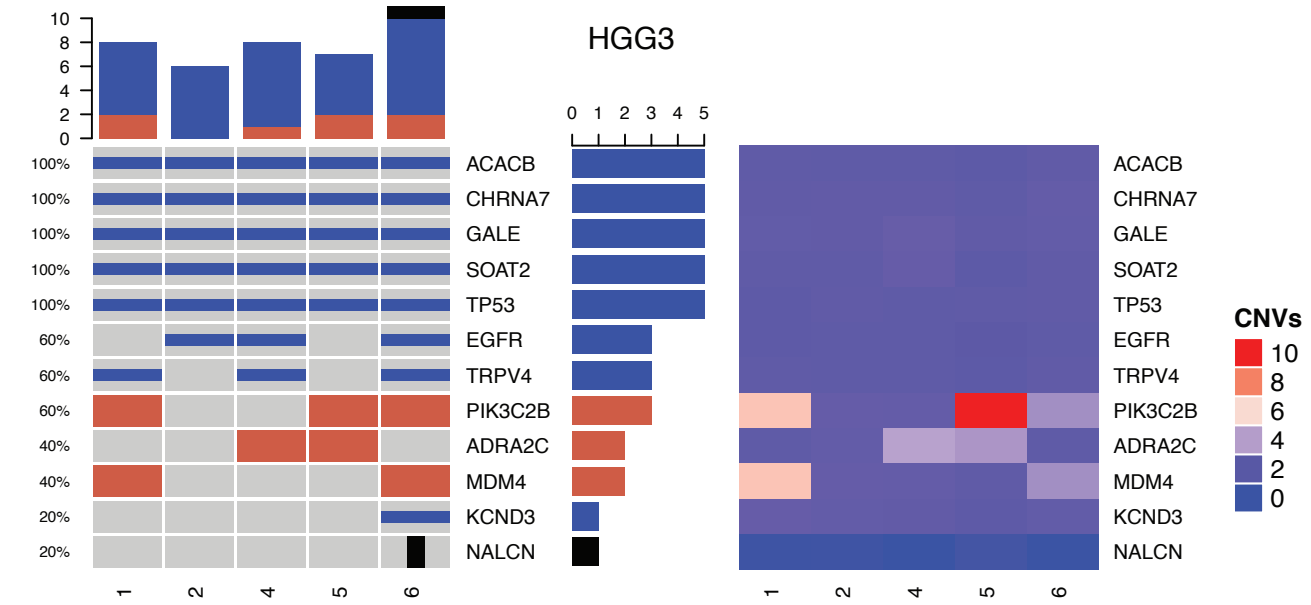

Supplementary Figure 15

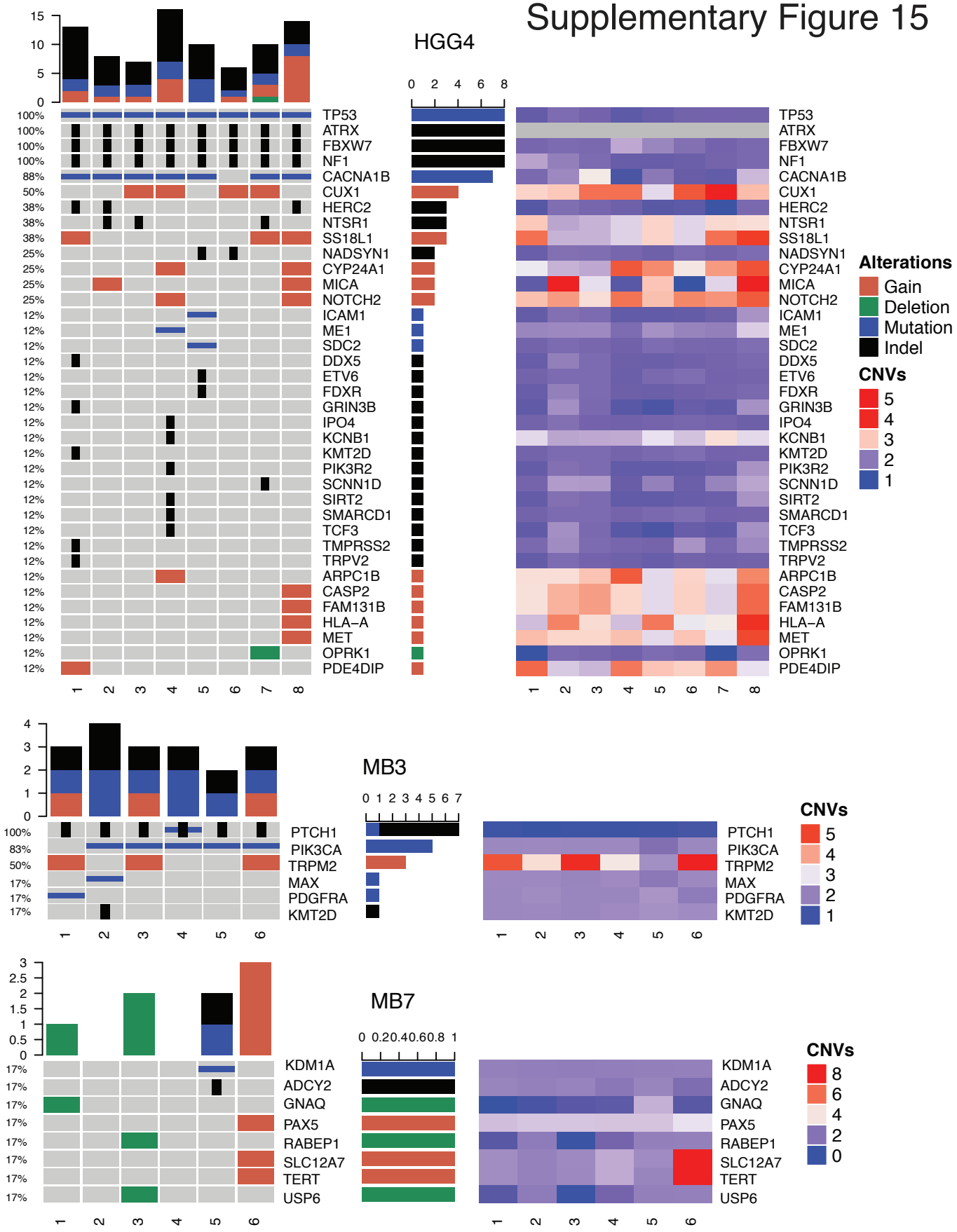

Supplementary Figure 15

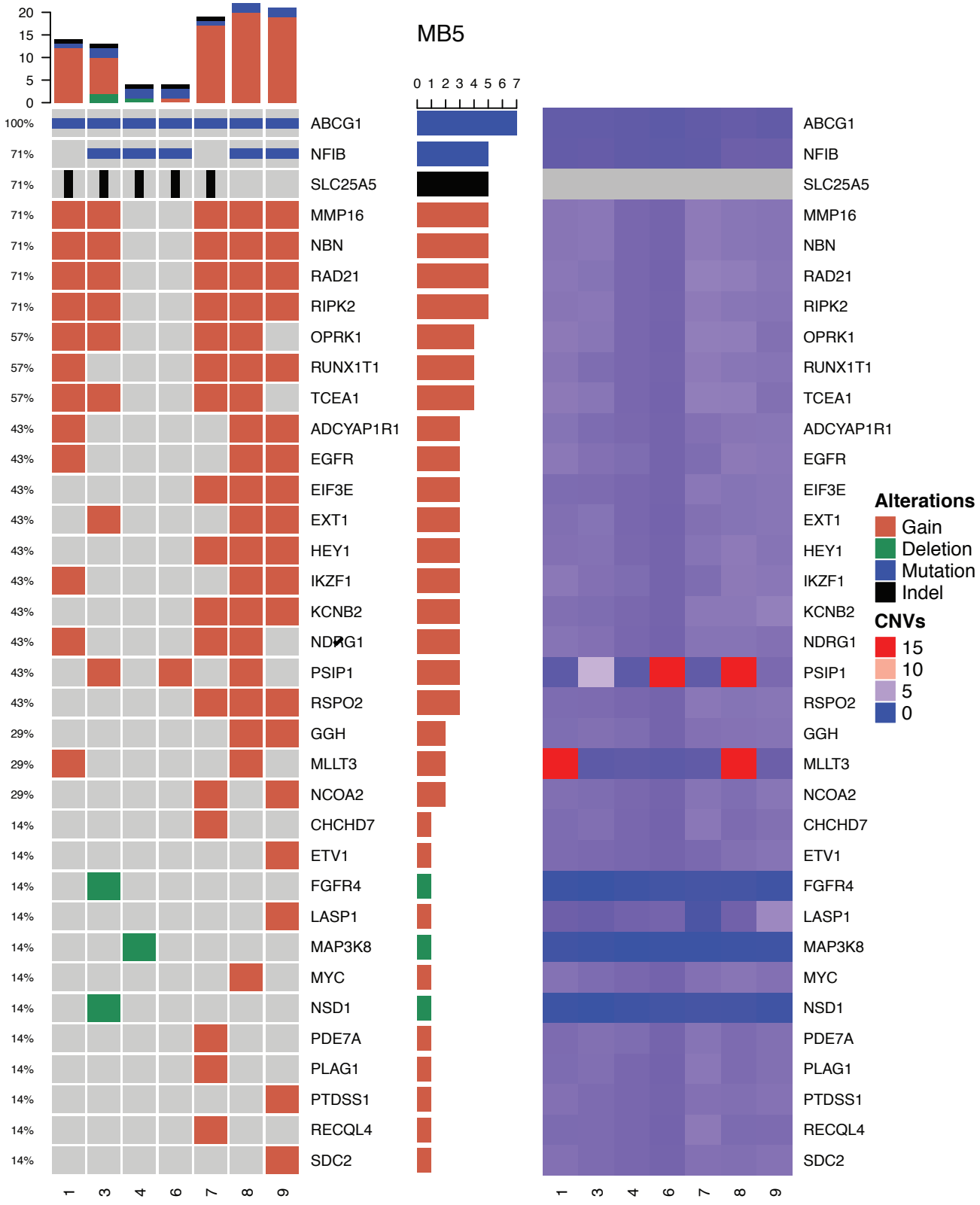

Supplementary Figure 15

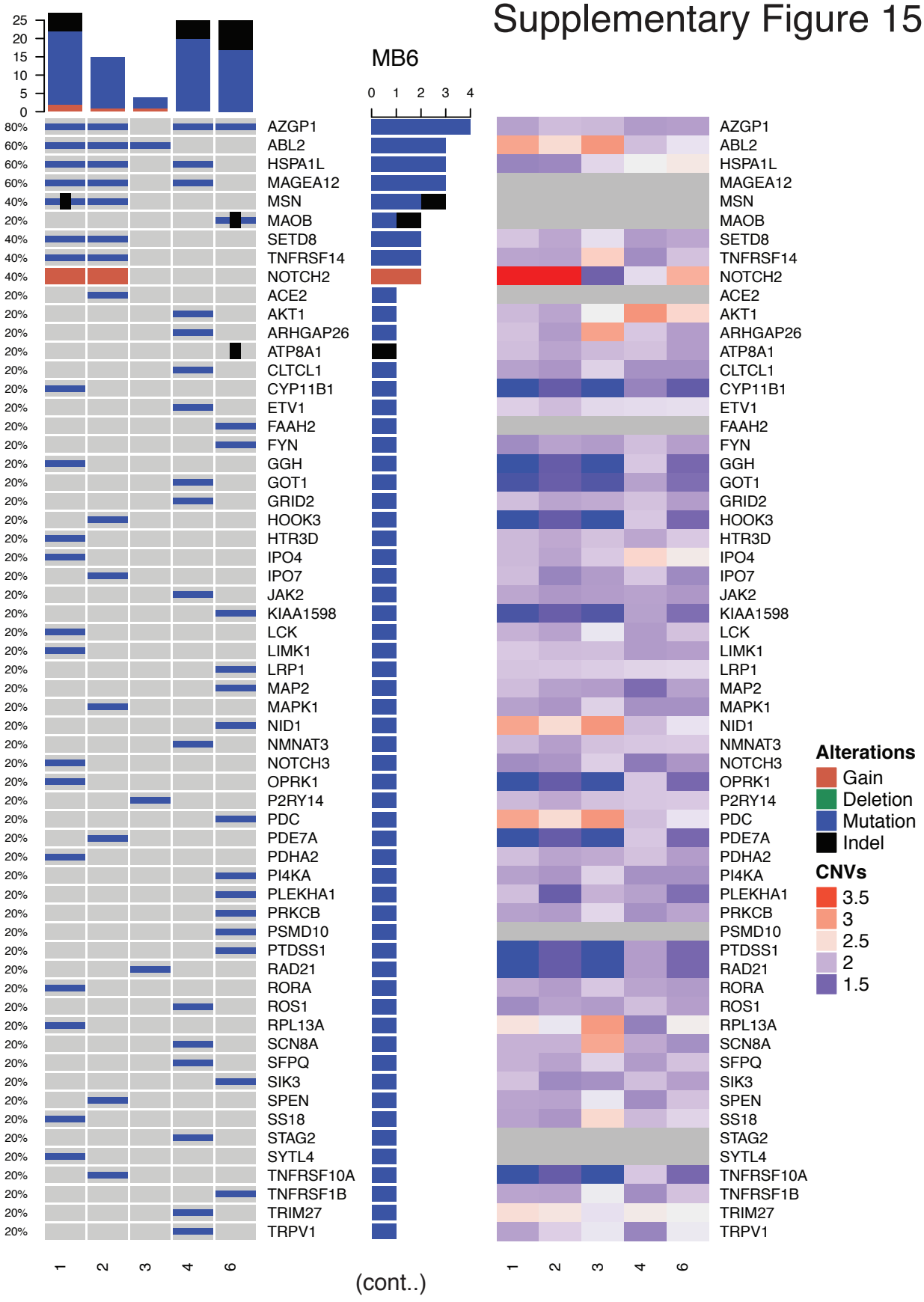

(cont..)

Supplementary Figure 15

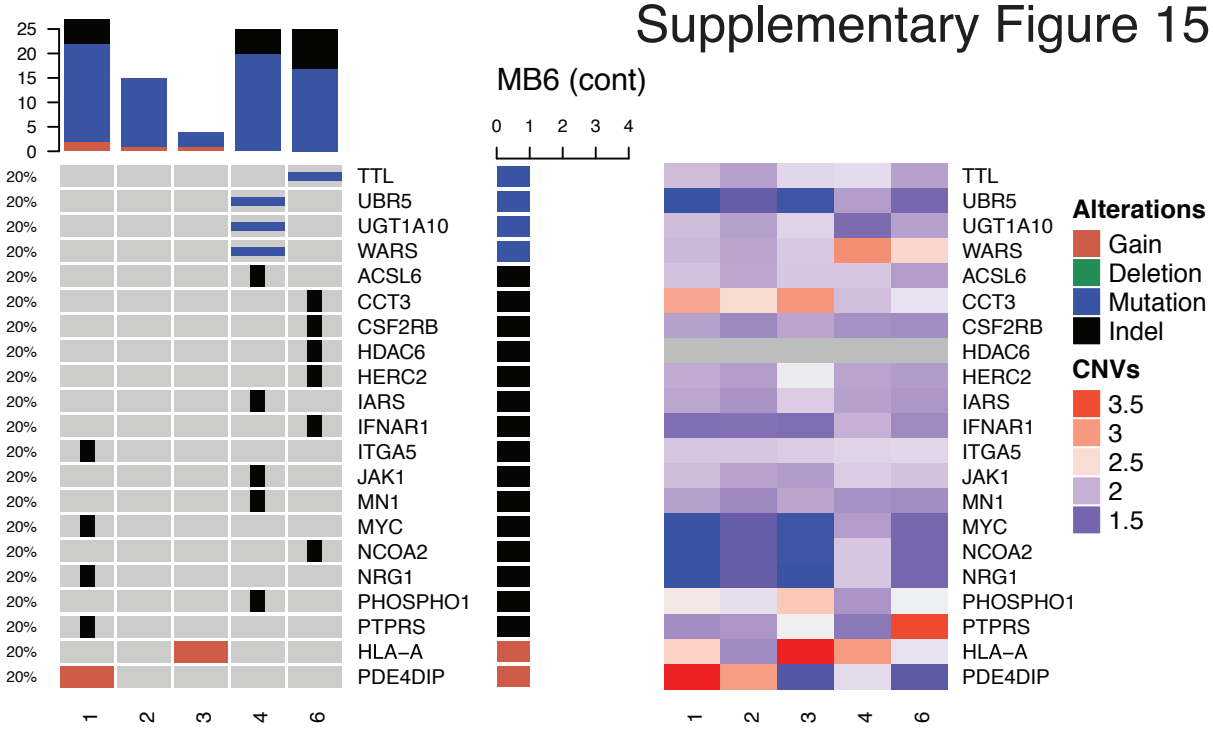

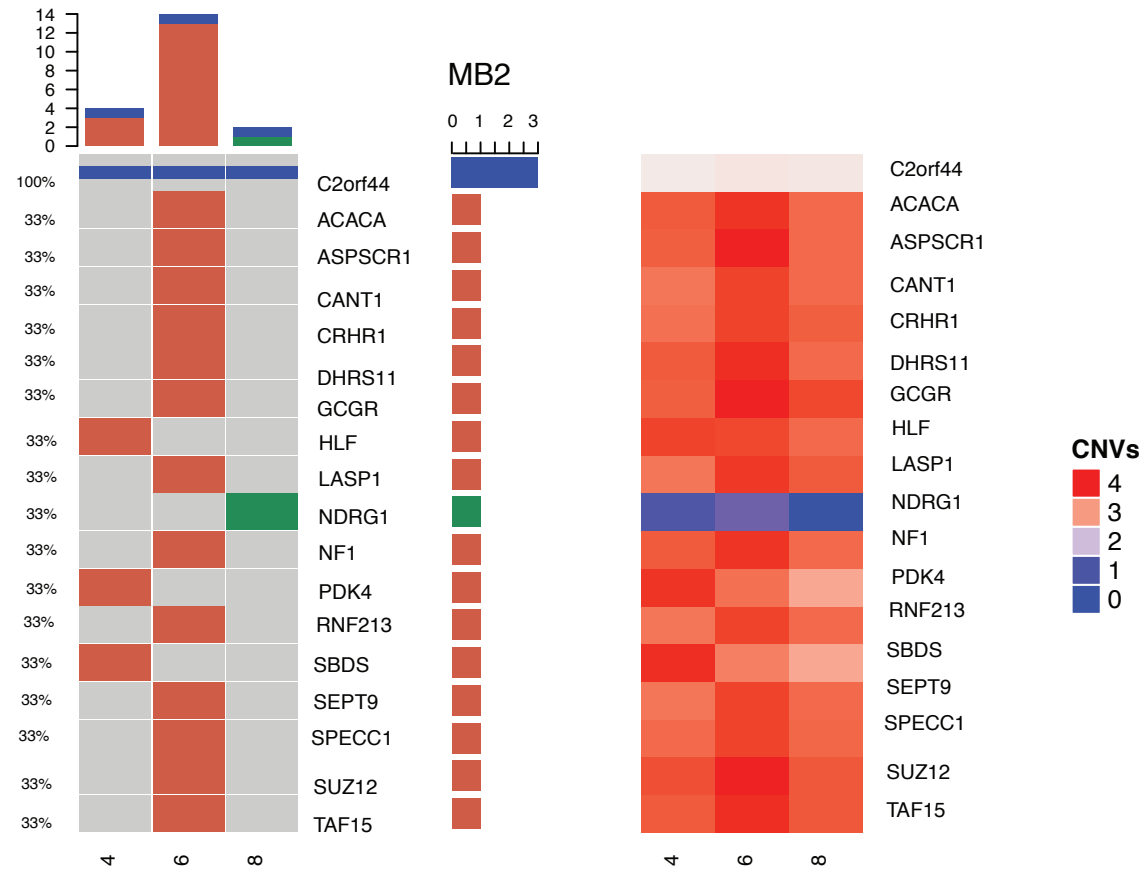

Supplementary Figure 15

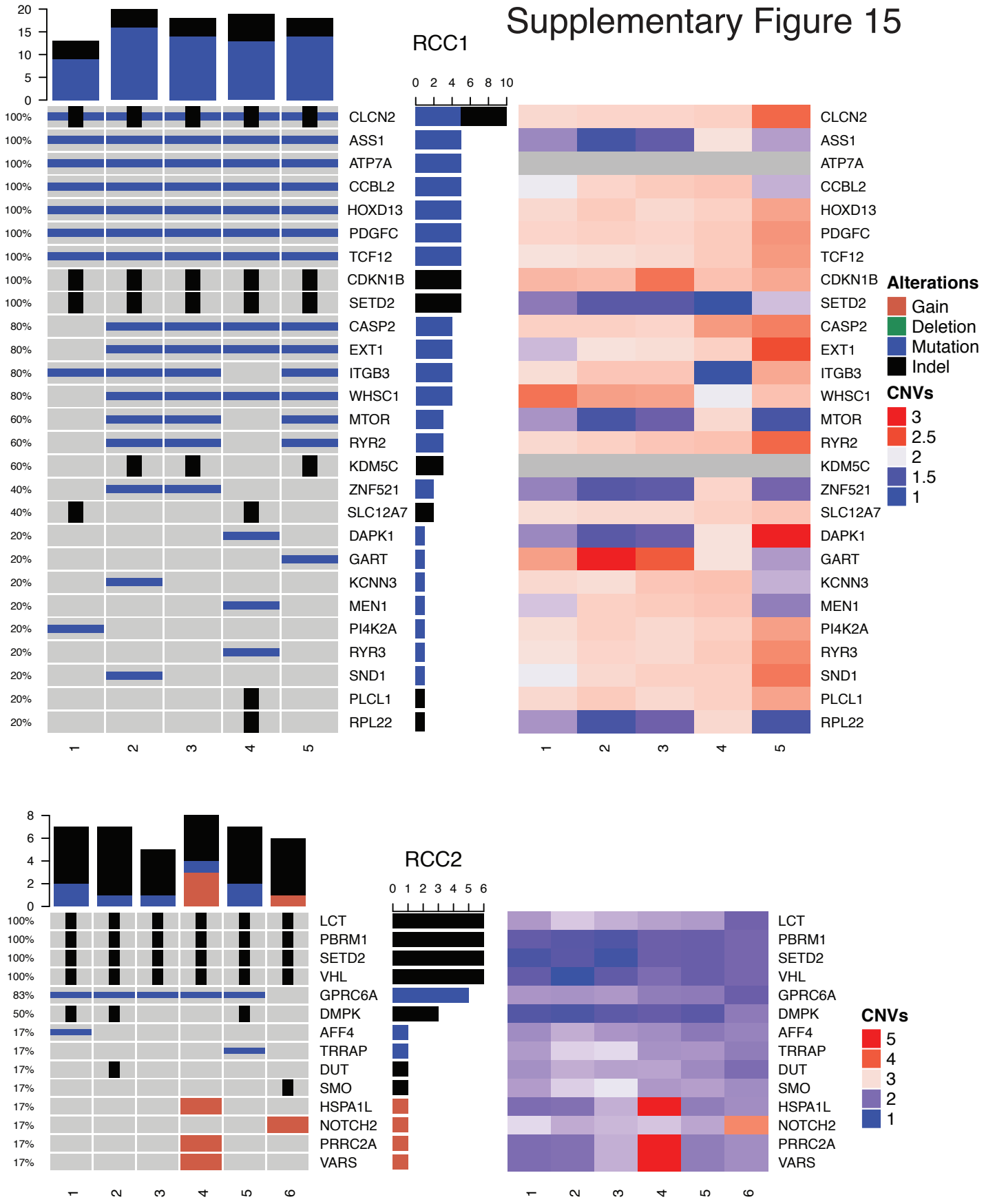

Supplementary Figure 15

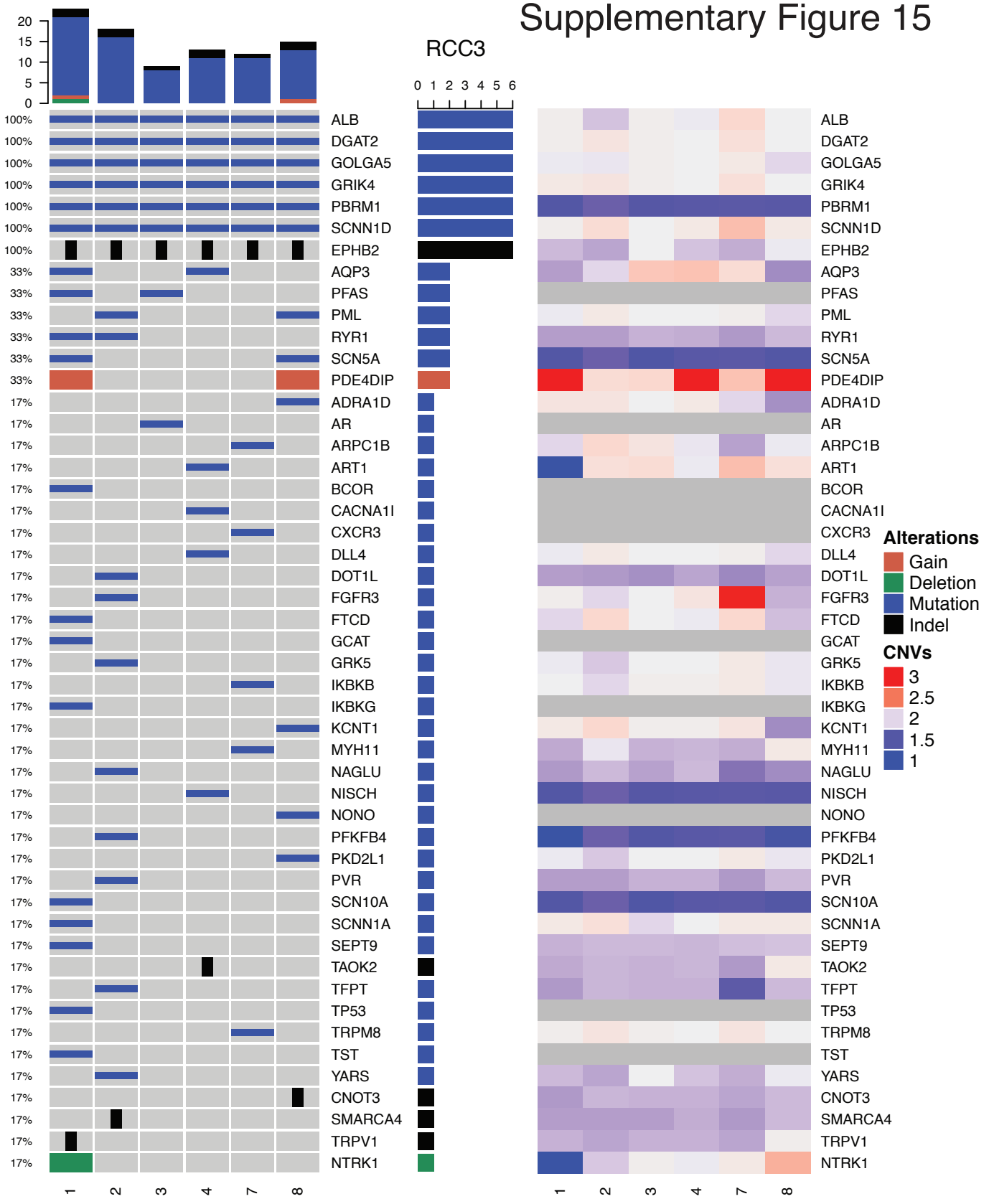

Supplementary Figure 15

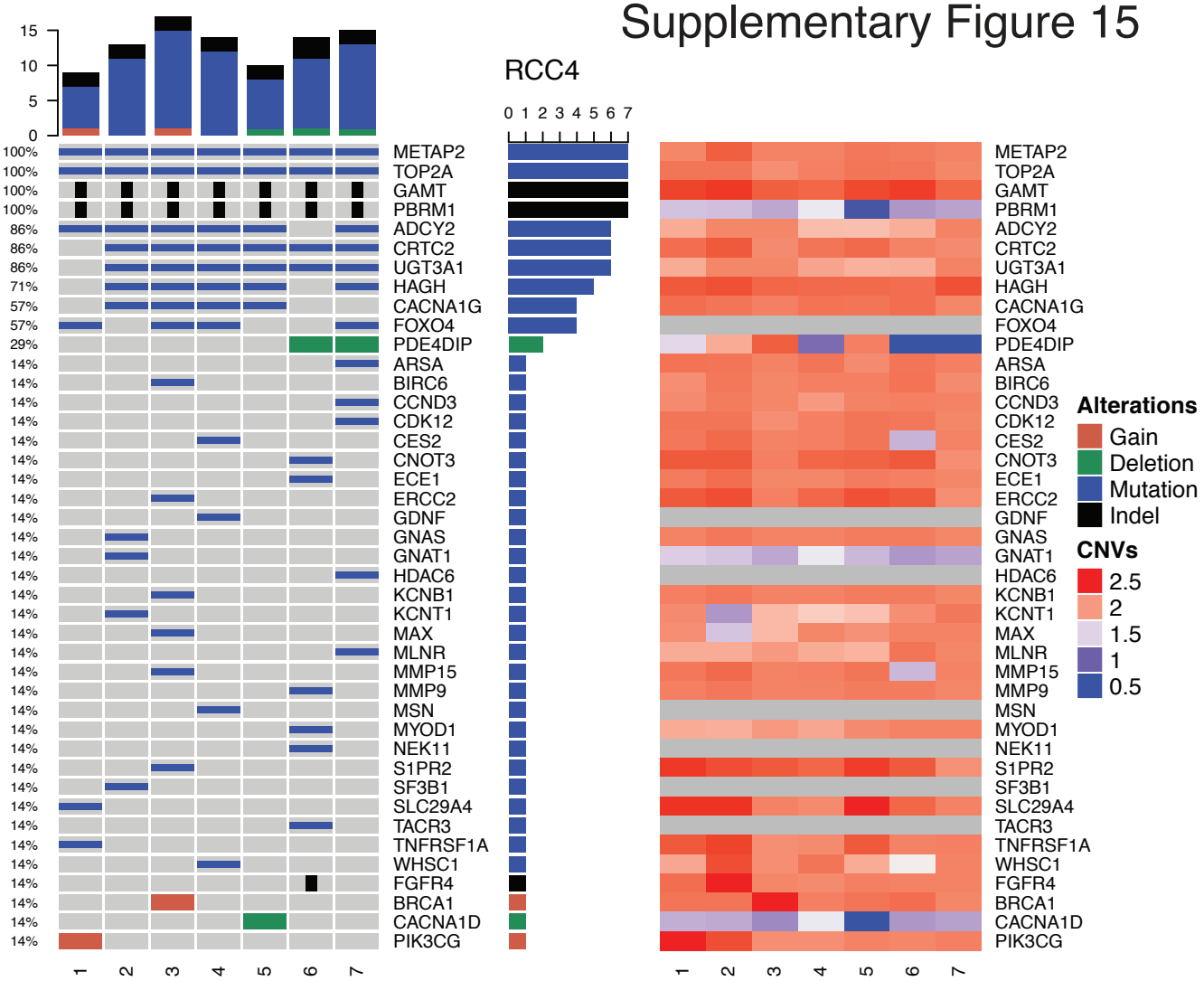

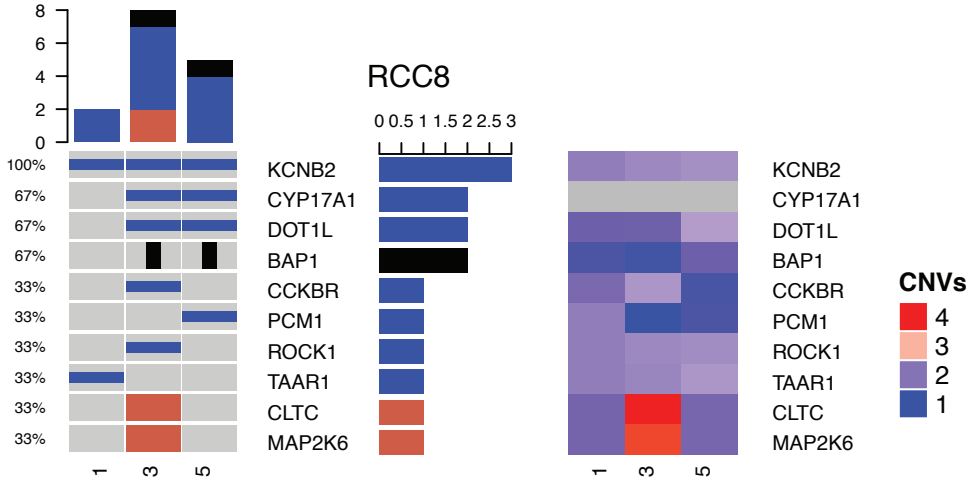

Supplementary Figure 15

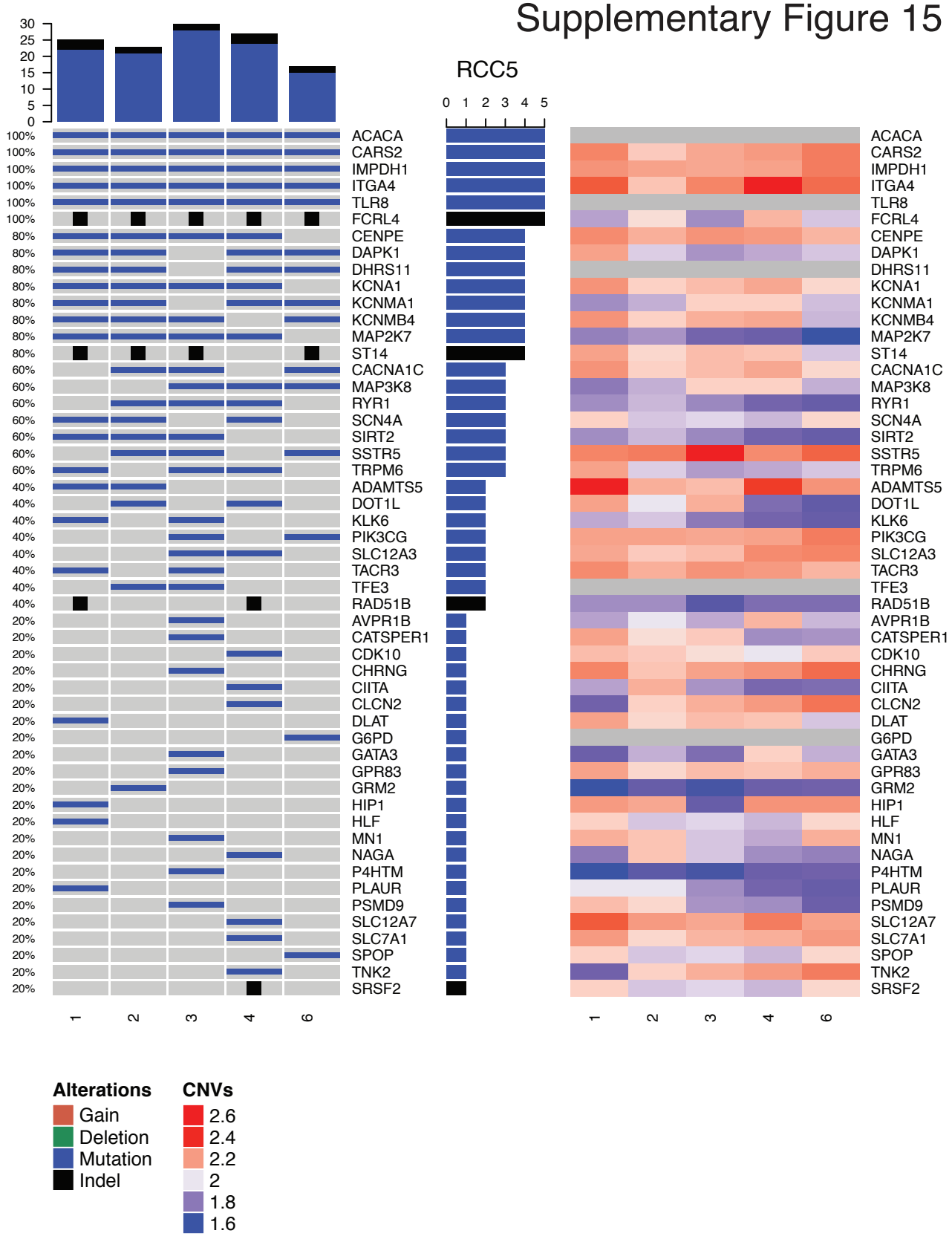

Supplementary Figure 15

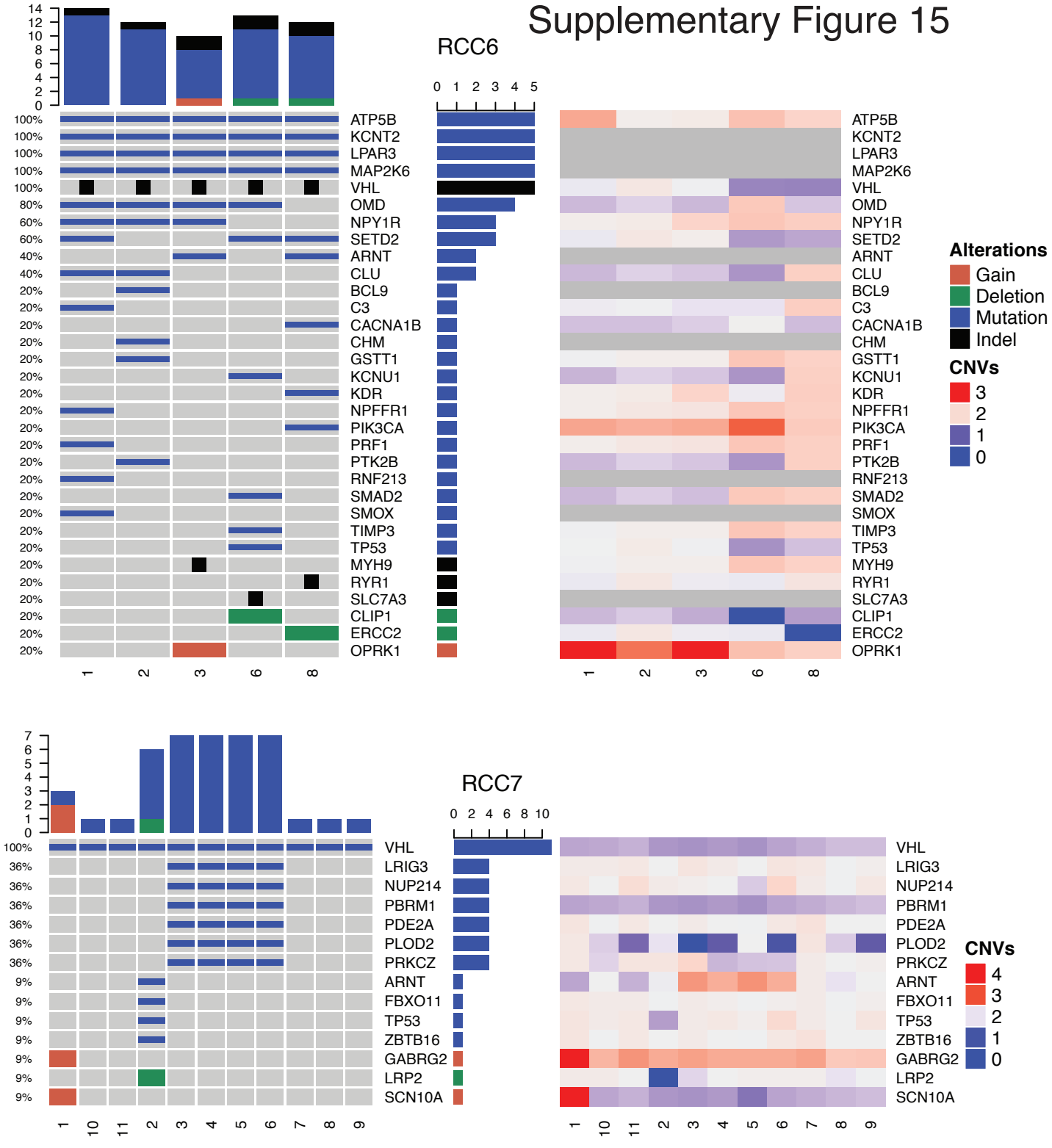

Supplementary Figure 15

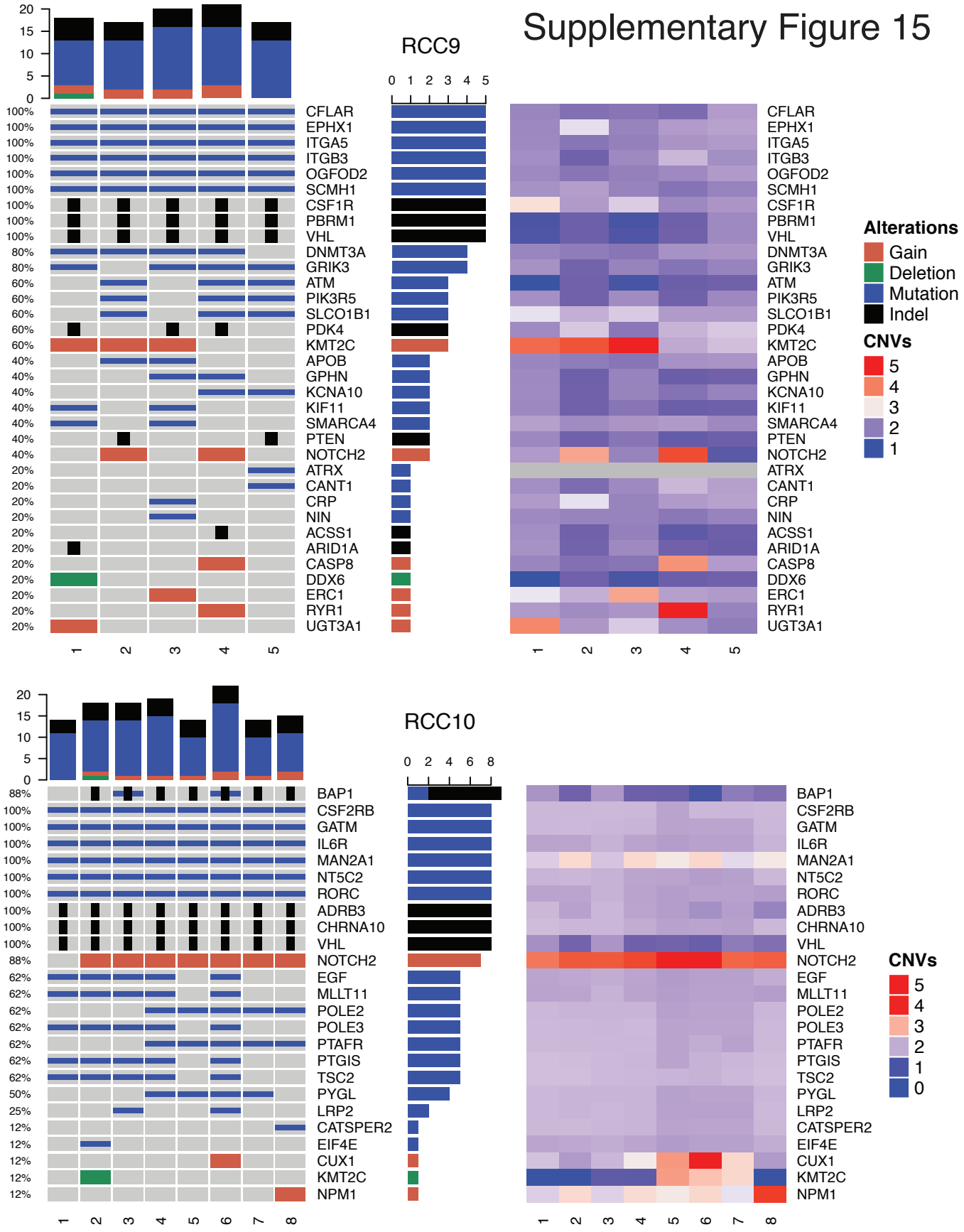

Supplementary Figure 15. Oncoprints of clonal candidate actionable and driver mutations (CNAs / SNVs / indels). Patient-specific oncoprints of candidate driver and actionable mutations, indels, and high-level amplifications or homozygous losses in genes from the Cancer Gene Census and the Drug-Gene Interaction Database. Columns correspond to data from individual biopsies, and rows correspond to genes with alterations. The percent of biopsies with clonal alterations in individual genes is shown on the left, and the total number of individual alterations is presented by a barplot on the right of each gene. Barplots above each biopsy column indicate the number and type of alteration identified. In most biopsies where mutations are not present, there is no correlation with homozygous deletions. Homozygous deletions and copy number gains (>4 copies) are shown in the left panels, while the copy number status of all genes in each biopsies is shown in the right panel. Copy-number color scale is individually scaled for each tumor (legend on the right panel).

Supplementary Figure 16

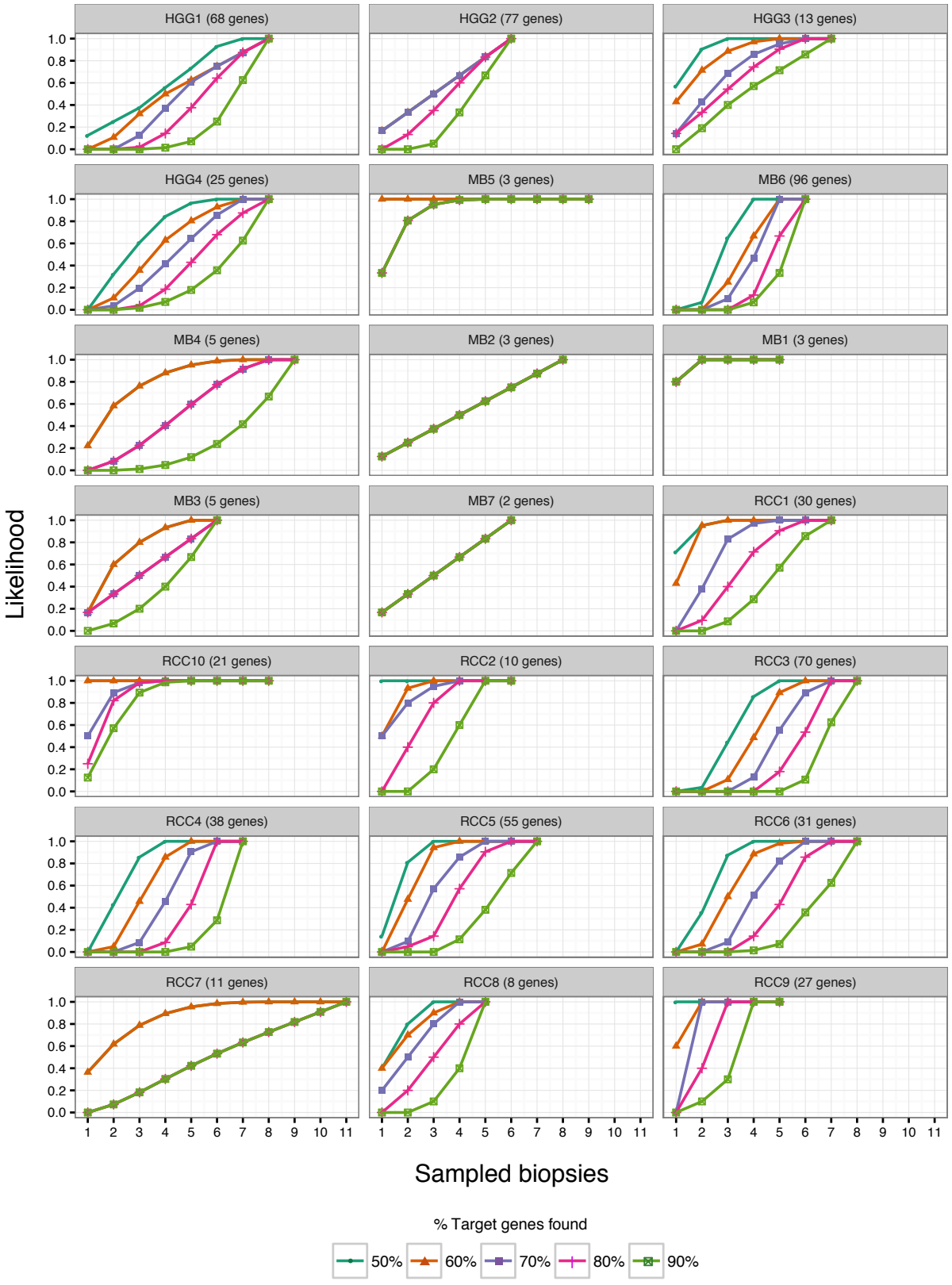

Supplementary Figure 16. Plateau of detection in each tumor. The likelihood of identifying a subset of all genes with clonal (?) driver/actionable mutations (i.e target genes) per tumor is shown as a function of biopsy number. The likelihood of finding x% of the target genes is calculated for each possible combination of biopsies at the current sampling level (for example all possible combinations of 3 biopsies), as the proportion of possible biopsy combinations where the % target genes is exceeded. For example, in RCC4, the likelihood of identifying at least 50% of the known altered genes with a single biopsy is 0% because no single biopsy contains that many of the mutations; however, there are multiple combinations of 2 biopsies that contain at least 50% of the known mutations (likelihood = 42%).

Supplementary Figure 17

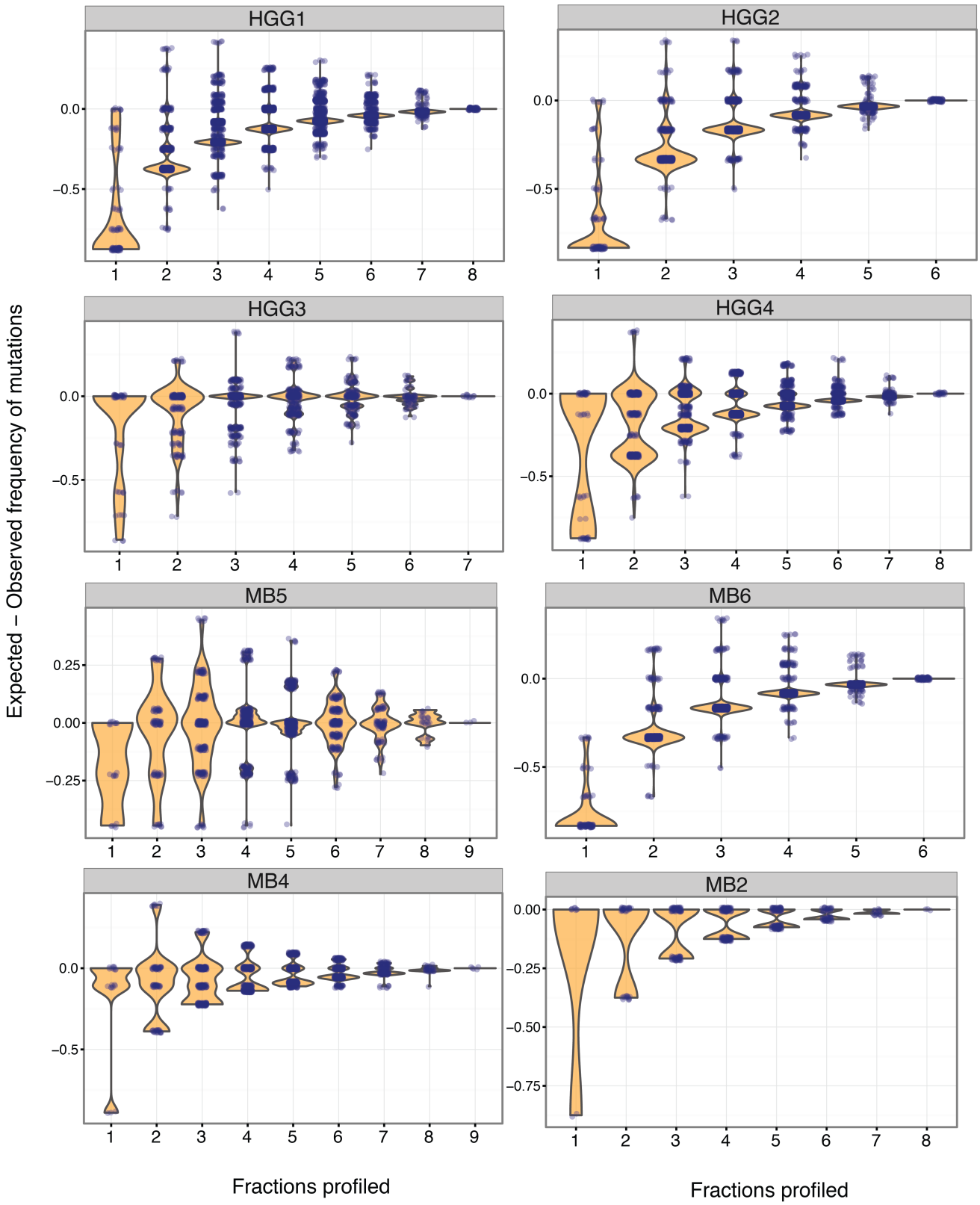

Supplementary Figure 17

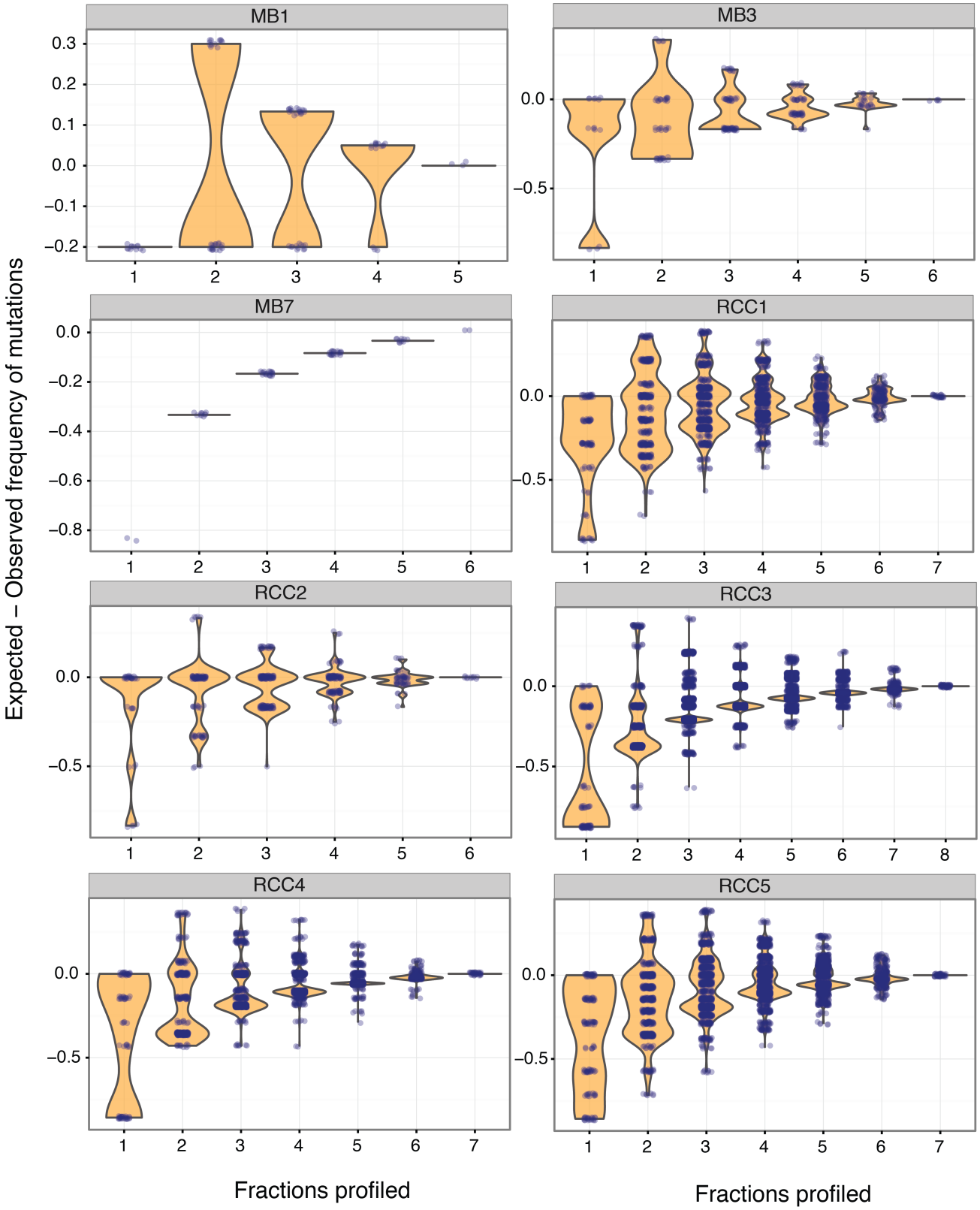

Supplementary Figure 17

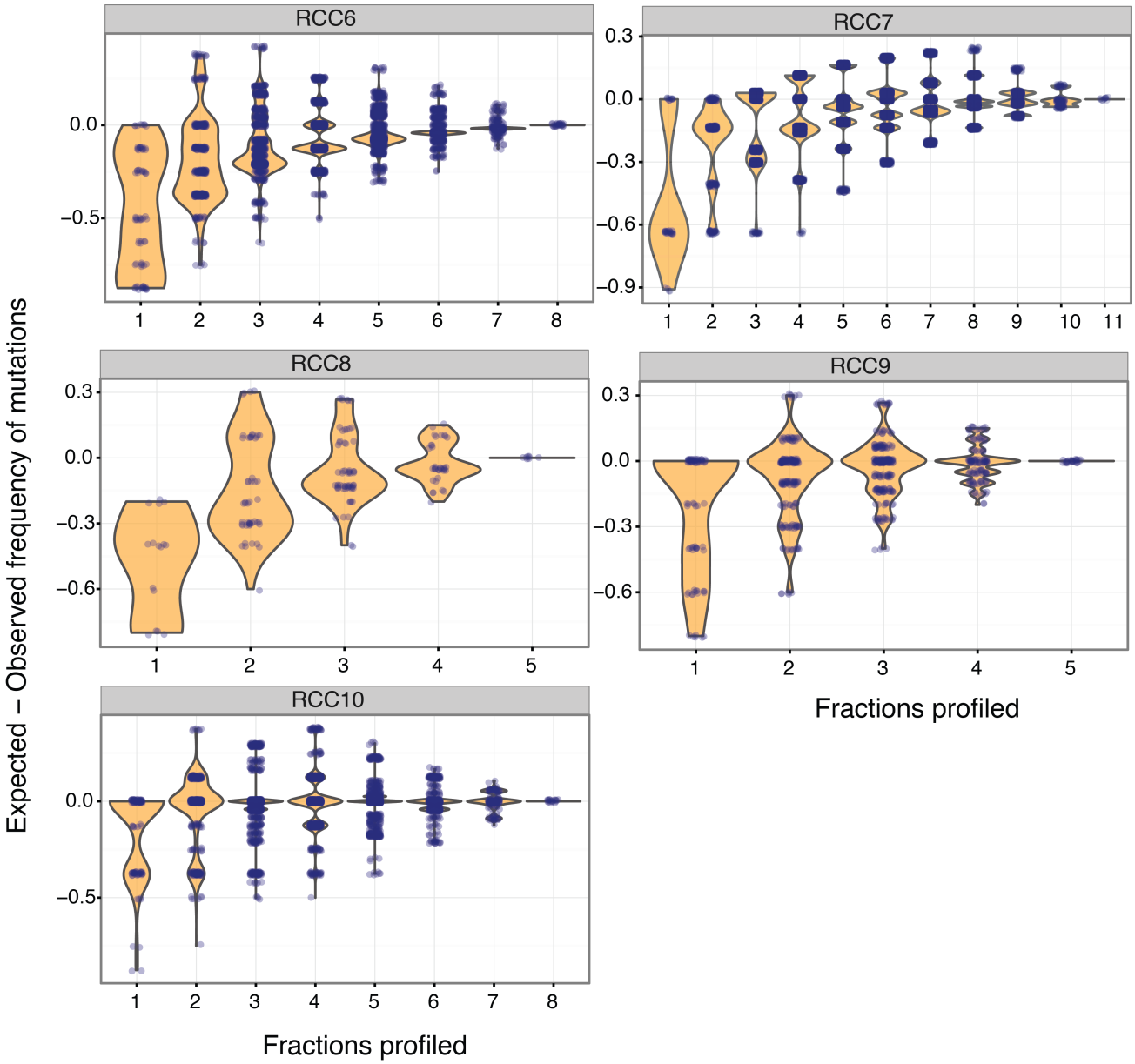

Supplementary Figure 17. Error inference of mutation frequency as a function of biopsy number. The inference error in determining the proportion of biopsies with a particular mutation is calculated for each mutated gene in each tumor, considering all possible combinations of x biopsies, where x is 1:n, and n is the total number of biopsies profiled in a given patient. Y-axis represents the difference between the known (expected) frequency of a mutation across biopsies, and the observed frequency in the current combination of x biopsies. Negative y-values indicate mutations where an observed mutation seems more frequent than it actually is; positive y-values indicate mutations where an observed mutations seems less frequent than it is, given the particular choice in biopsies considered; values at zero indicate mutations where the observed and expected frequency are identical. Violin plots show the major distribution of data points at each sampling level. More homogeneous tumors show a flat distribution with increasing biopsies (e.g. HGG3), while more heterogeneous tumors show an initial negative distribution that approaches zero as the number of biopsies increases (e.g. HGG2).

Supplementary Figure 18

a

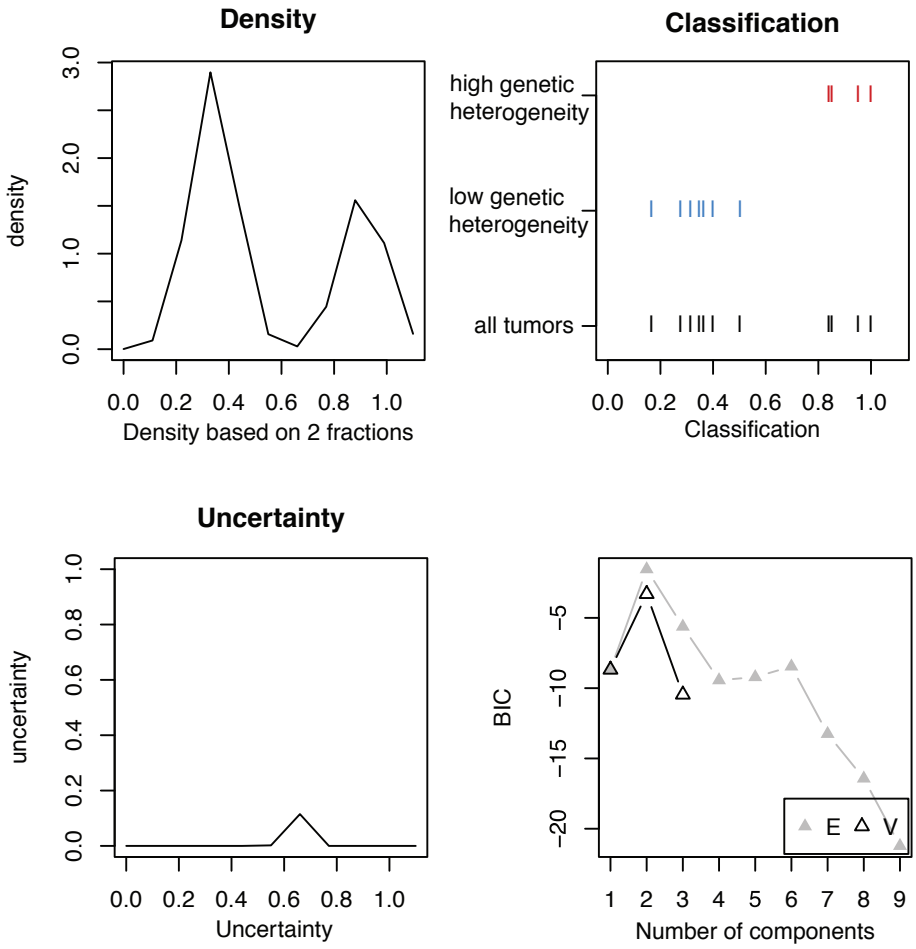

b

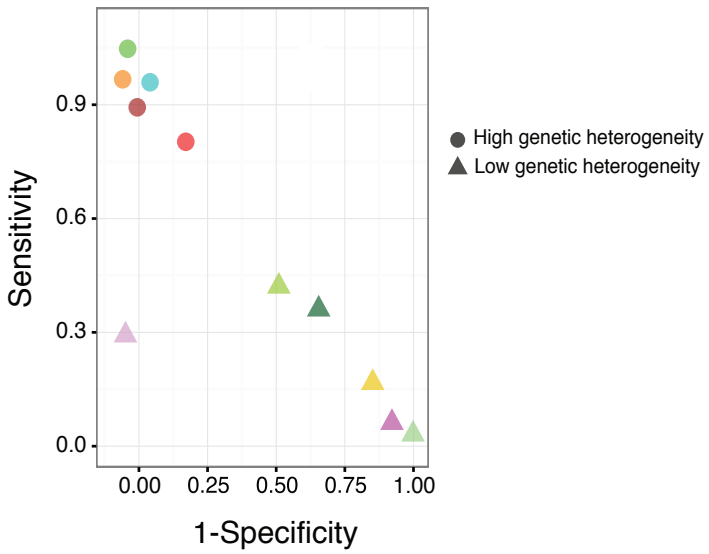

Supplementary Figure 18. High versus low genetic heterogeneity classification based on 2 biopsies. Classification results for MB and GBM tumors, based on the proportion of actionable/driver genes with mutations detected in 2 of 2 biopsies. **(a)** For each tumor we consider the subset of actionable/driver genes which are mutated in both sampled biopsies. Density plot of the proportion values shows that tumors are classified into 2 populations (2nd panel), consisting of tumors with high (blue) or low genetic heterogeneity (red). The uncertainty of classification and the BIC for each set of parameters are plotted in two lower panels. **(b)** Sensitivity and specificity is high for classification of tumors with high genetic heterogeneity. i.e. Based on the metric in (a), the vast majority of pairs of biopsies from tumors with high genetic heterogeneity have a low percentage of gene mutations found in both biopsies, such that they are always classified as heterogeneous tumors, and almost never as homogeneous tumors.

Supplementary Figure 19

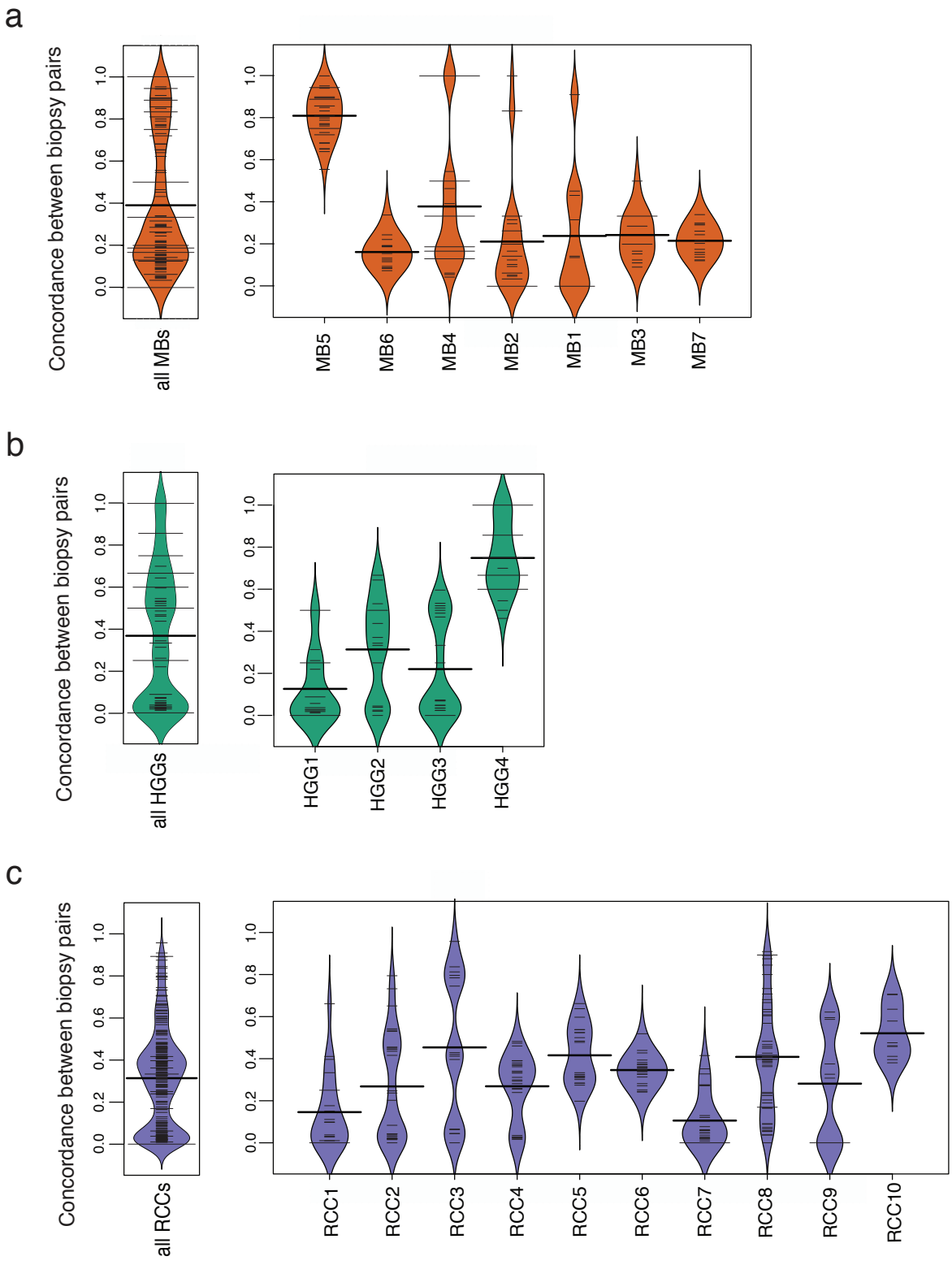

Supplementary Figure 19. Genetic similarity between pairs of biopsies in each tumor is presented for all MBs together and separately (a), and similarly for HGGs **(b)** and RCCs **(c)**. Concordance is measured as the number of somatic mutations in common between two biopsies, as a fraction of the total number of mutations present in both. Width of bean plots scale with the number of measurements with a similar y-value, showing data distribution. Thin horizontal lines indicate individual observations; multiple observations with the same value are added together to form a wider line; thick horizontal black bars indicate averages.

Supplementary Figure 20

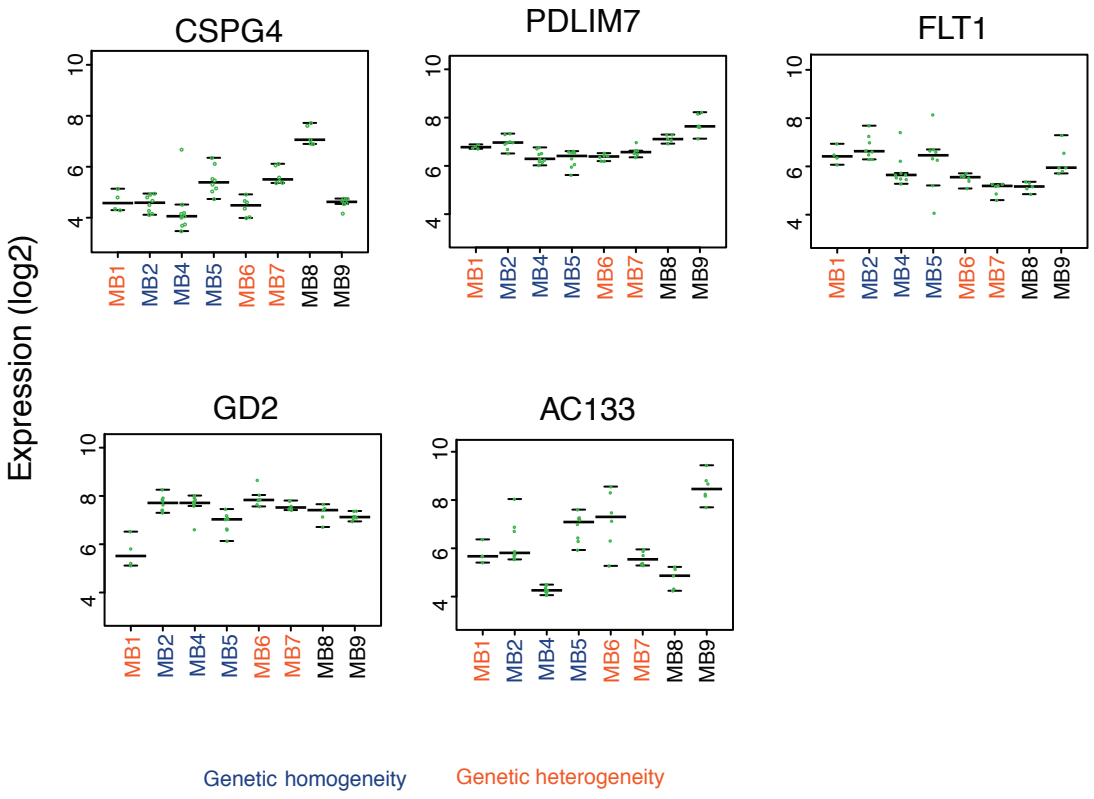

Supplementary Figure 20. Expression of CAR T-cell antigens of multi-region biopsies across 8 MB tumors. Expression of cell surface molecules with immunotherapies currently in clinical trials indicates that tumors with either high genetic heterogeneity (orange labels) or low genetic heterogeneity (blue labels) may respond equally well to CAR T-cell therapy. MB8 and MB9 (black labels) have not been classified due to a lack of genome sequencing data. Green points mark expression of a target gene in individual biopsies; long horizontal lines: median expression per tumor; lower and upper short horizontal lines: 25^{th} and 75^{th} percentiles of expression per tumor.